Improving Performance of Millimeter Wave Beamforming using Inaudible Acoustic Side-Channel

Author:
Moradi, Marjan

Publication Date:
2020

DOI:
https://doi.org/10.26190/unsworks/3950

Improving Performance of Millimeter Wave Beamforming using Inaudible Acoustic Side-Channel

Dissertation submitted in fulfillment
of the requirements for the degree of

Doctor of Philosophy

in

Computer Science and Engineering

Marjan Moradi

Superviser: Professor Mahbub Hassan

Co-supervisors: Dr. Ming Ding (Data61)

Dr. Kanchana Thilakarathna (USyd)

January 2020

Thesis/Dissertation Sheet

Surname/Family Name	:	**Moradi**
Given Name/s	:	**Marjan**
Abbreviation for degree as give in the University calendar	:	**PhD**
Faculty	:	**Engineering**
School	:	**Computer Science and Engineering**
Thesis Title	:	**Improving Beam Alignment in Millimeter Wave Communication Networks using Inaudible Acoustic Side-Channel**

Abstract 350 words maximum: (PLEASE TYPE)

Millimeter wave communication networks promise to offer ultra-fast internet download speed, but the access points must align the beams precisely to client devices. Efficient beam alignment for mobile users therefore is considered one of the most challenging problems facing millimeter wave networks. Existing approaches that use in-band beam alignment suffers from long alignment delays and low communication performance, especially when large number of mobile clients are connect to the access point. In this research, we explore out-of-band inaudible acoustic side-channel to assist and improve millimetre beam alignment. In particular, this thesis makes three fundamental contributions. First, we analytically study the beam alignment performance of 802.11ad and derive the required number of beacon intervals to complete antenna training in multi-users scenario for 802.11ad. Second, we propose the use of inaudible sound as a side channel to estimate the direction of client and assist beam alignment in millimeter wave access points. Using a combination of experimental and simulation analysis of the inaudible sound spectrum available in typical mobile phones, we demonstrate that the use of 50 Hz and 50 ms sound chirps with an array of two microphones provide efficient and reliable estimation of direction. We design a frequency division multiple channel access to correctly assign the sound source corresponding to the estimated angle on the receiver side. Third, we conduct a comprehensive simulation to evaluate the performance of the proposed sound assisted beamforming. First, the proposed analytical model to derive the required number of beacon intervals in 802.11ad for beam alignment is validated by simulation. Then we show that our proposed algorithm achieves up to 11 dB antenna gain when 10 users are connected compared to the default in-band beam alignment technique used in IEEE 802.11 ad. We believe that our findings shed new light on the fundamental benefits of acoustic-based out-of-band beamforming in crowded millimeter wave communication networks.

COPYRIGHT STATEMENT

Signed …….....

Date …17/01/2020…….....

AUTHENTICITY STATEMENT

‘I certify that the Library deposit digital copy is a direct equivalent of the final officially approved version of my thesis.’

Signed …….....

Date …17/01/2020…….....

ORIGINALITY STATEMENT

'I hereby declare that this submission is my own work and to the best of my knowledge it contains no materials previously published or written by another person, or substantial proportions of material which have been accepted for the award of any other degree or diploma at UNSW or any other educational institution, except where due acknowledgement is made in the thesis. Any contribution made to the research by others, with whom I have worked at UNSW or elsewhere, is explicitly acknowledged in the thesis. I also declare that the intellectual content of this thesis is the product of my own work, except to the extent that assistance from others in the project's design and conception or in style, presentation and linguistic expression is acknowledged.'

Signed ……..

Date ……..

INCLUSION OF PUBLICATIONS STATEMENT

UNSW is supportive of candidates publishing their research results during their candidature as detailed in the UNSW Thesis Examination Procedure.

Publications can be used in their thesis in lieu of a Chapter if:

- The candidate contributed greater than 50% of the content in the publication and is the "primary author", ie. the candidate was responsible primarily for the planning, execution and preparation of the work for publication
- The candidate has approval to include the publication in their thesis in lieu of a Chapter from their supervisor and Postgraduate Coordinator.
- The publication is not subject to any obligations or contractual agreements with a third party that would constrain its inclusion in the thesis

Please indicate whether this thesis contains published material or not:

☐ This thesis contains no publications, either published or submitted for publication
(if this box is checked, you may delete all the material on page 2)

☒ Some of the work described in this thesis has been published and it has been documented in the relevant Chapters with acknowledgement
(if this box is checked, you may delete all the material on page 2)

☐ This thesis has publications (either published or submitted for publication) incorporated into it in lieu of a chapter and the details are presented below

CANDIDATE'S DECLARATION

I declare that:

- I have complied with the UNSW Thesis Examination Procedure
- where I have used a publication in lieu of a Chapter, the listed publication(s) below meet(s) the requirements to be included in the thesis.

Candidate's Name	**Signature**	**Date (dd/mm/yy)**
Marjan Moradi		**17/01/2020**

Abstract

Millimeter wave networks promise to offer ultra-fast internet download speed, but the access points or base stations must always align the beams precisely to client devices. Efficient beam alignment for mobile users therefore is considered one of the most challenging problems facing millimeter wave networks. Existing approaches that use in-band beam alignment suffers from long alignment delays and low communication performance, especially when large number of mobile clients are connect to the access point. In this research, we explore the benefits of out-of-band inaudible sound assisted beam alignment to reduce the outage probability, thereby improving the performance gain of antenna in millimeter wave beamforming.

In particular, this thesis makes three fundamental contributions. First, we analytically study the beam alignment performance of 802.11ad in the presence of multiple devices while rotating with an applicable angular velocity. We come up with a probabilistic model for required number of beacon intervals to complete antenna training in multi-users scenario for 802.11ad. Second, we propose to take advantage of inaudible sound as a side channel to detect the direction of client and assist beam alignment in millimeter wave access points. Using a combination of experimental and simulation analysis of the inaudible sound spectrum available in typical mobile phones, we demonstrate that the use of 50 Hz and 50 ms sound chirps with an array of two microphones provide efficient and reliable detection of direction. Moreover, we design a filtering approach using FDM channel access to correctly assign the sound source corresponding to the estimated angle on the receiver side. Third, we conduct a comprehensive simulation in order to evaluate the performance of the proposed sound assisted beamforming on the gain of antenna. Initially, the

proposed analytical model is validated by the developed simulation platform. We show that our proposed algorithm achieves a significant 11 dB average gain of antenna for AP with 64 antenna sectors serving 10 users moving with walking speed of two different mobility model compared with IEEE 802.11 ad. This improvement is the result of using the proposed contention-free out-of-band sound channel to remove the existing contention-based channel access for beam alignment.

We believe that our findings in this thesis shed new light on the fundamental benefits of out-of-band beamforming in crowded millimeter wave network.

I dedicate this thesis to my son,

Barbod

who bore the burden on his little

shoulders, and to my beloved husband,

Javad

for his endless support.

Acknowledgements

This thoroughly enjoyable research is largely a result of the interaction that I have had with my supervisor Professor Mahbub Hassan who I feel very privileged to have worked with him. I owe a great debt of gratitude for his patience, support, inspiration, and friendship. I would like to thank him for his continuous efforts to show me the path to follow. I owe my gratitude to my primary co-supervisor, Dr. Kanchana Thilakarathna for his exceptional support, kind inspiration and his beautiful mind which enriched my growth as a student. I also express my genuine thanks to my co-supervisor, Dr. Ming Ding. He has always been available to provide the guidance, encouragement and the valuable feedback. I have been extremely lucky to have a very supportive co-supervisor as him. Sincere thanks to all my supervisory team members who tolerate my weakness and stayed in company with me to reach the peak of my PhD journey.

I cannot forget to acknowledge, with great pleasure, the financial support extended to me by University of New South Wales (UNSW) and Data61 (formerly known as National ICT Australia (NICTA)) during my PhD work. My gratitude is extended to my all my colleagues in Information Security and Privacy (ISP) Research Group in Data61, CSIRO. Finally, I would like to express my sincere gratitude to my parents for their love and support during the ups and downs of graduate school. I am grateful beyond words for all that they have given me.

Contents

List of Figures

List of Tables

Chapter 1

Introduction

The past few years have witnessed the global mobile data traffic growth with the estimated 63 percent in 2016. Overall mobile data traffic is expected to grow to 49 exabytes per month by 2021, a sevenfold increase over 2016 by Cisco forecast [1]. More than three-fourths of the world's mobile data traffic will be video by 2021 [2]. The demand for a high data rate and high integrity services will continue to grow in the foreseeable future. In this realm, Millimeter wave (mmWave) technologies promise to revolutionize wireless networks by enabling multi-gigabit data rates [3]. This trend conducts both research and industry to consider 60 GHz ISM band as a promising solution for data-rate demanding applications [4]. Demand for data-hungry applications such as uncompressed video streaming, instant file sync, wireless data centers and wireless fiber-to-home access, together with worldwide availability of the 60 GHz band, have fueled multiple standardizations, e.g., IEEE 802.11ad [5] and 802.15.3c [6]. Due to the smaller wavelength in millimetre wave (ranges from 1 to 10 mm), there is several dB more propagation loss as compared to the sub-6 GHz bands. To enable millimeter wave (mmWave) systems in practice and to guarantee sufficient received signal power (and data rate), large antenna arrays need to

be employed at both the transmitter and receiver [7]. The small wavelength (λ) in 60 GHz frequency permits multiple antenna solutions (with distance of $\lambda/2$ per antenna element). From this perspective, multiple antenna technology is a key enabler to efficiently utilize the millimeter wave band as it can increase the link capacity by employing directional communication. Millimeter wave radios, however, do not play well with mobile devices or dynamic environment, a key challenge that has been emphasized in the standards. The pseudo-optical nature of a beam renders it extremely sensitive to blockage, especially in indoor deployments with heavy human activity [8]. Searching for an alternative beam direction involves extensive overhead procedure at the presence of frequent movement. Thus, an overhead-free beam alignment is required for mobile millimetre wave communication.

With this introduction, the aim of this research is to improve beamforming performance in MmWave communication at the presence of mobility. In this study, we investigate the possibility of exploiting inaudible sound as a side channel to detect the direction of mobile devices and assist beam alignment in millimeter wave access points. Since all consumer devices, such as mobile phones, tablets, and laptops, include speakers, they can easily generate sound without requiring extra hardware. With falling costs and form factors of microphones and microphone arrays, sound-based DoA is practically realizable for next generation of access points. Finally, as there exists an inaudible bandwidth ($>$ 18 kHz) within the range of typical consumer speakers and microphones, it is possible to use sound for millimeter wave beam alignment without causing any sound noise in working environment. To the best of our knowledge, it is the first research to leverage microphone-speaker sensors embedded on the COTS devices for beam alignment in mmWave networks.

The remainder of this chapter is organised as follows. In Section 1.1, the

motivation for MmWave-based communication is examined in more detail. The research challenges of beamforming in MmWave networks addressed in this thesis are introduced in Section 1.2. Section 1.3 states the thesis contributions. Finally, the organisation of the dissertation is presented in Section 1.4.

1.1 Research Motivation

Millimeter wave (MmWave) networks are expected to offer multi-Gbps download speeds using 60 GHz frequencies. Millimeter Wave based communication standards including IEEE 802.11ad [5] supports up to 6.8 *Gbps* data rate enabling cordless virtual and augmented reality or ultra-high-definition video streaming. The following advantages and promising applications of MmWave communication have motivated us to design out-of-band beam alignment for next generation of mobile MmWave communication. Figure 1.1 illustrates just few of mmWave applications.

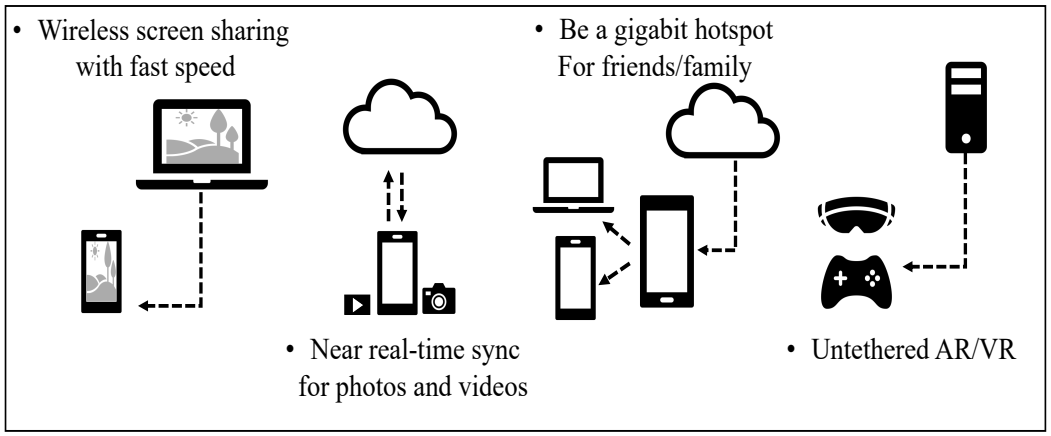

Fig. 1.1: Major mmWave applications

- Enabling the immersive service experiences
- Real-time interactive game

- UHD wireless video streaming
- Ubiquitous health care

This research study insights into the next generation of wireless communication considering the promising applications and opportunities brought by the Extremely High Frequency (EHF) communication interface.

1.2 Research Issues

Despite the immense potential of MmWave, its realization is challenging due to sever path loss, atmospheric absorption, and blockage. New MmWave networking standards, such as IEEE 802.11ad [5], mitigates these issues by employing multiple antenna sectors to establish a narrow directional communication beam between the access point and the client. MmWave beam performance, however, is highly susceptible to client mobility because a small displacement from the original location may misalign the selected sector pair of communication [9]. To keep beams aligned at all times, 802.11ad beam realignment process employs sector sweeping at both transmitter and receiver. The procedure, however imposes a high training overhead at the presence of clients' movement. This has led to the efforts of utilizing out-of-band information for beamforming and totally removing beamforming training overhead.

Despite the plethora of work in MmWave beamforming, a little has been done to investigate the impact of device population on beamforming. When there are multiple devices in the communication range of the 802.11ad WiFi access point which is often the case for office environment, each device is required to compete for one out of 8 dedicated time slots that occurs at every 100ms to perform beamforming. If a device fails to capture a slot in the current

beacon interval, it has to wait for another 100ms to retry beamforming. The higher the number of devices, the more severe the competition for securing a slot. Moreover, there is a limit of 16 frames per slot for the standard to exchange between transmitter-receiver pair. It means devices with up to 16 antenna sectors enable to complete antenna training within a slot, if they win it to access the channel. Devices with antenna sectors higher that 16, though, require wait for another 100 ms to catch more than 1 slot and finish antenna training. Thus, device population and more directional antenna lead to significant interruptions, especially in the case of beam misalignment due to device mobility. Nevertheless, to the best of our knowledge, this is the first study that thoroughly investigate the impact of device population on the performance of beam alignment in IEEE 802.11ad.

1.3 Research Contributions

This dissertation aims at proposing a novel beam alignment method to improve the performance of antenna training for mobile multi-users scenario in millimeter wave networks. The main contributions towards our objective are summarized in this section.

- We first reveal antenna training inefficiency of IEEE 802.11ad in a mobile multi-users network. We develop an analytical model for gain of Oracle-based model of directional antenna considering a practical mobility scenario of angular displacement for hand-held or body-worn devices. Moreover, an analytical model for the gain of antenna in IEEE 802.11ad is proposed followed by a probabilistic model for beamforming completion time in terms of required beacon intervals in the presence of multiple competing devices.

- We then propose a MmWave beam alignment framework, called Sound-Align, by exploiting inaudible sound as a side channel. In Sound-Align, mobile devices periodically generate short inaudible sound bursts or chirps, which are detected by a microphone array at the access point to work out the DoA. The DoA information is then used by the access point to select the right antenna sector for transmitting data to the mobile client.

- Using a combination of experimental and simulation analysis of the inaudible sound spectrum available in typical mobile phones, we demonstrate that sound chirps of only 50 ms can provide reliable detection of DoA, which provides low-latency beam alignment. We also show that Sound-Align chirps occupy only 50 Hz, which means that the limited inaudible bandwidth available for consumer devices can still accommodate up to 20 mobile users in the network.

- We further propose a filtering approach which is taking the advantages of FDM acoustic channel access to distinguish the corresponding channel of incident angles into microphone array. This approach leads the proposed beam alignment into a low computationally complex and low development cost using only two microphones to estimate DOA. Through extensive simulations for this scenario, we evaluate Sound-Align system performance for inaudible DoA estimation.

- Finally, We provide a comprehensive study to evaluate the performance of sound-assisted beam alignment method for MmWave directional communication. We examine the impact of different parameters on our proposed beam alignment algorithm. Various directional antenna configuration, different number of users in the network and different mobility

patterns are studied. The results prove the performance of the proposed beam alignment method compared with IEEE 802.11ad in a multi-users mobile scenario, specially for more crowded networks (10 users) and more directional antenna (64 antenna sectors).

1.4 Thesis Organisation

The rest of the thesis is organized as follows.

In Chapter 2, description of MmWave communication, its principals, challenges and applications are reviewed. We first review 60 GHz standard along with the most important procedures of IEEE 802.11ad amendment such as beamforming.

Afterwards, in Chapter 3, we categorize the related work on the area of MmWave beamforming into two main categories. Then, the existing research gap and related issues are addressed. Finally, considering the research gap and the explained research objective, we review the existing direction of arrival methods, particularly the acoustic based literature.

In Chapter 4, we analytically study the beam alignment performance of 802.11ad in the presence of multiple devices. In this chapter, we come up with a probabilistic model for required number of beacon intervals to complete antenna training in muti-users scenario for 802.11ad. We further consider a practical rotation movement for clients to investigate the deficiency of beamforming procedure proposed in the standard in a mobile applicable environment.

In Chapter 5, we propose an acoustic-based beam alignment assisting framework, called Sound-Align, to address the contention and latency problems associated with multiple-device connectivity. We initially perform a combination of experimental-simulation study to investigate the feasibility of direction of

arrival using inaudible sound emitted by the consumer electronic devices. We extensively evaluate the performance of inaudible sound DoA by employing the well-designed MUSIC algorithm. Simulation results and evaluations conduct us to design a direction of arrival method, called Sound-Align, using inaudible chirp signals to address DoA for multi-users scenario.

In Chapter 6, we extensively evaluate the antenna gain performance of the proposed Sound-Align method using simulation. The main challenge of IEEE 802.11ad beamforming in multi-users mobile scenario is addressed by the proposed method. We further evaluate the performance of Sound-Align for different antenna configurations, various number of users, and two different mobility models.

Finally, in Chapter 7, we conclude the dissertation and summarize the main future research directions.

Chapter 2

Background

This chapter gives an overview of millimeter wave communication and its promising applications. Moreover, path loss model for millimeter wave communication is discussed. Next, In Section 2.2, beamforming procedure of 802.11ad communication standard is reviewed and analyzed in the context of millimetre wave communication systems.

2.1 Millimeter Wave Communication

In this section we first introduce the capabilities and applications of MmWave communication. Next, we explain IEEE 802.11 ad amendment and its corresponding beamforming procedure, followed by Association Beamforming Training and Fast Session Transfer, as other MAC features of the protocol.

2.1.1 Principals, Capabilities, and Applications

In very broad terms, millimeter wave communication can be classified as occupying the electromagnetic spectrum that spans between 30 and 300 GHz, which corresponds to wavelengths from 10 to 1 mm. The extremely high fre-

quencies of millimeter waves offering maximum 6.7 Gbps achievable data rate [10] to make mmWave useful for a variety of applications. It is highly secure operation resulting from short transmission distances due to absorption loss and no wall penetration [11]. The newest standard IEEE 802.11ad [5] for 60 GHz industrial, scientific, and medical (ISM) band available in most of the countries and the related industry alliance named WiGig show that millimeter wave technology is really worth for multi-gigabit wireless communication.

However, the propagation characteristics of mmWave spectrum in free-space, which is frequency and distance related as with all propagation electromagnetic waves, impose higher path loss than other different unlicensed bands [12] (extra 22 dB loss at distance of 10 m compared to 5 GHz calculated by Friis equation [13]).

Although the high path loss at 60 GHz seems to be a disadvantage, directional communication can be a promising solution to compensate the extra loss. Based on this behavior, IEEE 802.11ad introduces a novel concept of "virtual" antenna sectors that discretize the antenna azimuth. In this case, the short wave length in the millimeter range allows significantly smaller antenna form factors compared to legacy WiFi at 2.4/5 GHz (approximately 140 times smaller [4]) and can be conveniently integrated into consumer electronic products. Moreover, the sector antenna concept is technically supported by introducing a beamforming procedure in the standard and providing directional communication. It seems beamforming is the key to unlock the potential of MmWave communication to provide multi Gbps data rate for next generation of wireless communication. In the following section, we discuss beamforming mechanism, in details.

2.1.2 Millimtre Wave Propagation Characteristics

As with all propagating electromagnetic waves, for millimeter waves in free space the power falls off as the square of the range. When the range is doubled, the power reaching a receiver antenna is reduced by a factor of four. This effect is due to the spherical spreading of the radio waves as they propagate. The frequency and distance dependence of the loss between two isotropic antennas can be expressed in absolute numbers by the following equation (in dB):

$$L_{free\ space} = 20 \log_{10}^{(\frac{2\pi R}{\lambda})} \tag{2.1}$$

where $L_{free\ space}$ is the free-space loss, R is the distance between the transmitting and receiving antennas, and λ is the operating wavelength. This equation describes line-of-sight (LOS) wave propagation in free space. It shows that the free space loss increases when the frequency or range increases. Also, that millimeter wave free space loss can be quite high even for short distances. It suggests that the millimeter-wave spectrum is best used for short-distance communication links. When the distance of the link $R = 10m$, path loss can be calculated using $(\frac{4\pi R}{\lambda})^2$.

Due to smaller wavelengths at millimetre wave frequencies, the free space propagation loss, which is inversely proportional to the wavelength, is several dB more as compared to the legacy sub-6 GHz bands. This aspect, however, needs to be interpreted in view of the additional directional antenna gains at the transmitter and receiver envisaged in millimetre wave systems. For the same antenna aperture size, the directional antenna gain is more considerably more as compared to an omnidirectional or sectored pattern antenna used in sub-6 GHz systems. Thus, the excess free space propagation loss in millimeter

wave communications can be compensated using directional antennas with beamforming [8]. Additionally, attenuation due to rainfall has an adverse impact on millimeter wave signal propagation depending on the rainfall rate [3]. Also, absorption due to atmospheric gases at certain frequencies including 60 GHz can lead to considerable attenuation if transmission distances exceed an order of few tens of metres. Therefore, the 60 GHz band is well suited for indoor short range millimeter wave communication for a maximum Tx-Rx separation distance of about 10m, whereas the 28 GHz, 38 GHz and 73 GHz bands are being investigated for their potential to support outdoor millimeter wave communication for medium range links of over 200m.

2.2 IEEE 802.11ad Standard

In this section, we focus on IEEE 802.11ad standard and provide introductory materials of beamforming procedure in the amendment. Moreover, we briefly summarize fast session transfer mechanism in the standard which has recently applied by some literature in the context of NLOS beamforming.

2.2.1 Sector Level Sweep

Beamforming (BF) training or beam alignment is a mechanism to train transmit antenna of both sides and achieve the necessary link budget [14]. IEEE 802.11ad amendment supports beamforming which is comprised by one mandatory phase, namely SLS, and 2 optionals, BRP and Beam Tracking. In this section, we briefly review SLS phase.

BF training is launched by transmitting a series of sector sweep frames (SSW) from initiator. The responder reports the best transmit antenna of initiator and the frame exchange process repeats for peer station till both

pairs find their best transmit sector. During this phase, the receiver transmits sector sweep frames for the $N_T^{(s)} \times N_R$ times, specified by a countdown parameter. Subsequently, the transmitter transmits sector sweep frames for $N_R^{(s)} \times N_T$ times. Thus, the total number of preamble transmissions in above beam switching is given by:

$$N_{SLS} = N_T^{(s)} N_R + N_R^{(s)} N_T \tag{2.2}$$

SLS comprises of 4 different steps to complete antenna sector training: Initiator Sector Sweep (ISS), Responder Sector Sweep (RSS), Sector Sweep Feedback (SSW-FB), and Sector Sweep ACK (SSW-ACK). In ISS, the initiator transmits SSW frames over all its antenna sectors. The responder should stay on omni-directional pattern for a specific time. In RSS, the responder transmit antenna is trained to find out the sector providing highest signal quality. The feedback for the responder is transmitted with a single SSW Feedback frame, on the determined optimum antenna configuration. Finally, the SSW Feedback frame is acknowledged with an SSW-ACK by the responder. Accordingly, The total time required for antenna training can be calculated as:

$$T_{SLS} = N_T^{(s)}.T_{TX-SSW} + S.(N_R^{(s)}.T_{RX-SSW} + T_{SSW-FB/ACK}) + T_{IFS} \tag{2.3}$$

where

$$T_{IFS} = (S+1)(N_T^{(s)} - 1).T_{SBIFS} + 3.T_{MBIFS} \tag{2.4}$$

where S shows the number of stations in the network for training and T_{IFS} denotes inter-frame space time which is defined by Eq.(2.4). T_{SBIFS} and T_{MBIFS} indicate short and medium beamforming inter-frame space and equals with $1\mu s$ and $3\mu s$, respectively.

Figure 2.1 illustrates the explained steps, schematically.

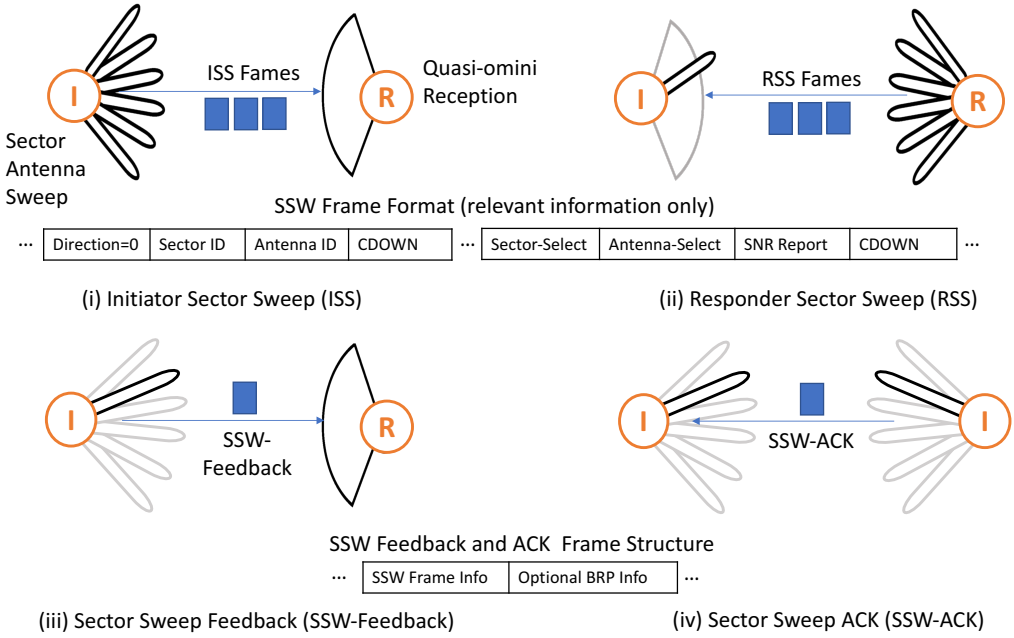

Fig. 2.1: SLS phase, 802.11ad Beamforming

2.2.2 Association Beamforming Training

The described general beamforming concept in section 2.2.1 integrates into IEEE 802.11ad medium access scheme and the association process. This section explains the association beamforming training, A-BFT, in details.

Channel access by a DMG station occurs during beacon intervals. Beacon interval is divided into different subdivisions called access period, namely BTI, A-BFT, ATI, and DTI. Beamforming in 802.11ad is performed within BTI and A-BFT. In BTI, ISS frames are transmitted by the AP to train its transmit antenna. The frame can be detectable by the devices in the network. During A-BFT, beam alignment performs for the devices which could detect the beacon frames within BTI period. A-BFT access period is slotted up to 8, each of which is a multiple of sector sweep with the maximum value of 16 SSW. This

access period implements a contention-based method to allow multiple devices get the chance of beam alignment. At the start of A-BFT access period, the devices invoke a random back off procedure to initiate antenna training. It is a collision avoidance model in which none of the devices picking the same slot could be trained. Hence, increasing number of devices will decrease the chance of channel access. Moreover, A device might be unable to complete its antenna training because its sectors exceed the number of SSW frames per slot. Thus, it requires to resume training during following BI, if could get the chance of channel access. Beam alignment architecture within beacon interval is illustrated in Figure 2.2.

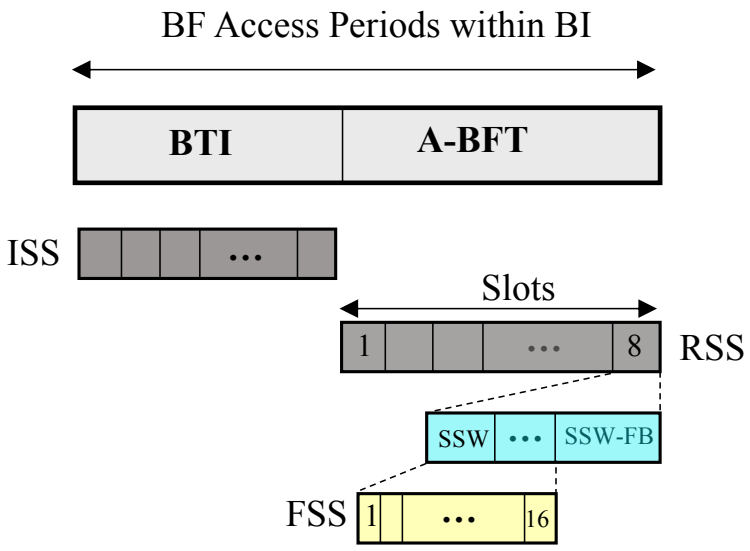

Fig. 2.2: 802.11ad beacon interval scheme

2.2.3 Fast Session Transfer

IEEE 802.11ad supports MAC features including Fast Session Transfer (FST), for directionally-communicate stations. FST provides the possibility of transferring the session in a multi-band device from a channel to another, in the

same or different frequency band. A multi-band capable device can manage operation over more than one frequency band/channel. The operation across the different frequency bands/channels can be simultaneous or nonsimultaneous [5]. FST, which is known as interface switching capability, supports traffic migration in between 802.11a/b/g/n/ac and ad [15]. With the recent acquisition of Wilocity by Qualcomm, the chip vendors trending towards multi-band chipsets (2.4/5/60 GHz) could be observed [16].

Besides, FST and interface switching impose an overhead in terms of the time elapsed between FST trigger and completely migrate into the different band/channel. The overhead has experimentally measured about 180 ms in [17] to the off-the-shelf Tri-band devices. Consequently, TCP performs poorly which causes to more than 500 ms end-to-end latency which is high for latency sensitive applications.

2.3 Summary

This chapter provided an overview of millimetre wave background and its propagation characteristics. As this research focus is on beamforming, this chapter contained introductory information on IEEE standards in the context of beamforming procedure.

Chapter 3

Literature Review

3.1 Introduction

Communication at millimeter Wave (mmWave) operating frequencies represents the most recent game-changing development for wireless systems [7]. Interest in mmWave is in its infancy and will be driven by consumers who continue to desire higher data rates for the consumption of media while demanding lower delays and constant connectivity on wireless devices [12]. The rapid growth of bandwidth demanding application in one hand [18], and the traffic trend foreseen by 2021 [2] on the other hand, will foresee mmWave plays a leading role of wireless communication in near future. Hence, In this section, we introduce the basic characteristics of millimeter wave communication and its areas of application.

This study is related to beamforming in Millimetre Wave (MmWave) mobile networks. therefore, in this chapter, we focus on different methods proposed for beamforming. We then focus on the studies concerned with beamforming in mobile environment in Section 3.2. The beamforming categorisation is presented in Section 3.3 and 3.4 for In-band and Out-of-band beamforming,

respectively. A brief overview of the issues related to beamforming is presented in Section 3.5. In Section 3.6 we concontrate on the concept of direction of arrival using antenna array and fundamental existing classes of direction finding is discussed. This section links the current out-of-band beamforming methods with the proposed beamforming method in this dissertation, i.e., Sound-Align beamforming in MmWave comminication. Finally, a summary of inaudible sound DoA methods is presented in Section 3.7.

3.2 Beamforming Taxonomy

Beamforming is essentially a spatial filtering operation typically using an array of radiators to capture or radiate energy in a specific direction over its aperture [10]. Considering baseband beamforming architecture, there is three different beamforming categorisation: *Analoge, Digital* and *Hybrid beamforming* [19]. Digital beamforming (DBF) has exploited by multiple-input multiple-output (MIMO) [20, 21, 22], where each antenna element is equipped with an RF-chain. This architecture is impractical at mmwave frequencies for LAN and IoT devices because of cost, size, and power consumption constraints [23]. In Hybrid beamforming (HBF) architectures [24, 25, 26] and [27], the precoding/combining operations are divided between the analog and digital domains, while using much fewer RF chains than antenna elements. The availability of multiple RF chains enables parallel, multi-stream processing and simultaneous multi-direction scanning. However, the antenna form factor for HBF is not match with the smart and wearable devices, such as smart phones. Thus, analog beamforming (ABF) represent the only feasible solutions [28, 29]. With this point of view, we address the research concentrating on ABF to be applicable on MmWave smart devices and LAN.

Establishing a directional narrow beamwidth in 60 GHz frequency band is a high overhead procedure at the presence of device rotation or movement [30, 31]. The number of sender-receiver sector pairs that needs to be matched multiplied by the number directional links to be trained in a network defines the amount of beam training overhead in a directional network [8, 10]. Mobility leads to frequent invocations of time-consuming and high-overhead mechanism for beam re-alignment, which deteriorate MmWave system performance. Thus, in this dissertation, beam search proposals in the literature can be divided based on the beamforming interfaces they are using into two main categories: (1) **In-band Beamforming** (explained in Section 3.3) and (2) **Out-of-band Beamforming** (addressed by Section 3.4).

3.3 In-band Beamforming

Using millimeter wave frequency signals for antenna search space and direction finding is known as In-band beamforming method. Angle-of-Arrival (AoA) estimation, as a potential technique for beamforming, is a challinging problem for analoge millimetre wave antenna arrays. For analog arrays, existing estimation schemes are mostly based on beam scanning and is time-consuming [32]. Recently, a research in [33] presented a virtual-subarray based recursive AoA estimation scheme for analog antenna arrays. While the method provides a fast AoA estimation for N antenna array, it increases the computational complexity by $O((2N)^3)$ due to its iterative procedure for BF updating.

The methods are generally categorised based on three challenges to be addressed: beamforming overhead, blockage, and multiuser beamforming. In this section, we briefly address the research proposed for In-band beamforming.

3.3.1 Beamforming Overhead

The majority of the literature aim to reduce beamforming overhead imposed by mobility such as [20, 34]. In this realm, one of the early research has been proposed in [35] by formulating the beam switching problem as a general optimization problem. The proposed method enables to significantly reduce the searching complexity compared with 802.11ad. The method, however, requires to form a predefined code-book and measure SINR value while dynamically adjusting the beam steering vector.

In order to reduce beamforming delay, Agil-Link has proposed in [36] to find the correct beam alignment without sequentially scanning the space. Instead, Agile-Link's design relies on a combination of smart hashes and voting. The method significantly reduces the latency compared with 11.ad and exhustive beamforming. However, the authors did not investigate the impact of multiple users on the delay performance.

3.3.2 Link Blockage

The next challenge for link degradation in MmWave communication is blockage. For outdoor millimeter wave communications, authors in [37] analyzed the effect of blockages due to building structures for urban cellular networks. For indoor environment, the method called MIDC, proposed in [29], focused on backup link and how to reserve it in blockage condition. MIDC also relied on codebook-based method and required to prepare an angle profile to find out best beam direction. The method capables to precisely detect the best link but at the expense of longer beamforming duration.

The challenge of link blockage in MmWave has studied in [38], for a user wearing VR while it has movement. The main objective was to design a beam-

forming system to cut the cords from VR headsets. To address this problem, the authors have proposed MoVR, a configurable mmWave reflector system. To find out the correct incident angle, MoVR applied a traditional beam-searching between AP and reflector to estimate the direction with maximum SNR. This step performed once, only at the installation time. The results confirmed the performance of the method at the blockage condition. However, the system scale-ability is small, just for a single user.

Signal blockage at the frequency of MmWave has recently studied widely in the realm of wearable networks in [39, 40, 41, 42]. The authors considered the problem of body blockages and reflections from surrounding objects and addressed the issue with stochastic geometry.

3.3.3 Multiuser concurrent beamforming

Existing indoor milliemter wave communication standards [43] [5] schedule a single transmission per time slot. However, the problem of mutual interference generated due to the concurrent links in short coverage area needs to be addressed. The authors in [44] propose a first-come-first-serve link scheduling strategy using beamforming information for SINR calculation.

The study proposed in [45], has consider the problem of dense MmWave network. Initially, the limited number of A-BFT slots has extended by the proposed SA-BFT method to alleviate high collision probability and low BF training efficiency. Simulation results, however, shown a small improvement on the number of successful stations to perform beam training compared with 802.11 ad. In the best case, less that 50% of the stations capable for beamforming training. Note that both explained methods carried out for HBD.

TakeAway: Using In-band training methods in the case of ABF (use

of a single RF chain) required further investigation and research in terms of network scale-ability, delay and beamforming overhead. Therefore, in the following section, we discuss the proposed Out-of-band methods for ABF in a mobile MmWave network.

3.4 Out-of-band Beamforming

As explained in previous section, configuring the antenna arrays is the main source of overhead in mmWave communication systems. In high mobility scenarios, the problem is exacerbated, as achieving the highest rates requires frequent link reconfiguration. Exploiting information coming from either sensors or other communication interfaces operating at sub-6 GHz frequency, known as **Out-of-band** beamforming [46], is a promising solution for mmWave link establishment. With this introduction, we initiate the section with the proof of concept to show the feasibility of out-of-band beamforming.

3.4.1 Proof of Concept

It is foreseen that out-of-band information will be the key to unlock the potential of mmWave communications in high-mobility scenarios [46]. In this section, we insight into the possibility of using out-of-band beamforming and proof of concept in the realm of mmWave communication band.

- Preliminary works have been considered the concept of exploiting information from one band to aid communication in another band, such as multi-radio collaboration with lower frequency in cellular communication and traffic management [47].

- MmWave infrastructures and routers/access points will likely be de-

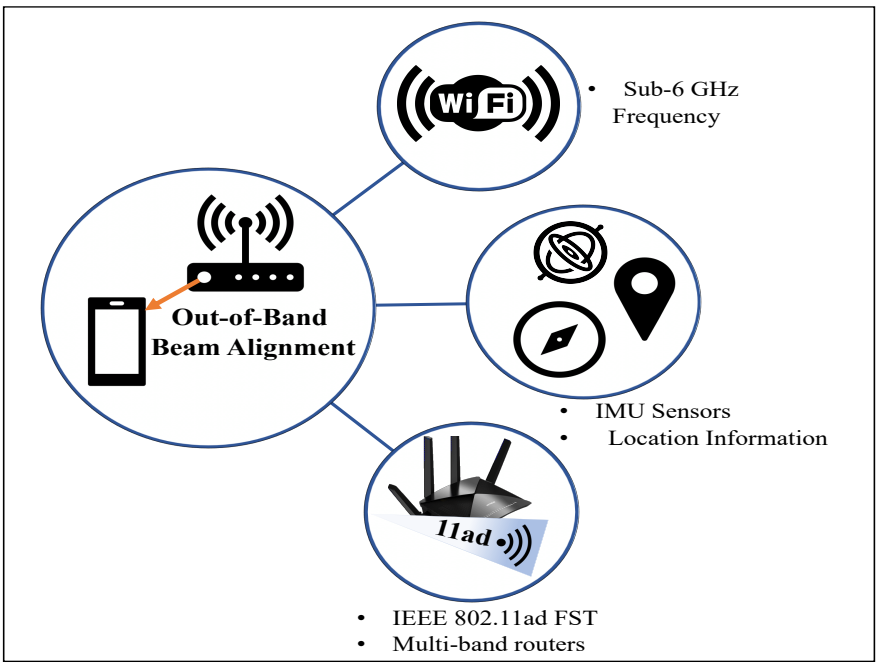

Fig. 3.1: Out-of-band beamforming entities in MmWave communication

ployed in conjunction with sub-6-GHz systems. COTS devices working with three bands such as [48] confirms the technical possibility of multi-band collaboration.

- Fast Session Transfer feature Supported by MAC layer in IEEE 802.11ad standard provides the possibility of interface switching. FST has discussed in section 2.2.3.

- Sensors are integrated everywhere and every time, or they can be easily installed in an mmWave base station or AP if required. These sensors enable to provide out-of-band hints for link establishment and/or communication.

Accordingly, we depicts the out-of-band concept and its essential modules exploited in mmWave beam alignment by Figure 3.1.

As obvious from the figure, there is two main sources of data fusion for

out-of-band beamforming:

i Radio frequency signal such as lower-frequency and sub-6 GHz wifi signals

ii Sensor fusion data such as information collected from IMUs and GPS

Accordingly, the existing out-of-band literature is classified into *RF-based* and *Sensor-based* methods. The following sections explain both categories, inclusively. Figure 3.2 illustrates the taxonomy of existing out of band literature. The methods are discussed by the following sections.

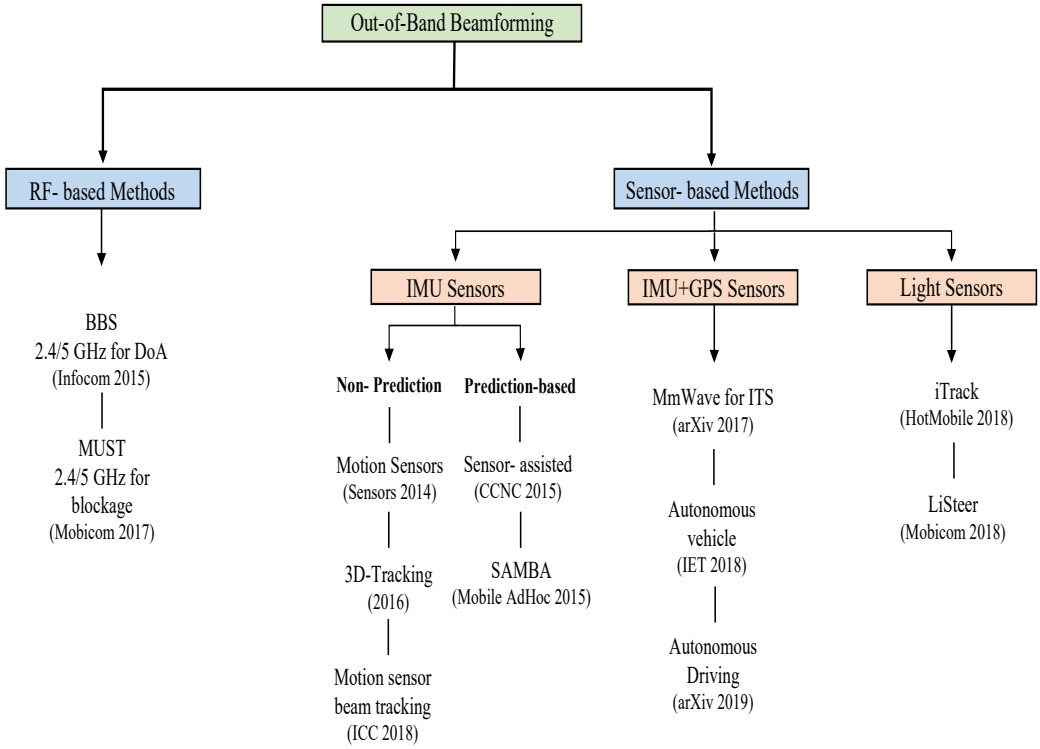

Fig. 3.2: Taxonomy of Mobile MmWave BeamForming Methods

3.4.2 RF-Based methods

Initially, a research has been done in [15] to remove SLS phase and in-band overhead for establishing directional MmWave communication using out of band beam searching. The designed system, Blind Beam Steering (BBS),

combined IEEE 802.11ad (MmWave) and IEEE 802.11ac/n interfaces with N-antenna omni directional array. Further, BBS has relied on the received signal strength information which has passively overheard at lower frequencies (2.4/5 GHz, named as detection band) with respect to the azimuthal incidence angel. RSS information have gathered in a profile named as angular profile. Within the angular profile, the strongest incidence angle has been assumed to match the direct path. Next, the estimated angle of the path must translate into mmWave band (named as application band) sector which matches the direct path and provides the highest signal quality. BBS has used MUSIC algorithm [49] for angle estimation in detection band. The performance of BBS has evaluated in terms of the accuracy of estimated degree and mapping to the correct sector in MmWave band. Results has shown the angle estimation error for 7° sector width in BBS achieved around 4° while at least 5 detection band antenna has required.

Recent research has been done in [17] to design MUlti-band Session Transfer (MUST). The study proposed a low latency interface switching when 60 GHz link establishment is not feasible due to blockage. While BBS has assumed LOS condition, MUST considered NLOS and has addressed beam misalignment at the presence of blockage. MUST switches to wifi once LOS blockage is identified by a probabilistic blockage model. Moreover, MUST tracks the angular shift of dominant path in 60 GHz band using successive time-domain snapshots of WiFi channel. For blockage detection, MUST has relied on the experimental finding which shown distinct SNR difference between 60 GHz and WiFi. The difference raising beyond a threshold (empirically put 3 dB) has provided the hint of blockage. Once blockage occurred, MUST triggers to collect the out-of-band WiFi channel information. It sends probe packets to the user from the WiFi interface and measures the channel response of the

received ACK. Then, the session has transferred to WiFi interface while reducing end-to-end latency from 4.35 s (for IEEE 802.11ad) to 232 ms (for MUST algorithm). In order to identify LOS blockage, MUST tracks the difference of the SNR of 60 GHz best beam and WiFi best path for a small interval Δt. In NLOS, SNR difference between 60 GHz and wifi shows higher variation. The algorithm has been implemented on the commodity 60 GHz devices (dual band Dell laptop as user side and 60 GHz modem as AP). Experiments from off the shelf 60 GHz shown that 802.11ad interface transfer has an average 4.17s switching latency, but MUST improved it significantly to 232 ms.

A summary of studies and detail performance of RF-based methods are provided in Table 3.1.

Table 3.1: RF based beamforming in out-of-band methods

Algorithm	**BBS** [15]	**MUST** [17]
Objective	• Removing in-band overhead	• Reducing FST switching latency
Antenna Setting	• Detection band: 5 omni-directional antenna • Application band: $7°, 20°, 80°$ beam-width horn antenna	• 32 for 60 GHz (Phased-array 4×8) • 3 antennas for wifi interface
Performance Evaluation	• Improve 11.ad training overhead up to 81% • Achieve 97% direction estimation accuracy	• TCP end-to-end latency from 4.35 s to 232 ms
Overhead	• Low performance for highly directional antenna (81% overhead and 4° DoA error for 7° beamwidth)	• Blockage detection and fast switching, only. (NLOS condition)

Takeaway: Although utilising RF is practicaly applicable for out-of-band beamforming, it has the following overhead:

- Radio frequency signals suffer from multipath propagation effect. Moreover, BBS method causes interference in frequency of signal, since it

utilises a single frequency,e.g., 5 GHz.

- Wifi and sub-6 GHz frequency is a crowded band.
- Delay caused by session transfer procedure in RF-based out-of-band beamforming (e.g., 232 *ms* in [17]) is not tolerable for delay-sensitive applications of mmWave such as online video streaming.

With this conclusion, we introduce *sensor-based* out-of-band beamforming in the following section.

3.4.3 Sensor-Based methods

Out of band beam alignment category is recently observed sensor-fusion or sensor-based trend. The combination of multiple streams of sensor data for a more accurate result is called sensor fusion [50]. The main objective is minimising the beam-tracking/training overhead of RF-based beamforming by recognising the causes of beam misalignment and recovering them, timely. Initially, sensor-based algorithms require to identify the source of link impairment. The established link is degraded due to blockage, rotation and displacement [9]. The sources of mis-alignment are schematically illustrated in Figure 3.3. Table 3.2 summarises these link impairment reasons and its corresponding recovery actions. Following, we discuss the existing sensor-based methods which are categorised based on the sensor type using for beam alignment.

3.4.3.1 IMU Sensors

Most of the existing proposed sensor-based beamforming methods have employed the data provided by IMUs such as accelerometer, gyroscope, and magnetometer. Accordingly, authors in [52] have proposed a method to apply

Table 3.2: Sources of Link Impairment in Beamforming Methods

Source	Description	Detection	Recovery
Rotation	• circular motion, for moving device in a circular fashion	• RSS drops beyond a threshold ($Th_{rotation}$)	• Mobile client requires to adjust its beam selection
Displacement	• linear motion for moving along a line at constant speed	• RSS drops beyond a threshold (Th_{disp})	• Both Mobile client and stationary AP must adjust beam selections
Blockage	• Transmission signal may block by objects due to users' activity	• Link breakage (Th_{block})	• Switching to a secondary path (using reflector [51])

sensor-fusion data and recognise/realign the beam misalignment. First, SLS phase is performed using RF signal and its received power. Once the power drops lower than a threshold, IMU values are obtained to track the beam, recognise the causes of error, and align the beam, accordingly. The motion sensors such as accelerometers, gyroscopes, and geo-magnetic sensor are composed of an attitude heading reference system (AHRS) and a zero-velocity detector (ZVD). The AHRS estimates the rotation angle and the ZVD detects whether the device moves.

The study has evaluated the performance of the tracking algorithm in three different scenarios: rotation (clockwise and counterclockwise), displacement, and blockage. The received signal power has measured, every 1 ms to detect misalignment. Once the power drops below a threshold value, named error handling (Th_{eh}), the possibility for rotation has examined and angle variation has measured using motion sensors. If the angle rotated more than 5°, (rotation threshold), then the client beam has realigned. In the rotation scenario,

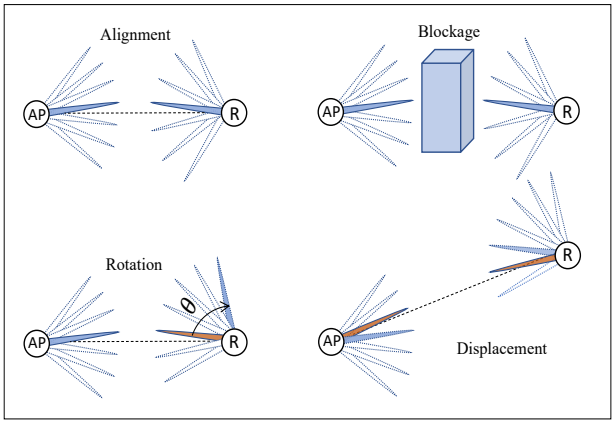

Fig. 3.3: Different sources of errors in beam-misalignment

the mobile client has been considered with the angular velocity of $800°/s$.The obtained AoA/AoD accuracy has reported as $1.5° - 2°$. If there were no rotation, it would be examined whether the client was displaced using ZVD sensor. Then, the link has been repaired by sector selection on both client and AP. In the case of blockage, both peers switched into a provided secondary path once the received signal power dropped below a threshold, (Th_{block}). The main performance metric was the number of switching for beam tracking in three different scenarios compared with the periodic non-sensor based beamforming methods. Results shown efficient number of switching for rotation and blockage, while there were no improvement in the number of switching for displacement. Though, the performance of the tracking algorithm were not evaluated at the presence of more realistic and faster angular rotation (e.g., $36°/100\ ms$ for web browsing action).

The primary study proposed by [52] has been extended by the research presented in [53] to consider three dimensional mobile user location tracking. The algorithm applied DoA and TOA combined with Extended Kalman Filtering (EKF) to estimate and track 3D location of user. The main drawback is high overhead caused by the periodic tracking update of mobile user.

Recently, a sensor-based beam alignment study has been presented in [50]. The method represent mathematical formulation of mobile user rotation angle in Quaternion coordinate system and attempt to adjust the misalignment degree. Accordingly, the mobile device requires to track attitude deviations instead of the absolute attitude and position in the global space. Thus, the method provide sensor feedback less frequently than other sensor-based methods. The coordinate system gives the chance of calculating optimum direction in local system corresponding to the base station in global coordinate system. Though, it still requires to observe SNR value, continuously for beam re-alignment. The authors also considered the angle deviation threshold to trigger beam re-alignment decision making. The results show the overhead reduction up to 0.7%. The explained sensor-based methods are summarised in Table 3.6.

Takeaway: The discussed literature considered the identification of sources of error to reduce beam searching overhead. The main objective has introduces as beam switching reduction. As a result, within the out-of-band beamforming class, sensor-based methods have the potential to provide higher data rate than RF-based methods in the case of rotation/displacement. This achievement is a consequence of detecting the source of beam misalignment before link outage problem and impair the link, in early stage.

So far, we explained sensor-based methods which are utilising IMUs to distinguish the sources of error and re-align the beam, accordingly. Following, we introduce IMU-based schemes which not only identify the sources of error, but also predict the next beam pair to avoid mis-alignment and provide seamless beamforming. They are categorised as prediction-based methods.

An algorithm presented in [54], has predicted the next beam pair to switch into, before the link quality drops. Indeed, an activity recognition algorithm,

Table 3.3: Non-prediction-based out-of-band beamforming using IMUs

Algorithm	**Motion sensors** [52]	**Motion-sensors Aided**[53]	**Misalignment Compensation** [50]
Objective	• Tracking the beam to reduce number of beam switching	• Mitigate beam forming overhead	• Sensor-based beam tracking to mitigate beam forming overhead • Less refinement overhead (less frequent sensors' feedback)
Sensor Type	• IMU	• IMU	• IMU
Mobility	✓ (Rotation speed : $800°/s$)	✓ Walking speed	✓ Walking speed
Antenna Setting	• 16 ULA in Base station • UCA in Mobile user	• 32 for 60 GHz (Phased-array 4×8) • 3 antennas for wifi interface	• ULA
Performance Evaluation	• Tx/Rx beam switching reduction to 10.4/1.4% during $4s$ interval and power/rotation threshold $-2dB/5.6°$		• Experimentally evaluate angle deviation • Beam searching and tracking overhead reduction up to 0.7%
Overhead	• RSS measurement every $1ms$ • Feedback from sensors for error detection/handling	• Interfering with moving objects and high-frequency noises	• Providing sensors feedback, frequently

namely k-NN was used to identify displacement, rotation, or blockage error. Different activities including standing still, turning, moving straight, and turning/moving were recognised by collecting samples from accelerometer and gyroscope within various window time. Once the activity was recognised, the prediction of the next beam sector was possible. Moreover, activity recognition could help to distinguish the source of error based on the sensor samples and the current identified activity. Though, the study could successfully reduce the number of beam realignments, the major drawback is its required time for activity recognition. In fact, rapid angular movement of users forces a very quick beam realignment, at the order of few 10 ms. On the other hand, the collected samples from IMUs (e.g., accelerometer with 100 Hz sampling rate) during this short window time provides less accurate activity recognition.

For example, during 100 ms window time, accelerometer provides 10 samples, causes to obtain activity recognition around 80% accuracy.

Another research proposed a method named SAMBA in [55] to predict the mobile device's next location given its sensor observation. The authors also came up with a novel codebook-based beamforming to proactively switch the beam into the predicted one, across the multi-level codebook. Indeed, the proposed design is a DFT-based codebook generating complex numbers as the weight vectors corresponding to the possible beam patterns. Once the codebook is generated by AP, beam adaptation is just limited to the task of changing the wight vector. The prediction step is required the distance measurement between AP and client using round trip time. SAMBA has dependency to the SNR value threshold for deciding about disconnection and initiates beam searching through the generated codebook. Then, the client continuously monitor sensor data and provide feedback to AP. The main considered metric is the percentages of connected time which has been improved by 80%. The explained prediction-based beamforming methods are summarised in Table 3.4

3.4.3.2 Out-of-band Beamforming using Light Sensors

Apart from the explained IMU-based out of band methods, a recent research presented in [56], named iTrack, to track the LED indicator of AP using light sensors. The main aim of the research was beam alignment maintenance without any training overhead. To address this objective, the angle of arrival of the light indicator in mobile devices has required to be estimated, continuously. The proposed system placed at least 6 light sensors on the six faces of a mobile device. In order to estimate AOA, the authors has presented a visible-light channel model which measured the received intensity of light corresponding

Table 3.4: Prediction-based out-of-band beamforming using IMUs

Algorithm	**Activity Recognition** [54]	**SAMBA** [55]
Objective	• Reduce the number of beam search (MAC overhead) and re-beamforming using sensor data for movement prediction	• In-advanced beam switching to maintain uninterrupted connection in mobile environment
Sensor Type	• IMU	• IMU
Mobility	✓ Walking speed	✓ Walking speed
Antenna Setting	25×25 Rectangular Array	• 2×8, 4×8 and 4×16 ULA
Performance Evaluation	• Achieve 80% success activity recognition within 100 ms time slot • Obtain 0.5% re-beamforming with power threshold $-4dB$ •Reduce re-beamforming overhead up to 12 times	• Improving connection time up to 80% using prediction method • Using a threshold (SNR_{ST}) to reduce overhead of constantly providing sensor feedback
Overhead	• Long delay for accurate error detection and beam prediction by activity recognition	• Delay caused by multi-level cood-book generation

to the incident angle. Then, both azimuth and elevation components of the arrival light beam has estimated from the measured light intensity by the six light sensors with known angular seperation. Indeed, the ratio of intensities at any two adjacent sensors has measured as a function of their AOA, only. The proposed AOA measurement has provided up to 4.5° accuracy. In the next step, the system utilised the estimated angle for sector selection in client side. Consequently, there is around 50% of times the correct client-side sector selection based on the estimated AOA, as the horn antenna with 7° beamwidth was using for experimental evaluation. Since iTrack communication is performed in MmWave band with directional antenna, incorrect sector selection causes

SNR degradation. Table 3.5 summarises the main attributes of iTrack.

Algorithm	**iTrack**[56]
Objective	• Passively acquire direction estimation to maintain beam alignment
Mobility	✓ rotation
Antenna	• 7° beam-width horn antenna
Performance Evaluation	• 50% Client-side sector selection success
Overhead	• Light sensor array installation on user's device • Distinguish ambient light from AP LED light • Frequently light intensity measurement (every 1° rotation)

Table 3.5: Light sensor

3.4.3.3 Out-of-band beamforming using Location information

Intelligent Transport Systems (ITSs) and Connected Autonomous Vehicles (CAVs) are another promising applications of MmWave communication while enables to satisfy the required multi-gigabit-per second data transmission. There is some research to develop beamforming for mobile millimeterwave vehicle-to-vehicle (V2V)/vehicle-to-infrastructure (V2I) communication. Sensor-based beam-alignment has also been introduced for MmWave-based autonomous vehicles. In this realm, the research presented in [57] introduced vehicle-to-infrastructure (V2I) MmWave communication. In this research, Road Side Unit (RSU) mounted on lighting poles has considered for communication with the vehicles. The only one single position and speed feedback of the vehicle has provided once it enters RSU covering region. Then, the trajectory of the vehicle has predicted by RSU and the beam is switched into the new one at the predicted time of arrival of the vehicle in the new beam. The main chal-

lenge is the speed estimation error which caused to outage and low rate. This challenge has addressed with designing beams with overlapping region. The switching timing could be scheduled when the vehicle arrived at the middle of the overlapping area to maximise the average rate. The main limitation of the proposed research is the constant speed assumption for vehicle.

The research has been presented in [58], using data fusion of inertial sensors and GPS, broadcast from connected vehicles to improve the efficiency. The vehicle transmits the velocity, motion data and the position information every 100 ms to its closest RSU. The motion changes of vehicle has measured by IMUs. The output is the angular velocity of vehicle (in rad/s) which has provided for RSUs. Thus, RSUs enable to predict the vehicle position relying on the updating feedbacks and the geometry. The major concern is the position estimation error which is caused for misalignment. Hence, the performance of the proposed method has been evaluated with different speed error, from 1 m to 3 m.

While the previously explained methods considered V2I MmWave communication, authors of [59] presented a technique for V2V beam alignment. The study has proposed an inertial sensor-based beam tracking system in which the antenna array is equipped with the inertial sensors. The aim was tracking the beam for the vehicles' stroke. To achieve this objective, surrounding vehicles has transmitted the prediction information of their movement for adjusting beam direction. In the proposed method, each antenna sector is equipped with accelerometer to provide the information of antenna dynamics. At the beginning of each beacon interval, the prediction information of other vehicles were provided to avoid extra signalling for beam alignment. The main challenge is to perfectly estimate the distance between 2 communicative vehicles with a constant 5 m distance. In very narrow beam-width configuration, e.g.,

0.2°, throughput dropped significantly with 30 *cm* distance measurement error.

Table 3.6: Out-of-Band MmWave Beamforming for Intelligent Transport Systems

Algorithm	**Beam Design** [57]	**SAMBA** [58]	**Autonomous Driving** [59]
Objective	• Beam-design optimisation to maximise data rate	• Beam-width adaptation to achieve maximum data rate	• Continues beam tracking to avoid beam re-alignment
Sensor Type	• GPS	• IMU+GPS	• IMU
System Design	V2I	V2I	V2V
Antenna Setting	• 10, 20, 40 number of beams	• 16 Sectors	• MIMO Antenna equipped with accelerometer on front and rear bumper
Performance Evaluation	• Prediction-based schedule for beam switching • beam design with overlapping region to avoid misalignment • Obtain up to 12 *Gbps* data rate with 80% beam overlap	• Overhead-free beamforming exploiting Vehicles sensory data (velocity, motion data, estimated position) • Achieve up to 3 *Gbps* average data rate for 25 vehicles	• Antenna array height & stroke dynamics prediction observed by sensors • Obtain higher throughput than 802.11ad
Overhead	• position prediction error (causes to outage)	• Low data rate at the presence of position estimation error	• Requires a perfectly estimated V2V distance

To conclude, the proposed sensor-based beamforming studies have generally taken the following steps:

I. A link is established by performing SLS phase and received signal power measurement (mutual step between most of the sensor-based and IEEE 802.11ad standard). Once the received power drops lower than a threshold, beam tracking must be performed for both error detection and error handling. Indeed, all the current IMU-based beamforming methods still requires to perform SLS, at least once they are establishing the beam.

II. An uninterrupted connection is desired to provide using sensor-assisted beamforming, especially in a mobile environment with frequently misalignment, e.g., every 54 *ms* [60]. Though, the number of beam realignment has reduced, the feedback collected from sensors of the device must be provided to AP for beam tracking (iTrack is exception while beamforming is established in the client side).

III. A prediction step has been taken in some studies to further reduce the number of rebeamforming and maintain the established beam. While sensor-based prediction methods improve the number of re-beamforming or SNR variation, the prediction procedure requires either a time (e.g., at least 500 ms using activity recognition) or complementary information (such as distance between AP and mobile user).

3.5 Research Gap

Despite the plethora of work in out-of-band beamforming to remove/reduce beamforming overhead, a little has been done to investigate the impact of device population on beamforming performance. Moreover, the proposed out-of-band mechanisms either require to continuously provide feedback to AP (e.g., sensor-based methods) or exploit 2.4/5 GHz legacy band which is a crowded band. Consequently, in this study we aim to exploit inaudible sound frequency to assist beam alignment and find the direction of arrival of signals in a crowded MmWave network. Accordingly, the following sections are dedicated to discuss the literature related to direction of arrival methods (Section 3.6) followed by presenting the existing methods utilising inaudible sound for direction finding (Section 3.7).

3.6 Direction of Arrival

The fundamental principle behind Direction of Arrival (DOA) estimation is to capture the phase information present in the signal picked up by receiver sensors [61, 62]. Let's consider the signal represented by a complex sinusoidal signal as $e^{i\omega_0 t}$. Thus, s_1 denotes the received signal by the reference element

antenna (usually the first element of antenna array) as follows:

$$s_1 = e^{j2\pi f_0 t} \tag{3.1}$$

and the received signal by the second element is the delayed version of the signal received by the first element. Hence,

$$s_2 = s_1(t-\tau) = e^{j2\pi f_0 t}.e^{-j2\pi f_0 \tau} \tag{3.2}$$

where τ denotes the occurred delay which is calculated by:

$$\tau = \frac{d\sin(\theta)}{c} = \frac{d\sin(\theta)}{f_0 \lambda 0} \tag{3.3}$$

where θ is the angle from which direction the signal is arrived, c denotes the signal travelling speed, and d denotes the distance between array elements. From the above equations, we get :

$$\begin{aligned} s_2 &= e^{j2\pi f_0 t}.e^{-j2\pi f_0 \frac{d\sin(\theta)}{f_0 \lambda_0}} \\ &= e^{j2\pi f_0 t}.e^{-j2\pi \frac{d\sin(\theta)}{\lambda_0}} \end{aligned} \tag{3.4}$$

with replacing $\phi = 2\pi \frac{d\sin(\theta)}{\lambda_0}$, we get:

$$s_2 = s_1(t)e^{-j\phi} \tag{3.5}$$

In this way, the received signal by the array antenna elements which is corrupted by noise is denoted as:

$$\begin{aligned} x_1(t) &= s_1(t) + N(t) \\ x_2(t) &= s_1(t-\tau) + N(t) \\ &\vdots \\ x_M(t) &= s_1(t-\zeta) + N(t) \end{aligned} \tag{3.6}$$

with M numbers of array antenna elements, it could be represented in a vector form by:

$$\begin{bmatrix} x_1(t) \\ x_2(t) \\ \vdots \\ x_M(t) \end{bmatrix} = S(t) \begin{bmatrix} 1 \\ e^{-j\phi} \\ e^{-j2\phi} \\ \vdots \\ e^{-j(M-1)\phi} \end{bmatrix} + N \tag{3.7}$$

where $N = \begin{bmatrix} n_1(t), n_2(t), ..., n_M(t) \end{bmatrix}^\top$. Given that there is K number of signal sources with center frequency, f_0, and directions $\theta_1, \theta_2, \ldots, \theta_K$ impinging on the M element array. Thus, the array output could be expressed as :

$$x(t) = \sum_{k=1}^{K} \alpha_k s(\phi_k) + N \tag{3.8}$$

where $\alpha_k s(\phi_k) = \begin{bmatrix} 1 & e^{-j(\phi_k)} & \ldots & e^{-j(M-1)(\phi_k)} \end{bmatrix}^\top$ is $M \times K$matrix of the steering vector. After obtaining the received signal model of k signals, the goal therefore is to estimate (ϕ_k), $k = 1$, ... , K.

DOA estimation method was first used in conventional beam forming algorithm [63]. Its main idea is: in a certain time, make all arrays estimate a

certain direction and measure the output power; for the output power, produce a maximum power of direction that is needed by DOA estimation. Following sections briefly discuss about the current DOA methods.

3.6.1 Classical Beamforming Method

The classical beamforming method of direction estimation is to estimate the spatial spectrum of incoming signal to array receiving antenna. Fourier Transform (FT) is one of the most popular spectrum estimation methods. Clearly, the direction of arrival can be estimated by locating the peak in the spatial spectrum. It could be achieved by first constructing the auto-correlation matrix of the received signals (of complex vector) within the equispaced linear array elements. Thus,

$$R_{xx} = E[xx^H] \tag{3.9}$$

where E and $(.)^H$ denote expectation operator and complex conjugate transpose, respectively. Next, the output power across the angular region is measured considering the array response vector or steering vector, $\alpha(\phi_k)$, and received signal auto-correlation matrix, as follows:

$$P_{CBF}(\phi) = \frac{\alpha^H(\phi) R_{xx} \alpha(\phi)}{\alpha^H(\phi)\alpha(\phi)} \tag{3.10}$$

where $P_{CBF}(\phi)$ is the output power as a function of angles of arrival and often terms as spatial spectrum. The most popular methods in this group is MVDR [64].

3.6.2 Sub-Space Method

There are some fundamental limitations in resolution in classical beamforming methods even though they are often successful and widely used. Thus, sub-space direction estimation algorithms have been proposed which is known as super-resolution algorithms Subspace-based methods depend on observations concerning the eigendecomposition of the covariance matrix into a signal subspace and a noise subspace.

One of the known techniques in this class has presented in [65] called ESPRIT which stands for Estimation of Signal Parameter via Rotational Invariance Technique. ESPRIT is an algebraic subspace DOA estimation method which does not require to search procedure. It explores the rotational invariance property in the signal subspace created by two sub arrays derived from original array with a translation invariance structure. The algorithm assumes that an antenna array is composed of two identical sub arrays. The sub arrays may overlap, that is, an array element may be a member of both sub arrays. The corresponding elements of the two sub arrays displaced from each other by a fixed translational (not rotational) distance. The array thus possesses a displacement (translational) invariance (i.e., array elements occur in matched pairs with identical displacement vectors). This property leads to the rotational invariance of signal subspaces spanned by the data vectors associated with the spatially displaced subarrays; the invariance is then utilized by ESPRIT to find DOAs. The two subarrays, m_1 and m_2 are displaced by distance d and the signals induced on each of the arrays are given by:

$$x_1 = A.s(t) + n_1(t) \tag{3.11}$$

$$x_2 = A.\Phi.s(t) + n_2(t) \tag{3.12}$$

where x_1 and x_2 are measurements due to displacement and Φ implies a diagonal matrix with entries correspond to the phase shift from one element to the next due to the delay for each individual k signal, thus:

$$\Phi = diag\left[e^{-j2\pi\frac{d}{\lambda}sin(\theta_1)}, ..., e^{-j2\pi\frac{d}{\lambda}sin(\theta_k)}\right] \tag{3.13}$$

and the correlation matrices can be defined as below:

$$R_{11} = E[x_1(t)x_1^H(t)] \tag{3.14}$$

$$R_{22} = E[x_2(t)x_2^H(t)] \tag{3.15}$$

From eigen-decomposition, we can construct the signal subspaces E_1 and E_2, and further, the following matrix,

$$C = \begin{bmatrix} E_1^H \\ E_2^H \end{bmatrix} \left[E_1(t)E_2\right] = E_c\Lambda E_c^H \tag{3.16}$$

where E_c and Λ are the eigenvectors and eigenvalues.

By further partitioning E_c,

$$E_c = \begin{bmatrix} E_{11} & E_{12} \\ E_{21} & E_{22} \end{bmatrix} \tag{3.17}$$

The rotational matrix,

$$\Phi = -E_{12}E_{22} - 1 \tag{3.18}$$

For the i^{th} eigenvalue, we can derive the angle of arrival by the following:

$$\theta_i = sin^{-1}\left(\frac{arg(\lambda_i)}{k\Delta}\right) \tag{3.19}$$

The algorithm works in signal subspace rather than in the noise subspace.

The most popular sub-space method is MUSIC [49], stands for Multiple Signal Classification. The basic idea of MUSIC algorithm is to conduct characteristic decomposition for the covariance matrix of any array output data.

Recall that the received signals from K sources at M-element array, expressed by equation (3.8), can be expressed as a linear combination of the incident waveforms and noise:

$$\begin{aligned} x(t) = [\alpha(\phi_1)\ \alpha(\phi_2)\ \ldots\ \alpha(\phi_K)] \begin{bmatrix} s_1(t) \\ s_2(t) \\ \vdots \\ s_K(t) \end{bmatrix} + \begin{bmatrix} n_1(t) \\ n_2(t) \\ \vdots \\ n_K(t) \end{bmatrix} \\ = \alpha\mathbf{s}(\mathbf{t}) + \mathbf{n}(\mathbf{t}) \end{aligned} \tag{3.20}$$

where $\mathbf{s}$ is $M \times K$ matrix denotes the vector of incident signals, $\mathbf{n}$ is the noise vector $\alpha(\phi_k)$ represents the array steering vector corresponding to the Direction of Arrival of k^{th} signal. As MUSIC is dependent on the correlation matrix of the data, the correlation matrix of $x(t)$ in eq.(3.20) could be written as:

$$\begin{aligned} \mathbf{R}_{xx} = E[\mathbf{x}\mathbf{x}^H] &= E[\mathbf{s}\alpha\alpha^H\mathbf{s}^H] + E[\mathbf{n}\mathbf{n}^H] \\ &= \alpha E[\mathbf{s}\mathbf{s}^H]\alpha^H + E[\mathbf{n}\mathbf{n}^H] \\ &= \alpha\mathbf{R}_{ss}\alpha^H + \sigma_n^2\mathbf{I} \end{aligned} \tag{3.21}$$

where σ^2 the noise power and I is unit matrix of $M \times M$. Considering eq.(3.21) as the eigenvalue equation, its corresponding eigenvalues are the values $\lambda_1, \ldots, \lambda_M$ such that:

$$|\mathbf{R}_{xx} - \lambda_i \mathbf{I}| = |\alpha \mathbf{R}_{ss} \alpha^H - (\lambda_i - \sigma_n^2)\mathbf{I}| = 0 \qquad i = 1, \ldots, M \tag{3.22}$$

Since α is comprised of steering vector which are linearly independent, it is a rank M matrix (corresponding to the maximal number of linearly independent columns of α). From linear algebra principals, it is concluded that when the number of incident signals, K, is less than the number of array elements M, $(M - K)$ number of $(\alpha \mathbf{R}_{ss} \alpha^H)$ eigenvalues are zero. That is, $(M - K)$ of $\mathbf{R}_{xx}$ eigenvalues are noise variance, σ_n^2. The eigenvalues of $\mathbf{R}_{xx}$ is sorted such that λ_1 is the largest eigenvalue, and λ_M is the smallest eigenvalue. Therefore,

$$\lambda_i = \sigma_n^2 \qquad i = 1, \ldots, M \tag{3.23}$$

This eigendecomposition of the received signal correlation matrix determines the noise eigenvalues as the number of small eigenvalues that are equal. Moreover, while the noise and signal subspaces are orthogonal, all noise eigenvectors are orthogonal to the signal steering vectors. Thus, power spectrum density or spatial spectrum of MUSIC given by:

$$P_{MUSIC}(\phi) = \frac{1}{\alpha^H(\phi) \mathbf{Q}_n \mathbf{Q}_n^H \alpha(\phi)} \tag{3.24}$$

where $\mathbf{Q}_n$ is one of the $(M-K)$ noise eigenvectors. MUSIC, therefore, identifies as the directions of arrival, the peaks of the function $P_{MUSIC}(\phi)$.

3.7 Inaudible Sound Direction of Arrival

In the previous section, we have explained DoA concept and its application on beamforming using an antenna array. Further, we have discussed the well-structured, high resolution DoA method, called MUSIC, in details. Recall that this research aims to ultimately exploit acoustic interface and inaudible sound signals as a side channel to assist beamforming in MmWave. Therefore, in this section, we review the literature utilising inaudible signals emitted by COTS devices, particularly the methods proposed to estimate acoustic DoA.

There is some research developed for acoustic-based data communication such as [66, 67, 68]. Moreover, an acoustic side channel has developed in [69] to address the contention overhead in wifi.

Apart from data communication in aerial acoustic channel, there is another research trend for gesture tracking using inaudible sound such as methods presented by [70, 71].

As can be seen, none of the above research has addressed inaudible sound DoA, though they have exploited the acoustic interface embedded on the devices. Moreover, despite the wide popularity of MUSIC algorithm as a subspace DoA method, MUSIC has not yet been leveraged for DoA in inaudible sound frequencies. Recently, just a method called DoAnet presented in [72], proposed a deep neural network to estimate the direction of arrival of multiple sound sources. The main aim of the research was to identified the number of active sources in different directions applying MUSIC algorithm.

In the following, we address the few methods developed for direction finding using inaudible sound signals.

A research proposed by [73] for acoustic direction finding between two devices such as phone-to-phone direction finding in social media application. The

method is based on the relationship between doppler effects and the relative motion from the phone to the acoustic source. 6 different acoustic channel has dedicated between 17 to 19.5 KHz. The phone gathers samples from the microphone and inertial sensors, when the user shakes the phone or walks in an arbitrary path. This is the main limitation of the method. Moreover, the accuracy provided by Swadloon is about 10° which is not tolerable for MmWave beamforming application.

The reseach presented in [74], called Daredevile, has been developed for indoor localisation of devices using sound signal. The primary step was addressed as the detection of sound angle of arrival emitted by smart phones. The method has dedicated single frequency of 18 KH in the range of inaudible sound to all smart devices. Using TDM approach to schedule channel access for multiple devices, Daredevile imposed a delay around 750 for direction finding. For example, with a single frequency band, the method can locate up to 40 phones every 30 seconds. The delay may be tolerable for indoor localisation, but it is a huge delay for MmWave beamforming.

Table 3.7 summarises the main attributions and achievement of the discussed inaudible sound DoA methods.

3.8 Summary

This chapter provided an inclusive overview of the proposed beamforming methods for mobile millimetre wave communication. Various methods have been classified into in-band and out-of-band beamforming based on the signal frequency utilised for beam alignment. We further categorised out-of-band beamforming into RF-based and sensor-based methods and discussed the studies, comprehensively. Finally, we have reviewed DoA concept and the popular

Table 3.7: Prediction-based out-of-band beamforming using IMUs

Algorithm	**Swadloon** [73]	**Daredevil** [74]
Objective	• Direction finding for mobile social networks and friending	• Acoustic-based indoor localization
Frequency	• Sinusoidal signal $17 \sim 19.5KHz$	• Chirp, $18KHz$
Channel Access	FDMA, $\sim 415Hz$ intervals	TDMA, $750ms$ (signal length: $500ms$, guard: $150ms$, delay : $100ms$)
Accuracy	• 5.8° (in 95% of time)	• 5° (mean error)
Performance Evaluation	• Phone shaking to produce doppler effect	• Angle of arrival estimation of received signal by microphone array comprises of 8 microphones based on TDOA
Overhead	• Sound receiver requires to shake the phone, gently	• Long delay caused by TDM

methods of DoA technique. Inaudible sound DoA methods were presented as well, to investigate the research gap in the context of inaudible sound direction finding for COTS devices. To conclude, this chapter prove the necessity of proposing a fast and accurate out-of-band beam alignment method for multiple users connecting to mmWave network. In the following chapters, we proposed, discuss, and evaluate the performance of inaudible sound assisted beam alignment method for multi-users mmWave network.

Chapter 4

Impact of Device Population on Beam Alignment Performance of 802.11ad

4.1 Introduction

In this chapter, we first develop an analytical model for the gain of antenna for a rotating device to emulate the scenario of angular displacement of hand-held or body-worn devices such as smartphones and virtual-reality headsets. Next, we probabilistically model the beacon intervals required to complete the beam alignment at the presence of competing multiple devices to access 802.11ad beam forming time slots. Then, we propose analytical probability of sector selection error in sensor-based beamforming and the obtained gain of sensor-based methods. Finally, using extensive simulations with practical device mobility patterns, we examine that loss of antenna gain.

The remainder of this chapter is organized as follows. Section 4.2 presents the analytical model of beamforming at the presence of rotation for oracle,

IEEE 802.11 ad in a multi-device scenario, and sensor-based beamforming. Next, we present our testbed followed by numerical results in Section 4.3. Finally, the conclusion is discussed in Section 4.4.

4.2 Performance Model for Mobile MmWave BeamForming

In this section, we aim to evaluate the performance of IEEE 802.11ad beam alignment in a multiple-device scenario. To this end, we first introduce directional antenna radiation pattern in Section 4.2.1 and develop a closed-form of Oracle-based scenario to evaluate the antenna gain in Section 4.2.2. Next, we derive a probabilistic model for a contention-based beam alignment by Section 4.2.3. We then formulate an analytical model to evaluate the performance of sensor-based beamforming in Section 4.2.4.

4.2.1 Antenna Radiation pattern

In this section, a generic directional antenna model is provided based on the implemented antenna in [75]. In this antenna model which is inherited from the base model in [76], the attributes of radiation pattern are defined mathematically. Let θ denotes the geometric angle between the direction of the transmitter and the receiver antenna. The gain of the directional antenna is then expressed as:

$$Gain(\theta) = \begin{cases} M(\theta) & \text{if } 0 \leq \theta \leq \Psi \\ \zeta & \text{otherwise} \end{cases} \tag{4.1}$$

where Ψ is the width of each antenna sector, which is computed by $\Psi = \frac{360^\circ}{N}$ for N sectors. If the receiver is covered by the main lobe of the transmitter antenna, the antenna gain of the link is $M(\theta)$. Otherwise, the gain is ζ. $M(\theta)$, main lobe or maximum gain, is calculated as:

$$M(\theta) = 10\log_{10}\left(\frac{1.6162}{\sin(\frac{HPBW}{2})}\right)^2 - 3 \times \left(\frac{2\theta}{HPBW}\right)^2 \tag{4.2}$$

Let $HPBW$ denotes the half-power beam width. For various sector widths, we have $HPBW = \frac{\Psi}{2.6}$. Besides, the side lobe gain ζ is calculated by:

$$\zeta = -0.4111 \times \log(HPBW) - 10.597 \tag{4.3}$$

The radiation pattern for a 4-sector antenna ($\Psi = 90^\circ$) is illustrated in Figure 4.1.

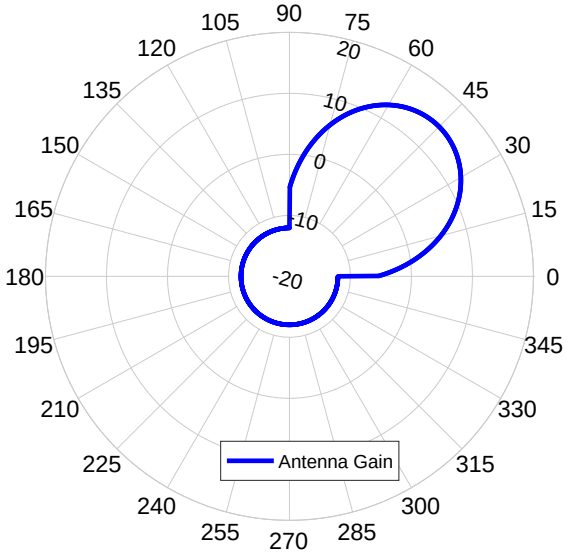

Fig. 4.1: Antenna Radiation Pattern for $\Psi = 90^\circ$

4.2.2 Performance Model of BeamForming: Oracle

It is desirable to maximize the antenna gain and achieve the link budget to deliver multi-Gbps data rates. Transmitter-receiver pair could be perfectly aligned to provide highest possible gain in a stationary environment and support high data rate applications. However, using mmWave link for moving or rotating devices such as VR headsets presents significant challenges []. In this light, we want to study the maximum antenna gain that can be achieved in a single-device scenario with device rotation.

Considering the discussed antenna radiation pattern in Section 4.2.1, we study the oracle-based model for the antenna radiation pattern with device rotation. To calculate the average value of the gain in the oracle model, $\overline{G_O}$, we need to calculate the integral of $M(\theta)$, the main lobe gain value, over all possible angles. Hence, the average antenna gain of the oracle model with device rotation can be formulated by:

$$\overline{G_O} = \frac{1}{\Psi} \int_0^{\Psi} 10 \log_{10} \left(\frac{1.6162}{\sin(\frac{\Psi}{5.2})} \right)^2 - 3 \times \left(\frac{5.2\theta}{\Psi} \right)^2 d\theta \tag{4.4}$$

The closed-form of $\overline{G_O}$ can be written as:

$$\overline{G_O} = -8.69 \times \ln \left(\sin(\frac{\Psi}{5.2}) \right) - 22.87 \tag{4.5}$$

It is apparent that $\overline{G_O}$ depends on the parameter of sector width, Ψ.

4.2.3 802.11 ad Contention-based Probability Model

One of the contributions of this research is to evaluate the performance of IEEE 802.11 ad beam alignment at the presence of multiple devices which are competing to access the channel. In order to evaluate the performance, we investigate the probability that the antenna training can be completed with a specific number of beacon intervals. Recall that the contention-based model of the protocol has been discussed in Section 2.2.2.

Let S denotes the number of devices in a network to compete beacon intervals for antenna training, each device having N sectors. Each beacon interval is divided into 8 slots and it is occupied by the devices in a contention-based method [5]. Thus, the maximum slot number that can be occupied by a device per beacon interval is 1. Moreover, the required number of slots for a complete training in 802.11ad is $k = \frac{N}{FSS}$, where FSS is the number of frames per slot.

Let $P[X = x]$ represent the probability of a random variable X, which is the number of beacon intervals that are required to complete one antenna training. Thus, we can calculate $P[X]$ by:

$$P[X = x] = \left(p\right)\left(C_{k-1}^{x-1}\right)\left(p^{k-1}\right)\left((1-p)^{x-k}\right) \tag{4.6}$$

The distribution has three parameters: $p \in [0, 1]$, k, and S. Here, p shows the probability that a device can successfully occupy a slot in a beacon interval during the competition with other devices. With the assumption that each device can occupy at most one slot in one beacon interval, p can be computed by $p = (\frac{N_s-1}{N_s})^{S-1}$, where N_s is the number of slots per beacon interval. In the current 802.11ad specification, we have $N_s = 8$. The key point of (4.6) is that, in x BIs, the last one must be a successful one to complete the antenna

training. In the remaining $x-1$ BIs, the device needs to occupy $k-1$ slots for antenna training, and miss the other $x-k$ slots during the training. In total, the device finishes the antenna training in k BIs. Plugging p into (4.6), yields:

$$P[X=x] = \left(\frac{N_{s-1}}{N_s}\right)^{S-1} \binom{x-1}{k-1} \left(\left(\frac{N_{s-1}}{N_s}\right)^{S-1}\right)^{k-1} \left(1-\left(\frac{N_{s-1}}{N_s}\right)^{S-1}\right)^{x-k} \tag{4.7}$$

As an example, we plot the derived Probability Mass Function, PMF, (expressed by Eq (4.7)) in Figure 4.2.

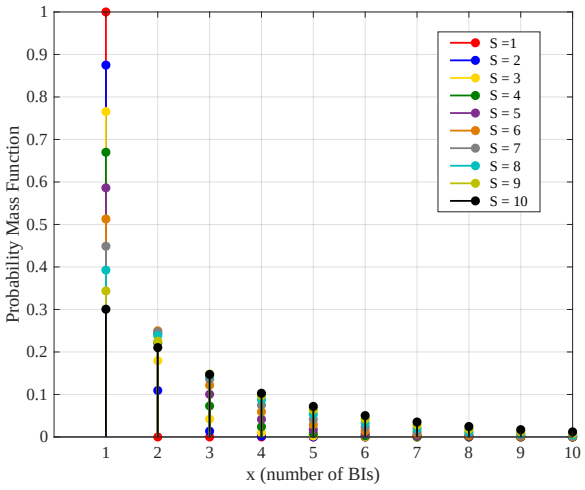

Fig. 4.2: Probability mass function of training completion in various number of BIs for $N = 16$

The figure plots the PMF of completing training with various numbers of BIs, $1 \sim 10$, at the presence of various numbers of devices, $1 \sim 10$. As observed from the figure, it is more likely to complete one antenna training with a less number of BIs in a less crowded environment with a smaller number of S. For example, the probability of antenna training completion with 1 BI is almost 90% for 2 stations, while such probability drops to 30% for $S = 10$. Moreover, a single device is guaranteed to be trained in 1 BI due to no contention in channel access. We also plot Empirical CMF (ECMF) of the derived probability for

further validation. Figure 4.3 displays empirical CMF of the discrete random value of X which is calculated by:

$$F_X(x) = Pr[X = x] = \sum_{k}^{x} P[X = x] = \sum_{k}^{x} p\binom{x-1}{k-1}(p)^{k-1}(p)^{x-k} \tag{4.8}$$

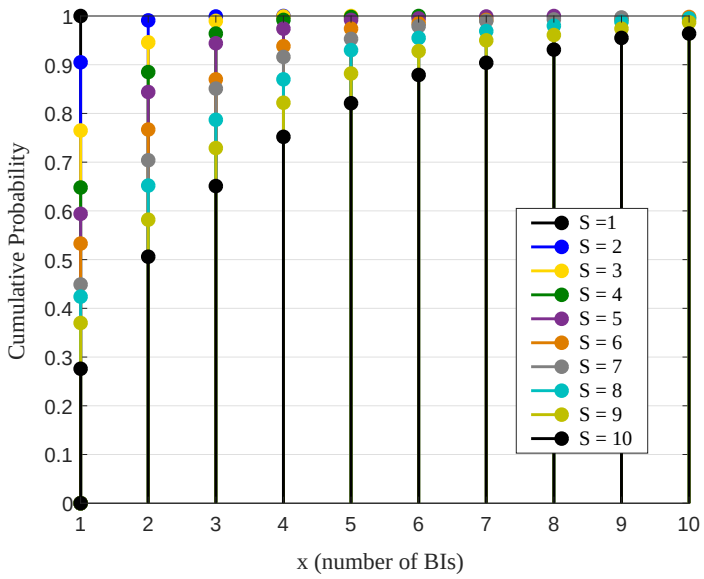

Fig. 4.3: Empirical CMF of various number of BIs for $N = 16$

As can be seen from Figure 4.3, the ECMF approaches one as the number of BIs increases. Additionally, we measure the expected number of required BIs to complete one antenna training for various antenna configurations. Such expected number is formulated as:

$$E[X] = \sum_{x_i=k}^{x} p(x_i) \times x_i \tag{4.9}$$

The result is measured by Eq.(4.9) and plotted in Figure 4.4. Three antenna configurations have been examined, i.e., $N = 16, 32, 64$.

As expected, the number of sectors and number of devices in a network

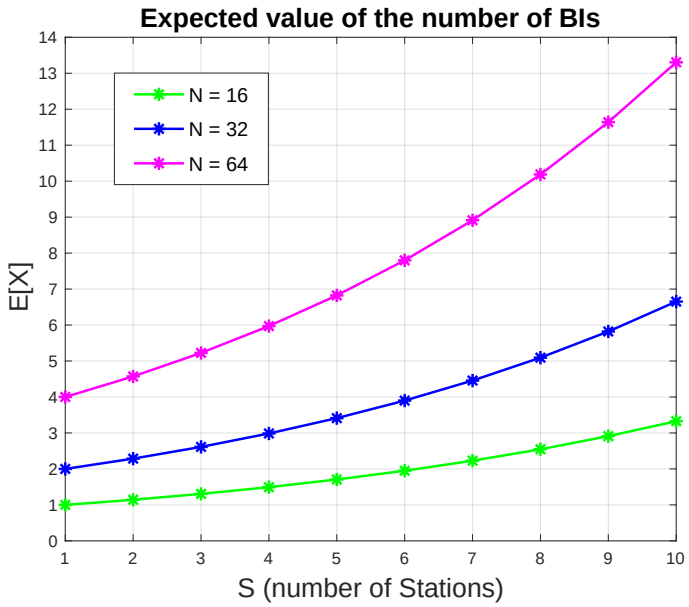

Fig. 4.4: Expected value for the number of BIs. $N = 16, 32, 64$

affect the expected number of required BIs for successfully antenna training. Intuitively speaking, more sectors and more devices lead to a higher expected number of required BIs for successfully antenna training.

4.2.4 Probability Model of BeamForming: Sensor based

In section 3.4, we have discussed about out-of-band beamforming schemes, particularly, sensor-based methods (by section 3.4.3). In this section, we insight into the performance evaluation of sensor-based beamforming. Consequently, the probability of the event of sector selection error is analyzed where sensors are employed for beam alignment. Recall that θ is the degree between boresight direction of transmitter antenna and the receiver orientation. Different sensors, i.e., IMUs [52] and light sensors [56], enable to measure θ with a specific measurement error. Let $\hat{\theta}$ denotes the degree measured by sensors which includes some degree of inaccuracy. Here, we assume Guassian distribution for

sensor measurement error. Hence, the probability density function of random variable $\hat{\theta}$ given that the mean $\mu = \theta$ is:

$$P(\hat{\theta} \mid \theta) \propto \frac{1}{\sqrt{2\pi\sigma^2}}.e^{-\frac{(\hat{\theta}-\theta)^2}{2\sigma^2}} \tag{4.10}$$

Recall that σ is the standard deviation and σ^2 is the variance of the distribution. Indeed, Eq.(4.10) denotes $X \sim N(\mu, \sigma^2)$ where $\hat{\theta}$ is the random variable, X, and θ considered as the mean value, μ. Accordingly, we formulate the probability of selecting a wrong sector as the result of angle estimation error (which has presented by Eq.(4.10)).

Now, we assume the estimated degree,$\hat{\theta}$, belongs to a specific sector with sector width $[0, \Psi]$ (which has discussed in section (4.2.1)). On the other hand, the event of Sector Selection Error,Γ_{SSE} Given that E_{SSE} denotes the event of sector selection error which is happened once θ lays down outside the sector in which $\hat{\theta}$ belongs to. In other words, E_{SSE} occurred if:

$$\theta \in [-180, 180] - [0, \Psi] = [-180, 0] \cup [\Psi, 180] \tag{4.11}$$

With this condition, the probability of occurring sector selection error for sensor-based BF scheme can be formulated by conditional probability. Thus,

$$P(E_{SSE} \mid \hat{\theta}) = \frac{P(E_{SSE} \cap \hat{\theta})}{P(\hat{\theta})} \tag{4.12}$$

Recall the condition of sector selection error, Eq (4.12) for $P(\Gamma_{SSE} \mid \hat{\theta})$ is replaced with: The numerator of the equation implies the set in which both probabilities occurred, i.e., the probability of sector selection error and degree estimation error. Thus, we substitute θ values written by Eq.(4.11) into Eq.(4.10), to acquire the numerator of the conditional probability. Thus:

$$P(E_{SSE} \mid \hat{\theta}) = \frac{\int_{-180}^{0} \frac{1}{\sqrt{2\pi\sigma^2}}.e^{-\frac{(\hat{\theta}-\theta)^2}{2\sigma^2}} d\theta + \int_{\Psi}^{180} \frac{1}{\sqrt{2\pi\sigma^2}}.e^{-\frac{(\hat{\theta}-\theta)^2}{2\sigma^2}} d\theta}{\int_{-180}^{180} \frac{1}{\sqrt{2\pi\sigma^2}}.e^{-\frac{(\hat{\theta}-\theta)^2}{2\sigma^2}} d\theta} \tag{4.13}$$

where the denominator shows the values with the probability of the estimated degree contains any error. It is obvious that the estimated degree could be any values within the set of $[-180, 180]$.

Considering error function which is denoted by erf(u) in mathematics, we have:

$$\text{erf(u)} = \int \frac{2e^{-u^2}}{\sqrt{\pi}} du \tag{4.14}$$

Thus, with substituting $u = \frac{\hat{\theta}-\theta}{\sqrt{2}\sigma}$ and $d\theta = \sqrt{2}\sigma du$, a specific integration is formed which could be solved by error function, erf(u). The next step is integrating and solving the problem which is expressed by Eq.(4.13). The following equation represents the probability of the event of sector selection error in sensor-based beamforming schemes:

$$P(E_{SSE} \mid \hat{\theta}) = \frac{\text{erf}(\frac{\hat{\theta}+180}{\sqrt{2}\sigma}) - \text{erf}(\frac{\hat{\theta}}{\sqrt{2}\sigma}) + \text{erf}(\frac{\hat{\theta}-\Psi}{\sqrt{2}\sigma}) - \text{erf}(\frac{\hat{\theta}-180}{\sqrt{2}\sigma})}{\left(\text{erf}(\frac{\hat{\theta}+180}{\sqrt{2}\sigma}) - \text{erf}(\frac{\hat{\theta}-180}{\sqrt{2}\sigma})\right)} \tag{4.15}$$

As obvious from the derived equation, the probability of sector selection error has two variables, sector width of directional antenna, (Ψ), and the standard deviation, σ, which implies the measurement accuracy of the utilised sensors. The next step is to formulate the expected value of the average gain for sensor-based methods. We can calculate the expected value of a measurable function,e.g., G_S, given that X has the probability density function $f(x)$.

In other words:

$$E[G_S(X)] = \int G_S(x) f(x) dx \tag{4.16}$$

With this definition, we can derive the expected value of average gain of antenna in sensor-based beamforming where $f(x)$ can be replaced by Eq.(4.15). Consequently:

$$E[\overline{G_S}(\theta)] = \frac{1}{\Psi} \int_0^{\Psi} M(\theta) \times (1 - P(E_{SSE} \mid \hat{\theta})) + S \times P(E_{SSE} \mid \hat{\theta}) d\theta \tag{4.17}$$

where $M(\theta)$ and ζ are the values calculated by Eq.(4.2) and (4.3), respectively.

With this error probability, the average gain provided by sensor-based beamforming methods, $\overline{G_S}$ could be measured by:

$$\overline{G_S} = \frac{1}{\Psi} \int_0^{\Psi} M(\theta) \times (1 - P(\Gamma_{SSE} \mid \hat{\theta})) + S \times P(\Gamma_{SSE} \mid \hat{\theta}) d\theta \tag{4.18}$$

where $M(\theta)$ and ζ are the values calculated by Eq.(4.2) and (4.3), respectively. The analytic equation derived for the average gain of sensor-based BF is based on two factors, the accuracy of the sensor and sector width for antenna. To conclude, we analytically derived the average gain offered by sensor-based beamforming approache at the presence of rotation.

4.3 Results and Evaluation

In this section, we present the numerical results for gain of antenna for Oracle, IEEE 802.11 ad and sensor-based methods at the presence of rotation. First, simulation model and parameter settings are discussed. Next, performance results for IEEE 802.11ad beamforming in a multi-device scenario will be pre-

sented. Then, results related to the performance evaluation of sensor-based beamforming is discussed.

4.3.1 Simulation Model

In this study, we consider a mmWave network includes a single access-point and S number of devices competing for beam alignment. Recall that we consider a free space environment with line of sight assumption. However, few researches consider the more practical NLOS communication such as [38] and [17] which address the blockage problem with installing relay to direct the beam to the receiver. As discussed in Section 3.3.2, the problem of blockage and NLOS has been considered by different research studies. Thus, in this research, we assume LOS condition and focus to address the problem of multi-users beam alignment in millimetre wave networks.

We depict the system model by Figure 4.5 to show the considered scenario. Both AP and devices are equipped with directional antenna with N sectors. We assume that AP is stationary with distance $d = 1m$ apart from the devices, but the devices are rotating with the angular velocity ω every 100 ms. Device rotation is assumed in this set of simulation to analyse the impact of mobility on beam misalignment. As a target scenario for millimetre wave network, we consider wireless VR/ARs which is worn by the player who turns her head to look around [36]. Thus, frequent rotation of devices is a critical problem which causes the beam misalignment and needs to be addressed to deliver multi Gbps data rate in mmwave future applications. In this case, frequent beam realignment is required to adjust the directional link. We configure ω as the value addressed by [9] from the range of $20° - 80°/100ms$ for various applications like web browsing/reading and playing games. This angular velocity is applicable

for our target scenario of wireless VR and mobile video streaming.

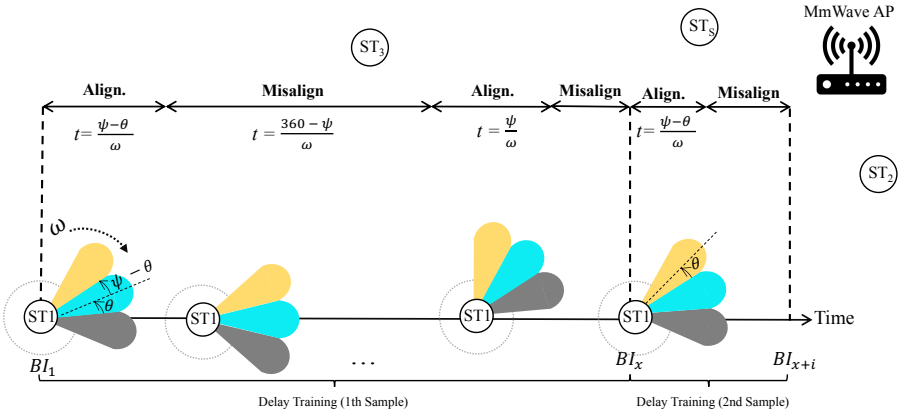

Fig. 4.5: System Model

Initially, a random orientation is selected (θ) to launch beam alignment. The station is aligned starting from this random seed and provide main lobe gain. It will be valid for the period in which the selected sector is faced with the AP. The aligned sector will be misaligned due to rotation. Since it is a multi-device scenario, a training delay is defined for the stations which takes to complete training and it is considered as a random discrete sample multiplied by $100ms$, the time of a single beacon interval. The random selection procedure has discussed in Section 4.2.3. Within each sample time, the receiver may provide side lobe or main lobe gain. We collect 100 samples to get the average gain of antenna and repeat the procedure 20 independent runs and have been averaged to mitigate the randomness of the results. The results have been collected through MATLAB simulation. Table 4.1 lists the variables, definition, and their values.

We consider three critical performance metrics. First, average running gain is measured as the mean value of the gain during running time of training period. This metric figures out the length of training to achieve average gain stability. Second, Instantaneous gain of antenna is measured as the corre-

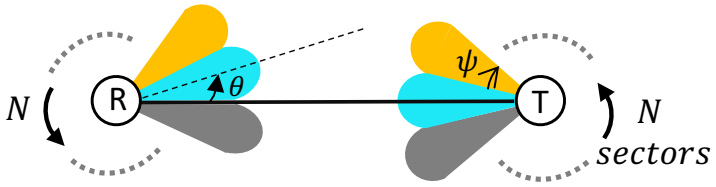

Fig. 4.6: Considered Scenario in Initial Position

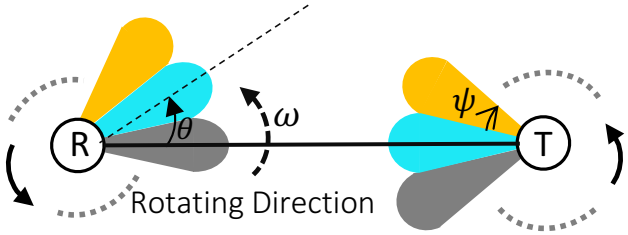

Fig. 4.7: Receiver orientation is changing once rotation starts

sponding gain per ms. Note that gain unit is dBi. To calculate the gain in this unit, the measured antenna gain is mapped to its corresponding linear value using $G_{Linear} = 10^{(\frac{Gain(\theta)}{10})}$.Then, it converts to decibel using the logarithmic transformation by $G_{dBi} = 10 \log_{10} G_{Linear}$.

Furthermore, outage probability of the average gain of antenna is measure to find the proportion of time that side lobe gain is imposed over the total training time.

4.3.2 Performance Evaluation of IEEE 802.11ad

To gain an understanding of the required length of simulation to obtain steady values for average gain, we plot average gain as a function of time for two different rotational speeds (see Figure 4.8a). First, we find that it takes about 24 seconds to reach steady state even with 16 antennas. In our subsequent experiments, we run each simulation for 100 training episodes, which ensures that the simulation always reach steady state.

In Figure 4.8a, we also note that the device achieves higher gain when

Table 4.1: Definition of parameters and their value

Symbol	Definition	Value
N	Number of Sectors	$4, 8, 16, 32, 64$
ω	Angular Velocity (per $100ms$)	$10° - 80°$
BI	Beacon Interval	$100\ ms$
S	Number of devices	$1 - 10$
N_s	Number of slots per BI	8
σ	Standard deviation	$1 - 5\ FSS$
Number of frames per slot	16	

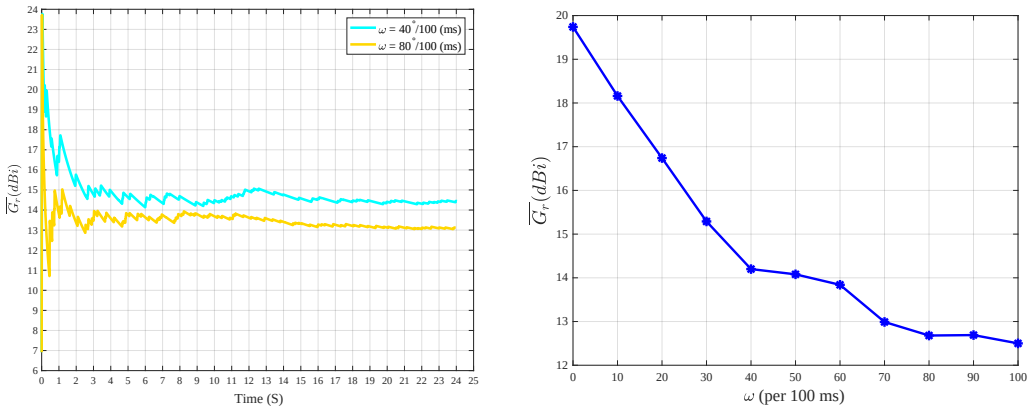

(a) Average gain as a function of time

(b) $\overline{G_{11.ad}}$ vs ω for $N = 16, S = 10$

Fig. 4.8: Angular velocity vs. $\overline{G_{11.ad}}$

rotating at a lower speed. To further investigate the impact of rotational speed on the average gain performance, in Figure 4.8b, we plot average gain against rotational speed for different number of competing devices in the network.

From the figure, we observe that initially antenna gain drops rapidly with increasing speed, but it saturates at a speed of about 70° per 100ms, beyond which the impact of increasing speed has no noticeable effect on gain. However, as the rotational speed varies between 40 to 80 degrees per 100ms in many applications the drop in antenna gain would be significant.

The gain drop due to higher rotation speed can be explained by examining the instantaneous gains for two different rotational speeds in Figure 4.9.

As we can see, the device spends more time in the main lobe when rotating

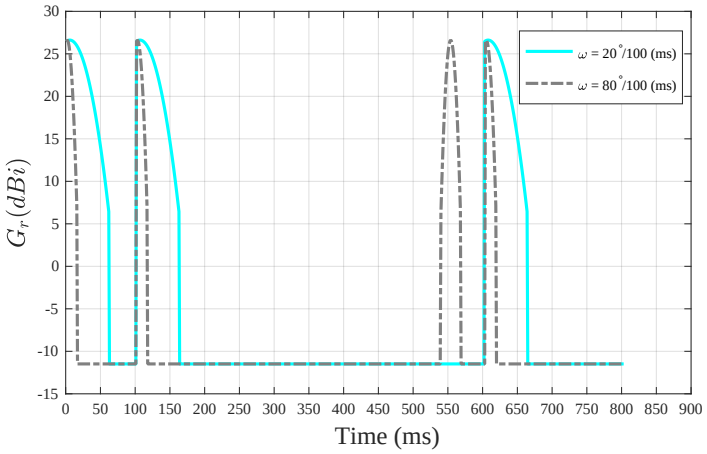

Fig. 4.9: Instantaneous gain for $\omega = 20°$ and $\omega = 80°/100ms$

at a lower speed, and vice versa, in a given cycle. As the main lobe has higher gain than the side lobe, the result is higher gain for lower speed. As shown in this figure, the gray curve ($\omega = 80°$) could provide main lobe gain at the time of 550 ms. It is interpreted by the fact that the aligned sector may have the chance of facing with the access-point if the training period is long enough.

In Figure 4.10a, we compare 802.11ad antenna gain against Oracle for different values of antenna sectors. As expected, Oracle always outperform 802.11ad, but the performance gap is more severe for larger number of antennas. For example, 802.11ad performs almost as good as Oracle when only two antennas are used, but suffers a whopping 7 dB loss if 16 antennas are employed to boost the network capacity. This implies that the current SLS mechanism is less efficient for higher speed applications, which require narrower beams (more antenna sectors). This can be explained by the fact that the narrower the sectors (larger the number of sectors), the less time the device spends in the main lobe. This behavior is plotted in Figure 4.10b for two different number of sectors, $N = 4, 16$.

Finally, in Figure 4.11, we study the outage probability for a rotating device

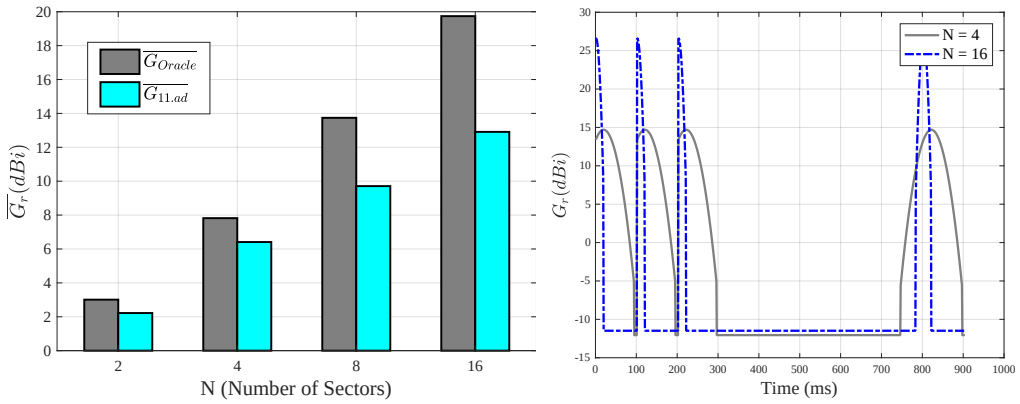

(a) Gain comparison for S = 10, $\omega = 80°$ **(b)** Instantaneous gain in $\omega = 60°$

Fig. 4.10: Directional antenna and gain comparison

under different number of competing devices. To study the effect of rotational speed, we vary ω from $20°/100ms$ to $80°/100ms$. We make the following observations:

- Under no competition (S=1), the outage probability increases significantly from 42% to 82% when rotational speed increases from $\omega = 20°$ to 80° per 100 ms.
- Outage probability increases with increasing competition, but it increases more rapidly for slower rotations.

4.3.3 Performance Evaluation of Sensor-based Beam-Forming

In this section, the numerical results related to sensor-based beamforming is presented. The assumptions, model, and the set values are similar with the discussed setting in Section 4.3.1. The probability for the event of sector selection error (Γ_{SSE}) is mathematically derived by Equation (4.15). It is formulated based on the measured degree by the sensors, $\hat{\theta}$ and σ. here, σ is

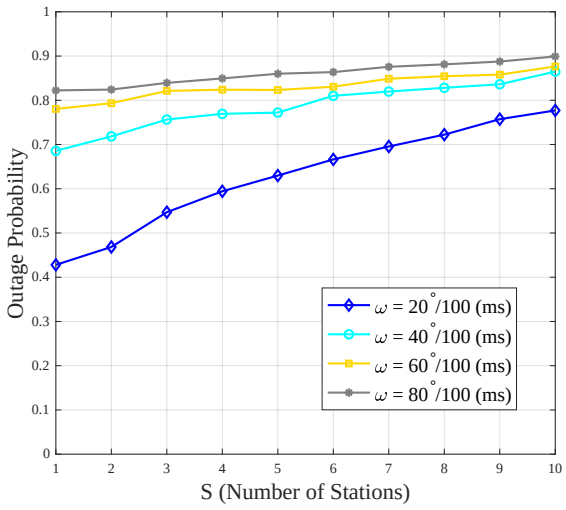

Fig. 4.11: Outage Probability for various angular velocity in $N = 16$

considered up to 5° variation in rotation measurement, based on conducted experiments for the current sensors. The probability of the event for $\hat{\theta} = [0° - 90°]$ ($N = 4$) and σ = 1-5 is reported in Figure 4.12.

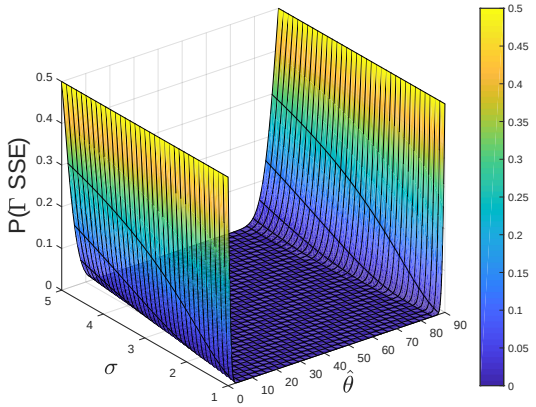

Fig. 4.12: The probability of sector selection error for $N = 4$ in various σ

As observed, the high probability for the error occurred near the sector border, in 0° and 90° for all values of σ. This measurement makes sense because real degree (θ), may or may not lay down at the same sector (e.g.,$\pm$1°for $\sigma = 1$). Intuitively, the higher the value of σ, the higher the error probability. Moreover, it is less likely to wrongly selecting the sector in the middle degrees

with the considered value of standard deviations.

Next, we insight into the impact of the number of sector, N (and consequently different beamwidth (Ψ)) on the error probability. Figure 4.13. The results for $N = 8, 16$, and 32 are illustrated in Figures 4.13.

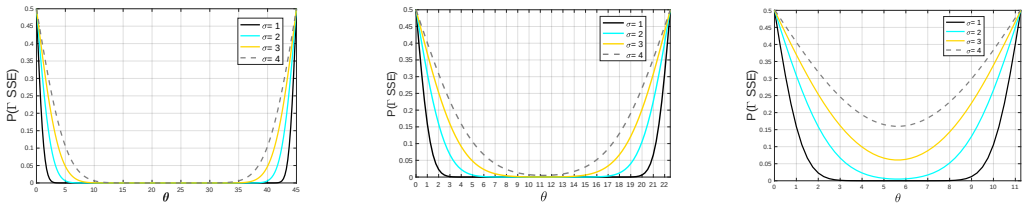

(a) $N = 8$ **(b)** $N = 16$ **(c)** $N = 32$

Fig. 4.13: Sector selection error probability for various antenna sectors

The common feature among the figures is that higher probability for the event of sector selection error occurs near the boarder of the sector. This behavioure is due to the asynchronous BI and sector switching. In fact, the current sector switches to the next one with greater offered gain in-between two BIs. The higher value of σ enlarges the degrees faced with the probability of the error. For example, in Figure 4.13a the probability initiates from 44° for $\sigma = 1$ but enlarges to start from 35° in $\sigma = 4$. The trend repeats for other value of the sector width, as observed by 4.13b and 4.13c. The impact of smaller degree of Ψ (the greater number of sectors of antenna) is non-negligible. The higher the number of sectors, the greater the value of the probability of the error. For instance, the probability of the error for $\sigma = 4$ for $N = 8$ (figures 4.13a) initiates from 0.1 in 40° but increases to above 0.3 in 22° for $N = 16$ (figure 4.13b) and 0.6 in 10° for $N = 32$ (figure 4.13c). To conclude, highly directional antenna are most vulnerable to the measurement error of sensors. This observation lead us to conduct another critical experiment to evaluate the impact of the sector selection error on the average gain of sensor- based BFs.

Table 4.2: $\overline{G_O}, \overline{G_S}, \overline{G_{11.ad}}$ vs. various N.

N	$\overline{G_O}$	$\overline{G_S}$	$\overline{G_{11.ad}}$
4	7.82	7.10 ($\sigma = 1$)	6.02
		6.76 ($\sigma = 2$)	
		6.46 ($\sigma = 3$)	
8	13.74	13.24 ($\sigma = 1$)	9.78
		13 ($\sigma = 2$)	
		12.80 ($\sigma = 3$)	
16	19.74	19.19 ($\sigma = 1$)	13.42
		18.93 ($\sigma = 2$)	
		18.71 ($\sigma = 3$)	
32	25.75	25.02 ($\sigma = 1$)	19.72
		24.63 ($\sigma = 2$)	
		24.27 ($\sigma = 3$)	
64	31.77	30.08 ($\sigma = 1$)	23.60
		29.98 ($\sigma = 2$)	
		29.22 ($\sigma = 3$)	

Finally, Table 4.2 report results in terms of gain comparison between the discussed BF approaches. The results collected from analytical model of oracle-based, IEEE 802.11 ad, and sensor-based beamforming. In sensor-based techniques, three different values of std is reported. Average gain for all approaches is calculated in dBW per degree of a sector. The gain is measured by the proposed platform. It runs for 100 rotations (36000 degrees) and average the gain per degree. The value are reported in the comparison table.

As obvious, sensor-based has maximum gain and sensor-based are mostly same for small value of std. IEEE 802.11ad has a lowest provided gain in rotation scenario. In the case where SLS delay is considered, $\overline{G_{11.ad}}$ decreases. The main facts which could be concluded is as follow:

- Highly directional antenna increases the gain for all the approaches. But, rotation causes to drop the gain in 11.ad than sensor-based.
- Highly directional antenna are more vulnerable to the value of std.
- Periodic BF such as IEEE 802.11ad provides lower value for gain in mobile scenario. SLS delay causes to reduce the gain of BF in IEEE 802.11ad.

4.4 Conclusion and Discussion

In this chapter, we analyzed the performance of beamforming mechanism for mobile millimeter wave communication in three different approaches: oracle-based, IEEE 802.11ad, and sensor-based. We derived the analytical model for oracle and sensor augmented BF based on the number of sectors in directional antenna and measurement accuracy of the sensors. Moreover, we developed a MATLAB-based platform for performance analysis of IEEE 802.11ad beamforming in a rotating scenario. The receiver gain comparison show the deficiency of periodic beamforming mechanism of the the protocol for multi-users scenario. This is because of two main reasons:(1) BF procedure dedicates 8 slots per beacon interval to be competed between devices. (2) each slot has 16 frames for antenna training. It means antenna configurations more than 16 sectors require to compete the next contention for slot access. Consequently, the average gain drops within the training procedure. Further, sensor augmented methods are still tackles with the gain lost near the boarder of the sector.

Chapter 5

Sound-Align: A Beam Alignment Framework using Acoustic Side Channel

5.1 Introduction

In this chapter, we investigate the possibility of exploiting inaudible sound as a side channel to detect the direction of client and assist beam alignment in millimeter wave access points. Since all consumer devices, such as mobile phones, tablets, and laptops, include speakers, they can easily generate sound without requiring extra hardware. With falling costs and form factors of microphones and microphone arrays, sound-based DoA is practically realizable for next generation of access points. Finally, as there exists an inaudible bandwidth ($>$ 18 kHz) within the range of typical consumer speakers and microphones, it is possible to use sound for millimeter wave beam alignment without causing any sound noise in working environment. To the best of our knowledge, it is the first research to leverage microphone-speaker sensors embedded on the COTS

devices for beam alignment in mmWave networks. Our study revealed that chirp signal emitted with 50 Hz frequency band and 50 ms time length could obtain an accurate and fast direction finding.

The rest of this chapter is structured as follows. Sound assisted system model is presented in Section 5.2 followed by the experimental methodology of the proposed sound align scheme in Section 5.3. We introduce our sound align algorithms in Section 5.4. Section 5.5 focuses on DoA performance of Sound-Align. Finally, the conclusion is discussed in Section 5.6.

5.2 Sound Assisted DoA System Model

The primary objective of Sound-Align is to leverage inaudible acoustic as an out-of-band channel for efficient beam alignment in MmWave networks, especially in IEEE 802.11ad networks. Fig. 5.1 illustrates the main steps involved in the beam alignment process. First, the mobile device generates a sound-chirp signal in the frequency range $18kHz$ to $19.2kHz$, which is further described in Section 5.2.1. The mobile device emits the sound-chirp signal using available speakers on the device. Then, we assume there exists a microphone array at the MmWave wireless access point (AP) to receive the sound-chirp. Sound-Align then utilize the MUSIC algorithm to estimate the direction of arrival (DoA) of the sound-chirp, which is further described in Section 3.6.2. Despite the wide popularity of MUSIC as a sub-space DoA method, MUSIC has not yet been leveraged for DoA in inaudible sound frequencies. Therefore, Section 5.4 presents a comprehensive simulation study based on experimental data collected from COTS smartphones to investigate the performance of MUSIC in inaudible sound frequencies. Along with the estimation of DoA, the AP determines the suitable MmWave antenna sector to communicate with the

respective mobile device.

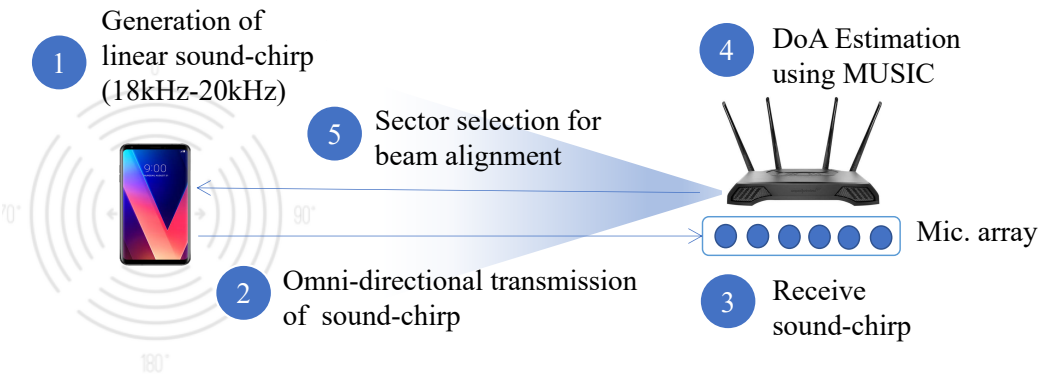

Fig. 5.1: Sound-Align beam alignment process system model and the chronological beam alignment steps

5.2.1 Chirp Signal

Chirp is a signal that varies in frequency over time. We propose to employ a linear up-chirp signal that sweeps the frequency from low to high, which is widely used for radar applications due to its capability of resolving multi-path propagation [67].

In a linear chirp, the instantaneous frequency, $f(t)$, varies linearly with time:

$$f(t) = ct + f_l \tag{5.1}$$

where f_l is the starting frequency (at time $t = 0$), and c is the chirpiness, which is constant:

$$c = \frac{f_h - f_l}{T_{Chirp}} \tag{5.2}$$

where f_h is the final frequency and T_{Chirp} is the time taken to sweep from f_l to f_h.

Without loss of generality, we utilize a sinusoidal linear chirp. The time-

domain funtion for sinusoidal linear chirp can be obtained as follows. Consider a sinusoidal signal with amplitude A, angular frequency ω_0, and initial phase ϕ as follow:

$$x(t) = A\sin(\omega_0 t + \phi) = A\sin(\theta(t)) \tag{5.3}$$

where $\theta(t)$ is instantaneous phase. The instantaneous phase of chirp signal can be obtained by taking the integral of the time-varying frequency function Eq.5.1. Thus,

$$\phi(t) = \phi_0 + 2\pi \int_0^t f(t)dt = \phi_0 + 2\pi(\frac{c}{2}t^2 + f_l t) \tag{5.4}$$

where ϕ_0 is the initial phase at time $t = 0$. The corresponding time-domain function for sinusoidal linear chirp is:

$$x(t) = \sin[\phi_0 + 2\pi(\frac{c}{2}t^2 + f_l t)] \tag{5.5}$$

5.2.2 Acoustic Channel and Path Loss Model

In this section, the path loss model for acoustic signal is presented. Sound pressure has effected by two main factors while damping: propagation loss and absorption loss. As acoustic wave has spherical propagation in air, the sound pressure decreases while the distance between source and destination increases. Let's assume $L_s(dB)$ denotes sound pressure level at source position. Sound pressure level in destination $L_d(dB)$ placed r meter apart from the source is measured as follow:

$$L_d(dB) = L_s(dB) - |20\ log^{\frac{1}{r}}| \tag{5.6}$$

It is also known as distance related loss. Apparently, it can be seen that sound pressure level reduces by 6 dB with doubling the distance.

Moreover, atmospheric conditions and propagation frequency have impact on the sound pressure level. The following equation formulates the absorption loss as:

$$P_{Abs} = \alpha.r \tag{5.7}$$

where α depends on temperature, humidity, and carrier frequency. In an indoor environment, with 20° temperature and 50% humidity, there is different values for α related to different frequencies [77]. For instance, in room environment and $f = 18KHz$, there is $\alpha = 0.443\,dB$ loss per 1 m the sound signal travelling.

To conclude, acoustic signal travelling in distance r has total loss which is modelled as:

$$Path\ Loss = |20\ log^{\frac{1}{r}}| + \alpha.r \tag{5.8}$$

For more clarification, path loss values plots in different distances, by Figure 5.2.

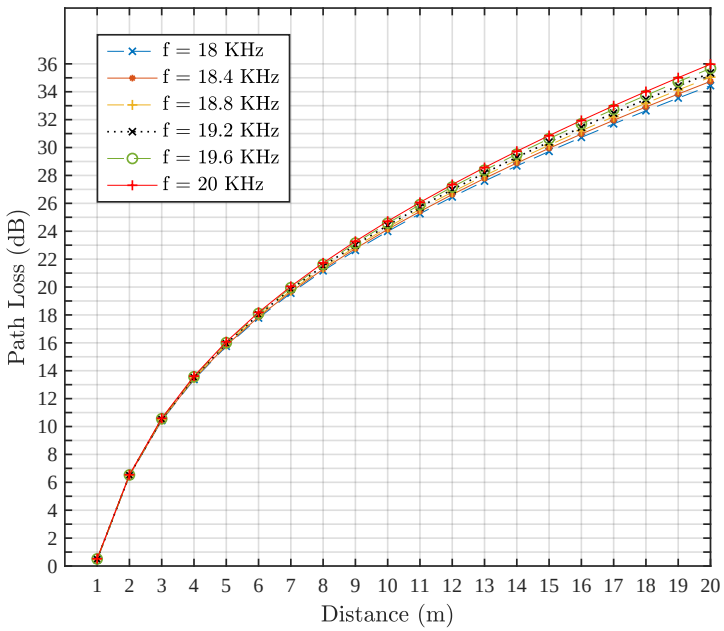

Fig. 5.2: Path Loss vs. Distance in Acoustic channel

5.3 Experimental Methodology

Propagation characteristics of inaudible signals transmitted by the COTS smartphones (as the transmitter) has not yet been well investigated. The only related experimental study of smartphones speakers reported the sound pressure level of the transmitted sound in 1kHz [78]. To leverage Eq. 5.6 in our simulations, it is first required to experimentally measure the (SPL) in the range of inaudible frequencies emitted from consumer devices at $1m$ distance. To this end, in Section 5.3.1, we first explain controlled experimental setup for SPL measurement in the range of inaudible frequencies. Next, we examine the available bandwidth to accommodate multi-users for DoA in Section 5.3.2. Finally, channel access and FDM approach is discussed in Section 5.3.3.

5.3.1 Controlled Experimental Setup

In order to measure SPL of inaudible sounds, we first, generated linear up-chirp signals in *Audacity*. Next, the generated up-chirps were transferred into a smartphone in the format of *.wav* files, and played using in-built speakers. The built-in microphones on a laptop computer placed at $1m$ distance was used as the receiver. The experiment was conducted in a quiet office room and there were no obstacles between the transmitter and the receiver. Fig. 5.3 depicts experimental setup and the step followed. The received signal was then analysed using *Audacity* to obtain SPL in dB.

We intentionally left silent intervals in between two chirps to record the background noise power.

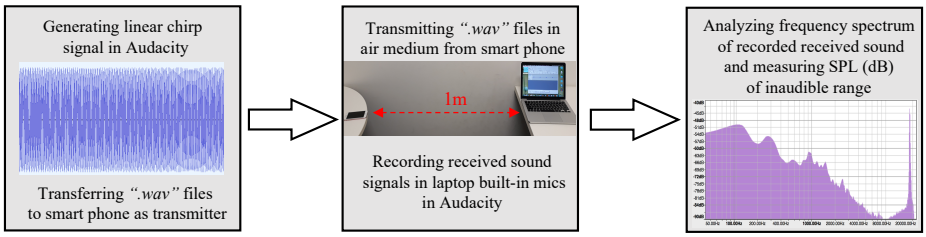

Fig. 5.3: Experimental setup: sound chirp generation, signal recording, and received signal analysis

5.3.2 Available Bandwidth

In order to investigate the practically applicable inaudible bandwidth among consumer devices, we establish an experiment of SPL measurement over inaudible range from 18 to $20KHz$. Fig. 5.4 shows the received SPL for a sine signal transmitted at single frequency among $18-20KHz$, every $100Hz$. Moreover, we report SPL values of some audible frequencies such as $2, 4, 6, 8$ and $10KHz$ (separated by the first red vertical line) for further comparison. The reported results average over 5 experiments at distance $1m$ between speaker and microphone (as shown in Fig. 5.3).

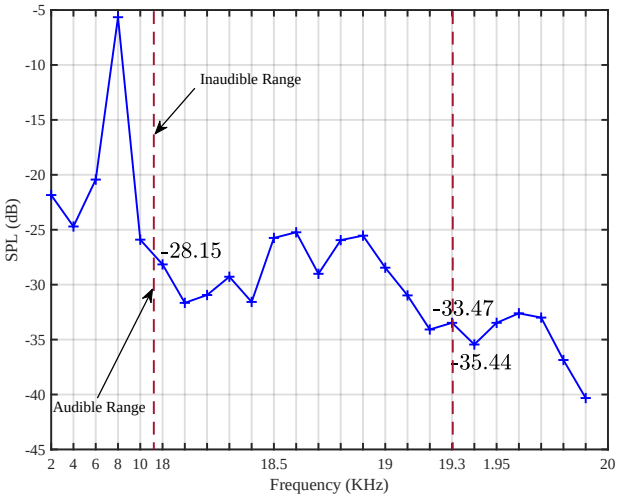

Fig. 5.4: Received sound pressure level at 1m: audible & inaudible SPL comparison

As obvious, SPL values drop significantly from audible to inaudible range.

It is due to the frequency selectivity of speaker/microphones on the consumer devices. Considering $18KHz$ as the low band of inaudible range with measured SPL of $-28.15\ dB$, the available bandwidth is capped at $19.2KHz$ where SPL has 6 dB loss ($-34\ dB$). Thus, total inaudible bandwidth for acoustic direction finding/ beam forming is 1.2 KHz. Figure 5.5 plots an up-chirp signal in frequency domain for the designed bandwidth,i.e., $18 - 19.2\ KHz$.

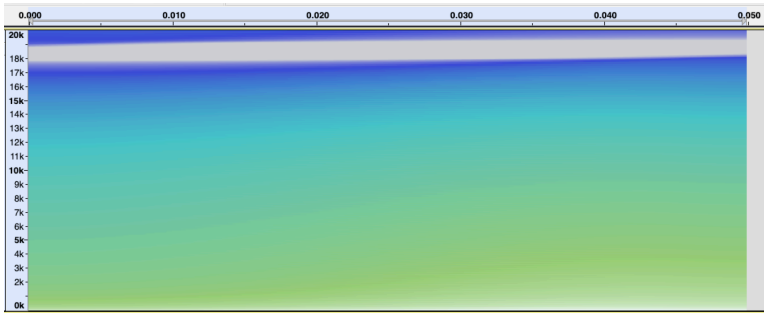

Fig. 5.5: Up-chirp signal in frequency domain for inaudible acoustic channel

5.3.3 Channel Access

In this section, we analyse the performance of inaudible sound when multi users share the available bandwidth. The main challenge of inaudible DoA is its limited bandwidth on the consumer devices. Moreover, it is desired to design a system to estimate the direction of multiple devices simultaneously, without collision. Accessing to the channel in a collision-avoidance manner is possible through either TDMA or FDMA. TDMA requires tight time synchronisation among the devices and AP. Moreover, between each user's transmission, a gap is required to avoid interference caused by delayed signals. The gap time

should be as short as possible to provide low latency and sufficiently long to avoid Inter Symbol Interference (ISI) [79]. The promising applications of MmWave communication are delay sensitive and requires fast beam tracking, such as real time video streaming or wireless VR/AR. For those applications, the devices require to track the beam every 30 ms (for $\omega = 40°/100$ ms and 32 antenna elements). Hence, TDMA could not be a proper choice for the proposed system design. In terms of FDMA channel access, the number of accommodated devices change based on the length of the frequency band and guard intervals. To find out the number of devices in FDMA, we conduct the following experiments to evaluate the system performance of Sound-Align. Thus, the very first step is to evaluate the separation of users on DoA, both angular and spectrum separation. We establish an experiment for two users in two different placement, i.e., far apart and neighbour placement, as shown in Fig. 5.6.

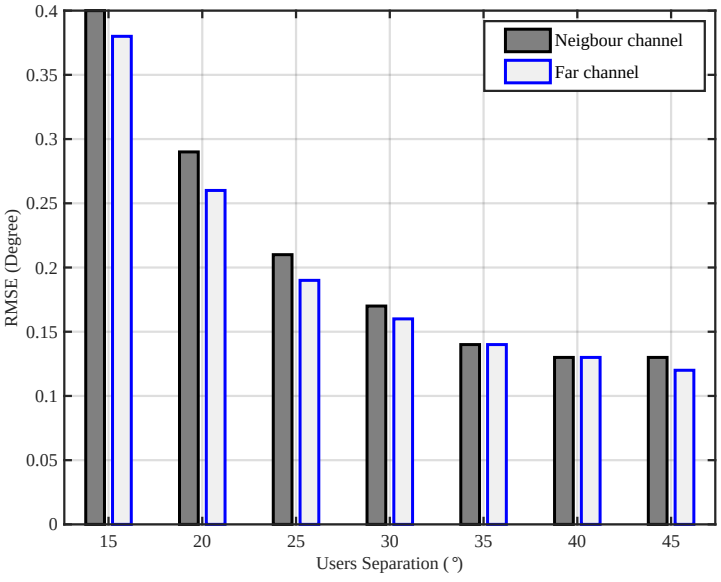

Fig. 5.6: Impact of angle-spectrum separation on sound DoA

In this experiment, RMSE has measured for two users placed at different angular separation, from 15° to 45°. It is obvious from the figure that sound

DoA accuracy is affected significantly by the angular resolution. Note that the minimum required spatial separation is 15°, with the assumed configuration (e.g., 2 microphones). Moreover, we examine the role of frequency interval between users, either neighbour channels (10 Hz guard band) or far channels ($1KHz$ guard band). It can be seen that the guard band has lower impact on RMSE, since both channel settings provide approximately similar DoA error.

5.4 Sound-Align Algorithm

Beam alignment in a mmWave multi-user scenario requires to perform fast for delay sensitive applications. As discussed in Section 5.3.3, we considered FDM channel access for sound assisted DoA to measure the direction of multiple sound signal. Dedicating the available bandwidth (discussed in Section 5.3.2) to various number of channels for simultaneous transmission is considered as an applicable and promising approach for multi-users direction finding. However, there is a fundamental challenge to identify the estimated angle (by microphone array) and the corresponding sound source. Indeed, MUSIC algorithm could accurately estimate the angle of arrival of multiple signals. But each estimated angle should be assigned to its relevant transmitted sound source (e.g., different users' devices). Thus, in this section, we develop a step for assigning the estimated angle by MUSIC into the relevant transmitted sound source using filtering approach. Algorithm 1 describe the approach, step by step.

Given a total of ΔBW inaudible acoustic bandwidth in COTS devices. We divided BW into i various channels with different carrier frequencies Δf_i for chirp signal generation (line $1-2$). Recall that we have explained the experimental methodology for channel assignment in Section 5.3. Next, channel matrix is formed comprises of i defined channels (line 3). Then, we consider

the network comprises of k multiple mobile users aim to align their beam with AP, continuously. Each user is dedicated with a random channel for sound chirp generation (line 5). The users, then, transmit chirp signals based on its dedicated channel and frequency band (line 6). Upon receiving inaudible sound signals, the key step is to filtering out the received signal with channel matrix. Hence, in our implementation, the acoustic samples pass through the channel matrix. In other words, the received sound signal is dot multiplication with the derived channel matrix to distinguish its frequency band and the corresponding user. (line 7). Finally, the angle of each individual filtered signal is estimated using MUSIC algorithm (line 8).

Algorithm 1 Sound-Align Direction of Arrival Algorithm

1: $(\Delta f_i = \{f_{Li}, f_{Hi}\}, i \in I) \leftarrow$ Bandwidth dedication into $I = \{1, 2, \ldots, i, \ldots, 20\}$ channels
2: $x(t)_i \leftarrow$ Chirp signal generation for defined frequency bands in step.1 using Equation 5.4
3: $CH = \begin{bmatrix} x(t)_1 & \ldots & x(t)_i \end{bmatrix} \leftarrow$ Channel matrix
4: **for** $k = 1 : N_{user}$ **do**
5: $\quad (x(t)_k \in CH) \leftarrow$ Random channel assignment per user
6: $\quad Rec_k \leftarrow$ Received signal of the emitted sound by $x(t)_k$
7: $\quad Filter_k \leftarrow Rec_k \cdot CH$
8: $\quad \theta^{(k)} \leftarrow$ Direction estimation using MUSIC algorithm
9: **end for**=0

In Figure 5.7, we depict dedicated channel and filtered frequency received from a particular user.

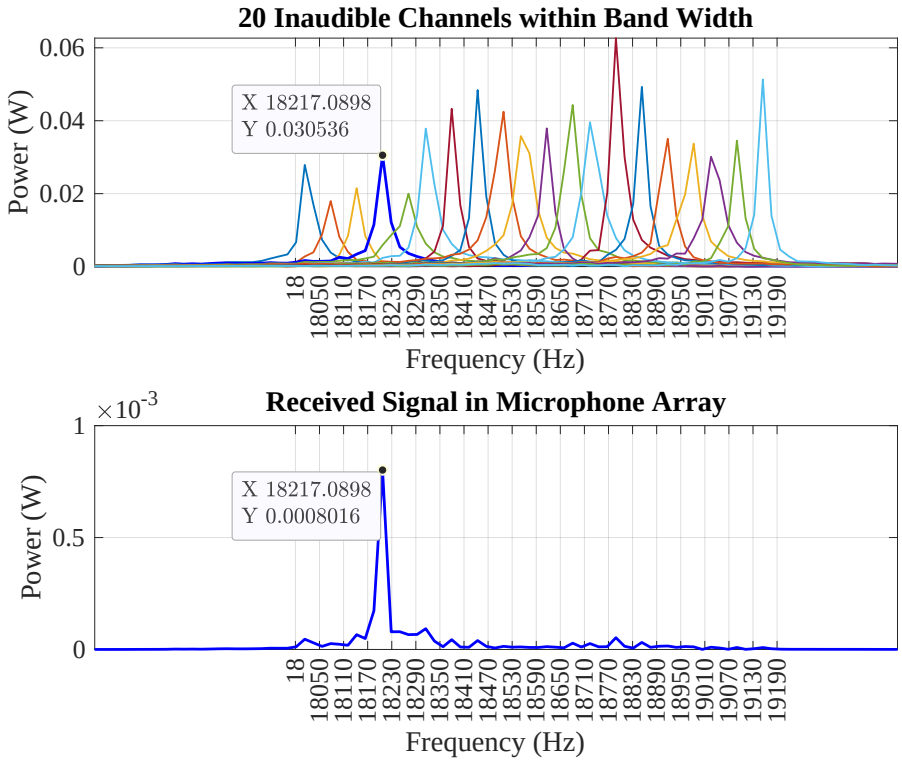

Fig. 5.7: Frequency Filtering Approach for 20 inaudible sound channels

5.5 Performance Evaluation

In this section, we present the performance results of Sound-Align DoA scheme. First, we present simulation model and setup in Section 5.5.1. Then we extensively evaluate the performance of the proposed sound assisted DoA algorithm in terms of chirp band, chirp length, and border effects as follows.

5.5.1 Simulation Model and Setting

MATLAB simulation model was developed to evaluate the performance of Sound-Align. We consider a sinusoidal up-chirp signal in the range of $18 - 19.2\ kHz$ transmitted by a smartphone. The received signal at the AP is modeled based on path loss model in Eq. 5.6. The SPL at 1 is taken from the

experiments described in Section 5.3.1.

The angular Azimuth space covered by ULA is from $-90°$ to $90°$. In order to compensate the impact of microphone array borders, we delimit the users' movement between $-70\circ$ to $70°$. Further, the Region Of Interest, ROI, is bounded between 1 to 5 m vertically apart from the microphone array (and AP, consequently). Moreover, Table 5.1 lists the simulation parameters and the corresponding definition and values.

Table 5.1: Simulation parameters and values

Parameter	**Value**	**Definition**
f_l	18 KHz	Starting frequency
ΔB	$30 - 150$ Hz	Chirp bandwidth
BW_{total}	1200 Hz	Total inaudible band
N_{Users}	$1 - 8$	Number of users
N_{mics}	2	Number of mics
d_{ele}	9 mm	Mics inter-space
T_{Chirp}	$10 - 100$ ms	Chirp length
D	$1 - 5$ m	T/R distance

5.5.2 Performance Impact of Microphone Array Border

The arrival angle on the microphone array plays a role on the estimated error of DoA. The microphone array has different gain in different broadside angles which causes to provide different direction estimation error. To investigate this effect, RMSE of a single user has measured for different ground truth angles as shown in Fig. 5.8.

DoA estimation error increases exponentially when the incident angle approaches 90 degrees from either side. In this experiment, two different antenna settings has examined, e.g., $N_{mic} = 2,\ and\ 8$, and both array sizes have similar pattern despite RMSE is much lower for higher number of microphones.

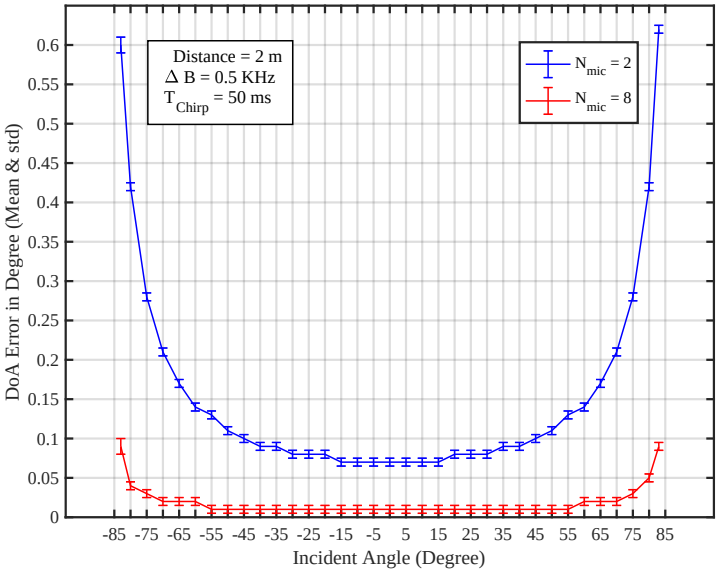

Fig. 5.8: Impact of border of microphone array on sound DoA accuracy

5.5.3 Performance Impact of Chirp Bandwidth

The available inaudible bandwidth in consumer devices is limited to $1.2kHz$ as shown in Fig. 5.4. Therefore, the chirp bandwidth has to be less than that. We vary the chirp bandwidth (ΔB) from $30Hz$ to $500Hz$, where the lower (starting) frequency is $18kHz$. RMSE and 95% confidence interval is shown in Fig. 5.9.

Increasing chirp bandwidth often makes the signal robust to noise and consequently improves RMSE of DoA estimation. For instance, $\Delta B = 30Hz$ estimates the angle with around 1.2° error, while $\Delta B = 150\ Hz$ offers more accurate DoA with 0.7° accuracy. However, in this particular case, when increasing the ΔB, RMSE reduces rapidly at lower bandwidths and then stay relatively stable for ΔB greater than $50Hz$. The same pattern is visible for all three distances considered. The increase in RMSE with distance is due to the signal attenuation which is about more than $6dB$ for doubling the distance (c.f. Eq. 5.8).

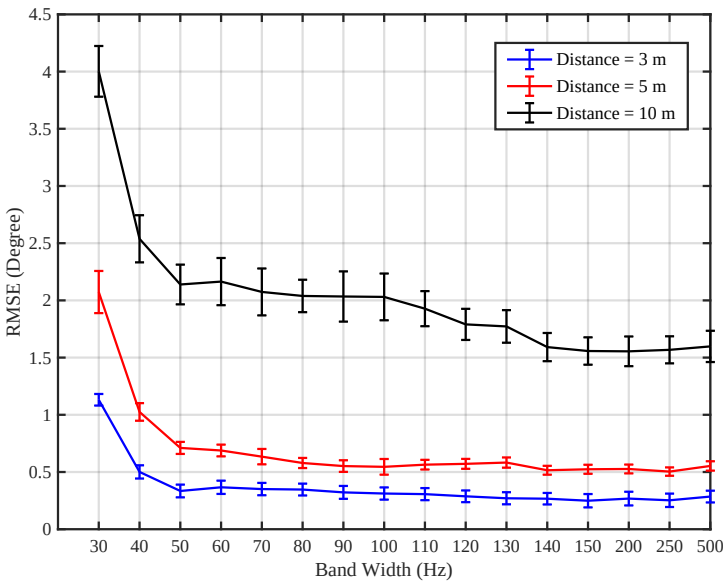

Fig. 5.9: Impact of chirp frequency band on DoA Performance

5.5.4 Performance Impact of Chirp Length

Fig. 5.10 shows RMSE of DoA for chirp length, i.e., the time duration of the chirp signal, from 10ms to 100ms. As expected longer the chirp, better the performance. Similar to chirp bandwidth, performance of chirp length also saturates after a certain value, 50-60ms to be exact.

It is desired to finding DoA as fast as possible to support the real time applications of mmWave communication. To investigate how fast DoA is applicable, we performed an experiment with various chirp length, from 10 to 50 ms. Measured RMSE values are reported on Table 5.2.

Table 5.2: RMSE (degree) for various chirp length and 12 $mics$

$T_{Chirp}(ms)$	1 m	2 m	3 m	4 m	5 m
10	3.01°	✗	✗	✗	✗
20	2.33°	✗	✗	✗	✗
30	1.10°	4.18°	✗	✗	✗
40	1.00°	3.63°	✗	✗	✗
50	0.34°	0.75°	1.51°	2.92°	4.2°

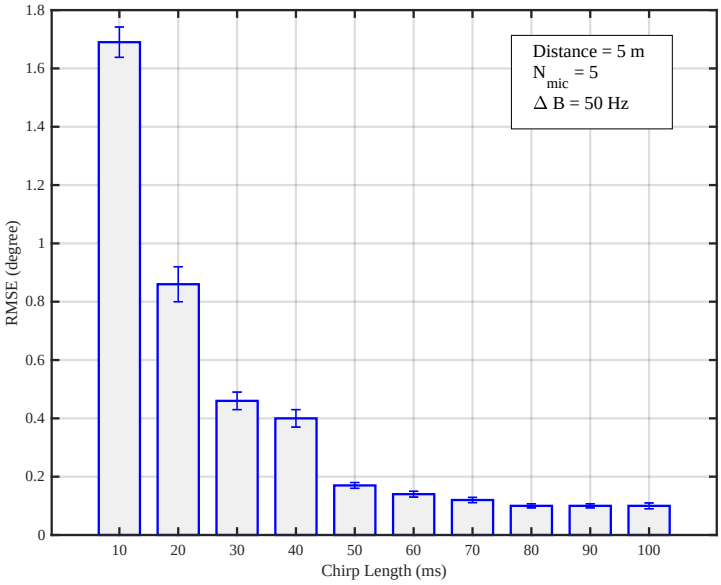

Fig. 5.10: Impact of chirp duration on DoA performance

It can be seen from the table that T_{Chirp} must be long enough to provide sufficient number of samples for direction finding, specially for longer distances (with higher path loss). The cross-marks on the table imply that direction finding is infeasible with the corresponding chirp length, such as $T_{Chirp} = 10\ ms$ and 20 ms in $d > 1\ m$, while it is possible for 2 m for $T_{Chirp} = 30\ ms$ and 40 ms with 4.18° and 3.63° accuracy, respectively.

In order to investigate the reason of low accuracy for multi-users scenario with short chirp lengths, we plot Figure 5.11 which evaluate $3dB$ Bandwidth for different chirp lengths, namely 10 and 50 ms. Both transmitted and received signals were shown in this figure. As shown, $3dB$ Bandwidth for $T_{Chirp} = 10\ ms$ is about 219 Hz which means the required frequency gap must be over this value.

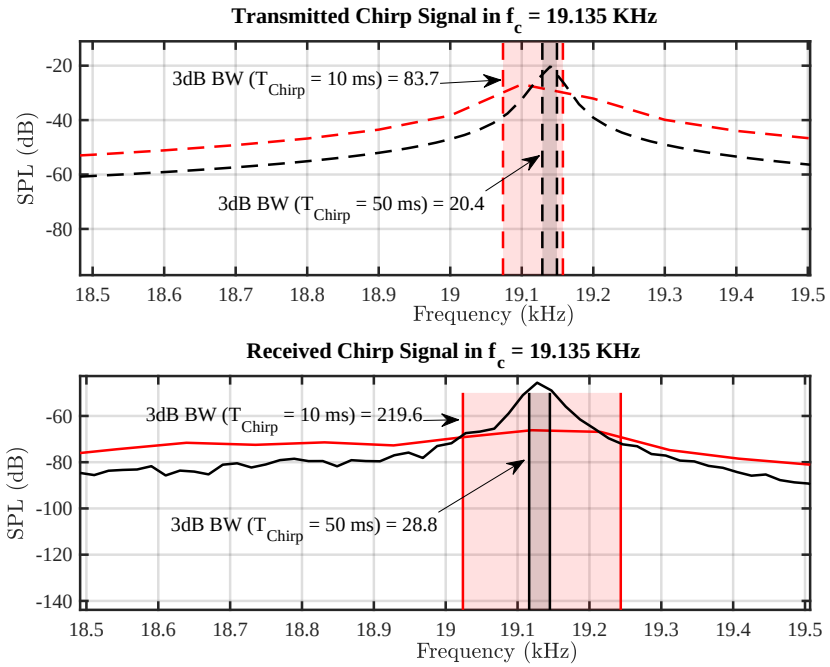

Fig. 5.11: 3dB BW for $\Delta B = 50Hz$

5.6 Conclusion and Discussion

In this chapter, we have presented an inaudible sound-based beam alignment framework, Sound-Align, for MmWave communication. We have initially established a combination of experimental-simulation experiments to find out the feasibility of chirp signal for DoA using MUSIC algorithm, the well-established high resolution direction finding method. Using a combination of experimental and simulation analysis of the inaudible sound spectrum available in typical mobile phones, we have demonstrated that the use of 50 Hz and 50 ms sound chirps provide efficient and reliable detection of direction. Moreover, the proposed inaudible sound DoA has a low computational/implementation cost using just two microphones. This achievement has led by the proposed filtering FDM approach of sound channel access.

In summary, Sound-Align system parameters are as follows:

- Bandwidth: RMSE in DoA estimation does not reduce beyond 50 Hz. The accuracy is less than 1° in short distances (less than $5m$) which can be the case for many indoor environments.

- Chirp length: RMSE improves with increasing size of chirp length. However, there is no performance gain beyond 60ms chirp length.

- Incident angle: Higher incident angles, i.e. at the border of gain pattern, causes higher error in DoA. This impact could be compensate delimiting region of interest for border area.

In next chapter, we will investigate the performance of the developed inaudible sound DoA in mmWave beam alignment in a mobile multi-users scenario.

Chapter 6

Performance Evaluation of Sound Align

6.1 Introduction

In Chapter 5, we designed and investigated inaudible sound Direction of Arrival (DoA) for consumer electronic devices, in order to estimate the direction of multiple devices in the RoI. We considered practical limited bandwidth available on the COTS devices to address DoA for multi-users scenario. Moreover, we have shown that the proposed sound DoA design is significantly fast (at the order of 50 ms) and low cost/less complex in the infrastructure design (microphone array comprises of only 2 microphones).

Now in this chapter, the aim is to investigate the performance of the designed DoA method for mmWave beam alignment in multi-users scenario. Further, we evaluate the system performance in the case that all users on the network are freely moving within the network boundaries with walking speed. Moreover, we thoroughly investigate the sound-assisted beamforming for MmWave communication with various antenna sectors and directional-

ity. The performance of the system with two different mobility model is also explored. The results showed Sound-Align outperforms IEEE 802.11 ad by 11.39 dB and 10.59 dB average gain for $N_{Sec} = 64$ and $N_{User} = 10$ in Random WayPoint and Back& Forth mobility models, respectively.

The rest of this chapter is structured as follows. The system model is presented in Section 6.2, followed by performance metrics in Section 6.3. We then review our proposed beam alignment algorithm briefly in Section 6.4. In Section 6.5, the simulation results are presented. Finally the conclusion is discussed in Section 6.6.

6.2 System Model

In this section, we define the various elements that make up the simulation environment. In particular, we describe Region of Interest (RoI), the users mobility model, and millimeter wave sectored antenna and degree of coverage per sectors in RoI.

6.2.1 Region of Interest

Figure 6.1 illustrates the Region of Interest for users' movement.

We assume an office environment in $5m \times 5m$ and covered by microphone array with $(-90°, 90°)$ azimuth angle (left side figure). We consider the effect of border of microphone array on DoA, as discussed in section 5.5.2, thus the Region of Interest is delimited by $(-70°, 70°)$. Moreover, users are moving $1m$ apart from the microphone array which has considered as the reference distance for inaudible acoustic communication in section 5.2.2. Hence, the testing environment defined by the explained boundaries are plotted in 6.1 (right side figure). Note that we assume the system model in a $2D$ environment while

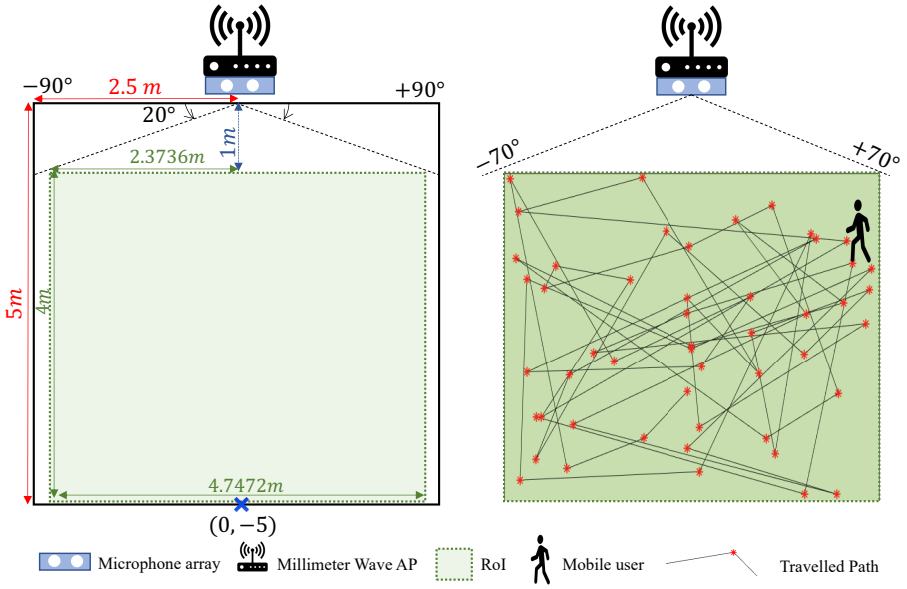

Fig. 6.1: Region of Interest and RWP mobility model

both AP and users' devices are at the same height (constant z coordination value). $2D$ deployment is an applicable assumption for most of the typical AP installments in indoor environments.

6.2.2 Mobility Model

In this section, we describe the mobility models examined to evaluate the performance of the proposed beam alignment method. We assume all users have mobility within the RoI. Two different applicable mobility models have considered, Random Way Point (RWP) and Back and Forth (B&F).

- **Random Way Point (RWP):** It is a commonly used mobility model. In this model, each user selects a random destination within the RoI independent of other users, and moves there following a straight trajectory. We assume that all the users are moved at the usual walking speed of $v = 1.4\ m/s$ [80]. Upon reaching the destination, users select next destination and move toward.

- **Back & Forth (B&F):** In this mobility model, all users are walking through a straight horizontal line while keeping constant distances from AP. Upon reaching the border of RoI, the user turns around to change direction and keep walking with the constant speed of v. Figure 6.2 denotes the paths travelled by users in B&F mobility.

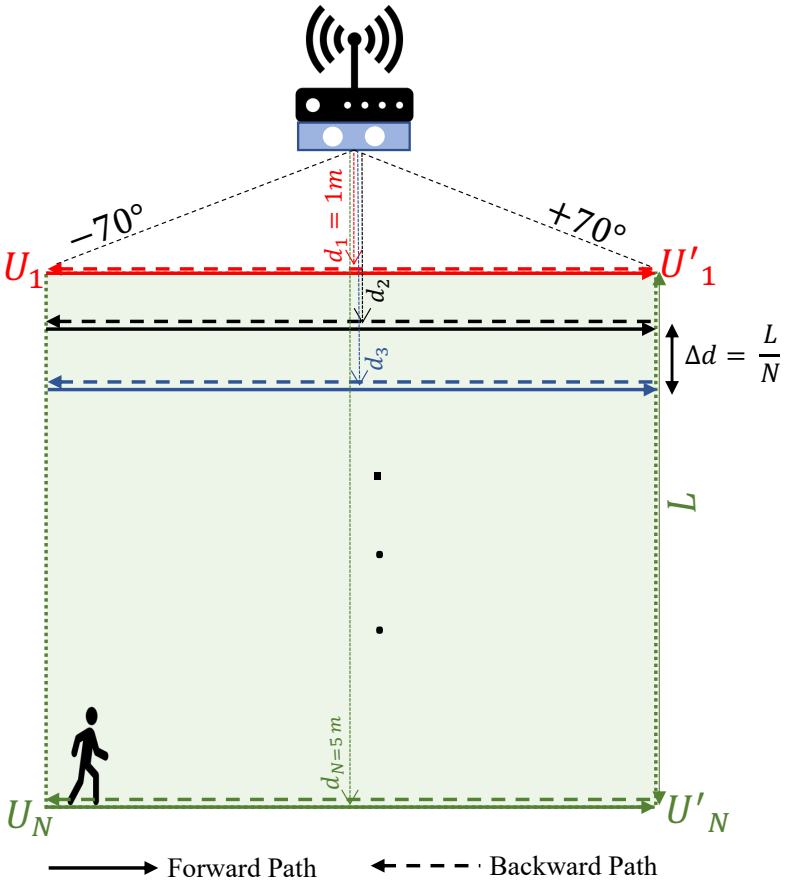

Fig. 6.2: Back & Forth Mobility model

Note that U_N and U'_N denote starting and turning points of user N, respectively.

6.2.3 MillimeterWave Antenna Coverage

MillimeterWave AP is assumed to be equipped by a circular array antenna directional antenna with N_{Sec} different sectors. Total 360° is simply divided by N_{Sec} and allocate a beamwidth of $\phi° = \frac{360}{N_{Sec}}$. Each beamwidth, then, covers an area of RoI equivalent with $\phi°$. Considering the geometry of system model shown in Figure 6.1, AP has assumed to be installed in the middle of horizontal side. RoI, therefore, is covered by $N_{Sec}/2$ while the users are faced with half-circle. Figure 6.5 illustrates the sectored RoI with $N_{Sec} = 16$ and 64.

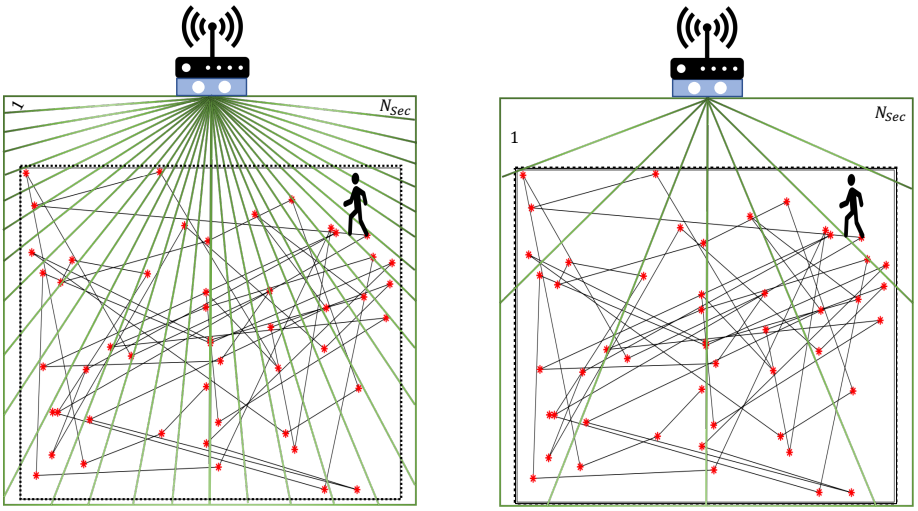

Fig. 6.3: Sectorised RoI by $N_{Sec} = 64$ & 16

6.3 Performance Metrics

Here, we define the required metrics in order to evaluate the system model and its performance.

6.3.1 Direction of Arrival Accuracy

Accuracy of direction of arrival is one of the main metrics used to evaluate the system performance since accurate estimated angle conducts to select the appropriate sector and vice versa. Thus, we report DoA accuracy by measuring RMSE of estimated angle, $\widehat{\theta}$, corresponding to the ground truth, θ, in degree. Equation (6.1) is used to compute DoA accuracy among observation time slot, T_{obs} :

$$RMSE_{DoA} = \sqrt{\frac{\sum_{t=1}^{T_{obs}} (\widehat{\theta}(t) - \theta(t))^2}{T_{obs}}} \tag{6.1}$$

6.3.2 Sector Selection Success Rate

In the considered mobile users system, we define a metric to evaluate performance of the proposed alignment method. Assuming that $Sec_{\theta}(t)$ denotes the align sector at time t. Thus, sector is successfully selected by the proposed method if:

$$\text{Success}(t) = \begin{cases} 1 & \text{if } Sec_{\theta}(t) = Sec_{\widehat{\theta}}(t) \\ 0 & \text{Otherwise} \end{cases} \tag{6.2}$$

where $Sec_{\widehat{\theta}}(t)$ denotes the selected sector by the proposed beam alignment method. According to the definition of sector selection success, the sector selection success rate, $Rate_{SSS}$, of the method in percentage, can be written as:

$$Rate_{SSS}(\%) = \frac{\sum_{t=1}^{T_{obs}} (Success(t) = 1)}{T_{obs}} \times 100 \tag{6.3}$$

6.3.3 IEEE 802.11ad Slot Access Rate

Beamforming procedure in IEEE 802.11ad is a contention-based scheme, as discussed in Section 2.2.1. In each BF cycle, all users have to compete to catch a slot for antenna sector training and alignment with AP. Each user may or may not be successful to achieve the slot within a beacon interval. Slot access within ith beacon interval can be expressed as:

$$\text{Slot Access}(i) = \begin{cases} 1 & \text{if user wins a slot} \\ 0 & \text{Otherwise} \end{cases} \tag{6.4}$$

Accordingly, we define slot access rate within each beacon interval to report the rate in which the user can successfully win a slot. Recall that slot access contention happens in multi-users scenario. Consequently, we report average slot access rate of all N users on the network within different beacon intervals. In other words,

$$\text{Slot Access Rate}(\%) = \frac{\sum_{n=1}^{N_{Users}} \sum_{i=1}^{BF_{cycles}} (Slot\ Access(i) = 1)}{BF_{cycles} \times N_{Users}} \times 100 \tag{6.5}$$

where N_{Users} and BF_{cycles} show number of users on the network and total number of beamforming cycles, respectively.

6.3.4 Alignment Percentage

In this section, we investigate the impact of dynamic movement of users within the RoI. Maintaining alignment at the presence of mobility is a challenge for mmWave communication. The aligned sector direction is quickly misaligned due to users' mobility. Thus, we evaluate the system performance using align-

ment percentage metric every ms which is denoted by $M_{Lobe}(t)$. Recall that in a particular time t, a device is aligned if it lies between the main lobe antenna. Thus,

$$A(t) = \begin{cases} 1 & \text{if } M_{Lobe}(t) \\ 0 & \text{Otherwise} \end{cases} \tag{6.6}$$

Accordingly, we measure the percentage of time that the user provides main lobe gain, per ms over the specific time, T_{Obs}. Note that the alignment percentage is averaged by the total number of users who are individually moving around the RoI. The metric can be expressed as:

$$Alignment(\%) = \frac{\sum_{t=1}^{T_{obs}} (A(t) = 1)}{T_{obs}} \times 100 \tag{6.7}$$

6.3.5 Average Gain

One of the main aim of this research is to improve the performance of mmwave directional communication in a mobile multi-user scenario. Therefore, the antenna gain is considered as one the performance metric in this chapter. Accordingly, we measure the achieved average gain of antenna per ms per user, $\overline{Gain}(t)$, and compared with the corresponding gain in 802.11ad. The antenna pattern of mmwave and the gain equation has previously discussed in Section 4.2.1. Since the user is moving randomly, its incident angle with the microphone array is changing, continuously. Let's $g_t(\theta)$ denotes instantaneous gain of mmwave directional antenna as a function of its incident angle. Thus, $\overline{Gain}$ can be written as:

$$\overline{Gain}(t) = \frac{\sum_{i=1}^{N_{Users}} \sum_{t=1}^{T_{obs}} g_t(\theta)}{T_{obs} \times N_{Users}} \tag{6.8}$$

6.4 Sound-Align Algorithm

In this section, we explain the proposed sound assisted beam alignment method. Algorithm 2 is presented to align the beam with a directional mmWave antenna.

In this algorithm, at first, every user selects a random starting point within the RoI (line 1), and a random destination to set it as next target point to reach it (line 2). Alongside the path between starting and destination points, user's location is frequently obtained per ms using Equation 6.9 (line 3). Next, user's coordination is measured every 100 ms, e.g., beamforming cycles (line 7). Then, sound DoA is measured using Sound-Align algorithm (line 8) and its corresponding sector is obtained (line 9). Recall that mmWave directional antenna sector coverage has explained in Section 6.2.3. DoA and sector selection steps are repeated per ms (line 11-12). $Sec_{\widehat{\theta}(t)}$ is compared continuously with $Sec_{\widehat{\theta}(bf)}$, every ms (line 13) to obtain main lobe or side lobe gain (line 14-16). The procedure continues till the user reaches beamforming position (line 20). Then, the next beamforming cycle will be obtained to reach the destination point, (X_d, Y_d) (line 21-22). Once the user reaches the destination point, traveling path continues with assigning the current destination point as starting point (line 24). Now, a new destination point is randomly selected (line 25) and the procedure repeats to cover all considered N_{cycle}s (line 26-27).

Algorithm 2 Sound-Assisted MmWave Beam Alignment Scheme

$(X_{(s)}, Y_{(s)}) \leftarrow$ Random Selection $(x, y) \in$ RoI
$(X_{(d)}, Y_{(d)}) \leftarrow$ Random Selection $(x, y) \in$ RoI
$(X_{(t)}, Y_{(t)}) \leftarrow$ Equation 6.9 for $t = 1\ ms$
$N_{cycle} \leftarrow n \in \mathbf{N}$
for $N = 1 : N_{cycle}$ **do**
  if $(X_{(t)}, Y_{(t)}) \neq (X_{(d)}, Y_{(d)})$ **then**
    $(X_{(bf)}, Y_{(bf)}) \leftarrow$ Equation 6.9 for $t = 100$
    $\widehat{\theta}(bf) \leftarrow$ using *Sound-Align* Algorithm
    $Sec_{\widehat{\theta}(bf)} \leftarrow \theta_l \leq \widehat{\theta}(bf) < \theta_u$
    while $(X_{(t)}, Y_{(t)}) \neq (X_{(bf)}, Y_{(bf)})$ **do**
      $\widehat{\theta}(t) \leftarrow$ using *Sound-Align* Algorithm
      $Sec_{\widehat{\theta}(t)} \leftarrow \theta_l \leq \widehat{\theta}(t) < \theta_u$
      if $Sec_{\widehat{\theta}(t)} == Sec_{\widehat{\theta}(bf)}$ **then**
        $g_t(\theta) = M(\theta)$
      else
        $g_t(\theta) = \zeta$
      end if
      $t \leftarrow t + 1$
      $(X_{(t)}, Y_{(t)}) \leftarrow$ using Equation 6.9
    end while
    $bf \leftarrow bf + 100$
    $N \leftarrow N + 1$
  else
    $(X_{(s)}, Y_{(s)}) \leftarrow (X_{(d)}, Y_{(d)})$
    $(X_{(d)}, Y_{(d)}) \leftarrow$ Random Selection $(x, y) \in$ RoI
  end if
end for=0

6.5 Evaluation and Simulation Results

In this section, the performance of the proposed beam alignment scheme is evaluated through extensive simulation by MATLAB. We evaluate the performance of both single and mulit users scenario where all users have mobility according to the explained mobility models in Section 6.2.2 within the entire RoI expressed in Section 6.2.1.

6.5.1 Simulation Setup

We use MATLAB to simulate the proposed sound assisted beam alignment system with multiple mobile users. Table 6.1 lists the parameters and their values used in this chapter. We used same parameters for inaudible sound signals and acoustic channel as obtained in previous chapter. Note that microphone array includes 2 mics has utilised for sound DoA and mmWave directional antenna with N_{Sec} different sectors has exploited for multi Gbps wireless communication.

Table 6.1: Simulation parameters and values

Parameter	**Value**	**Definition**
N_{Users}	$1-10$	Number of Users
v	$1.4\ m/s$	Walking speed
N_{Sec}	$4, 8, 16, 32, 64$	MmWave antenna sector
$d_{vertical}$	$1-5\ m$	Vertical distance
BF_{cycle}	$100\ ms$	Beamforming intervals
N_{mic}	2	Number of microphone

Our preliminary simulation results show that the system performance becomes stable after 500 beamforming cycles, e.g., 50000 ms. As a result, we run all simulations for 1500 cycles (150000 ms) to mitigate the randomness of the results.

6.5.2 Performance Impact of Single user on the ROI

In this section, we first consider a single user within the RoI which is moving along RWP and B&F mobility model. Performance of the single user is compared through different metrics against the benchmark beamforming method, IEEE 802.11 ad.

Let us start with random path traveling by the single user. Figure 6.4 illustrates movement path of single user within RoI. Note that movement boundaries is vertically limited from 1 m to 5 m apart from Ap ($[-1, -5]$). Moreover, the furthest point has shown on the figure for further investigation throughout the following subsections.

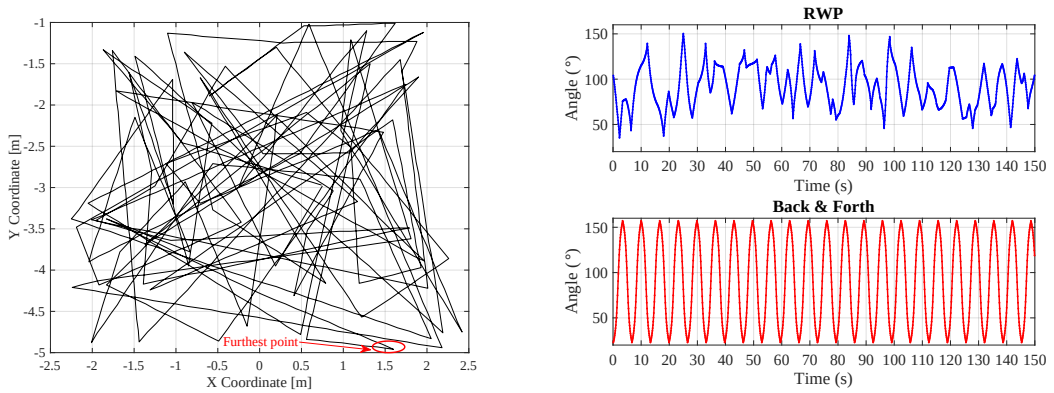

Fig. 6.4: User mobility pattern and angle variation for RWP and B&F

Given that $[X_s, Y_s]$ and $[X_d, Y_d]$ show coordination of starting and destination points of user, respectively. Let us m denotes the slope of the line which connects starting and destination point. It simply can be obtained by $m = \frac{Y_d - Y_s}{X_d - X_s}$. Thus, the user's coordination per $t = 1$ ms, $[X(t), Y(t)]$ can be written as:

$$\begin{cases} X(t) = X_s + \frac{v \times t}{\sqrt{(1+m^2)}} \\ Y(t) = Y_s + (m \times (X(t) + X_s)) \end{cases} \tag{6.9}$$

Recall that v shows the users walking velocity. Consequently, ground truth angle per ms, $\theta(t)$ can be obtained as:

$$\tan^{-1}(\theta(t)) = \frac{X(t)}{Y(t)} \tag{6.10}$$

Accordingly, Figure 6.4 (upper right side) plots ground truth angle variation, θ, of mobile user over the time per ms. The lower plot in the figure illustrates angle variation corresponding to a user who is moving along Back & Forth mobility model (explained by Figure 6.2). As expected, angle variation corresponding to Back & Forth mobility model obtained periodic and repetitive behaviour.

6.5.2.1 Sector Tracking Graph

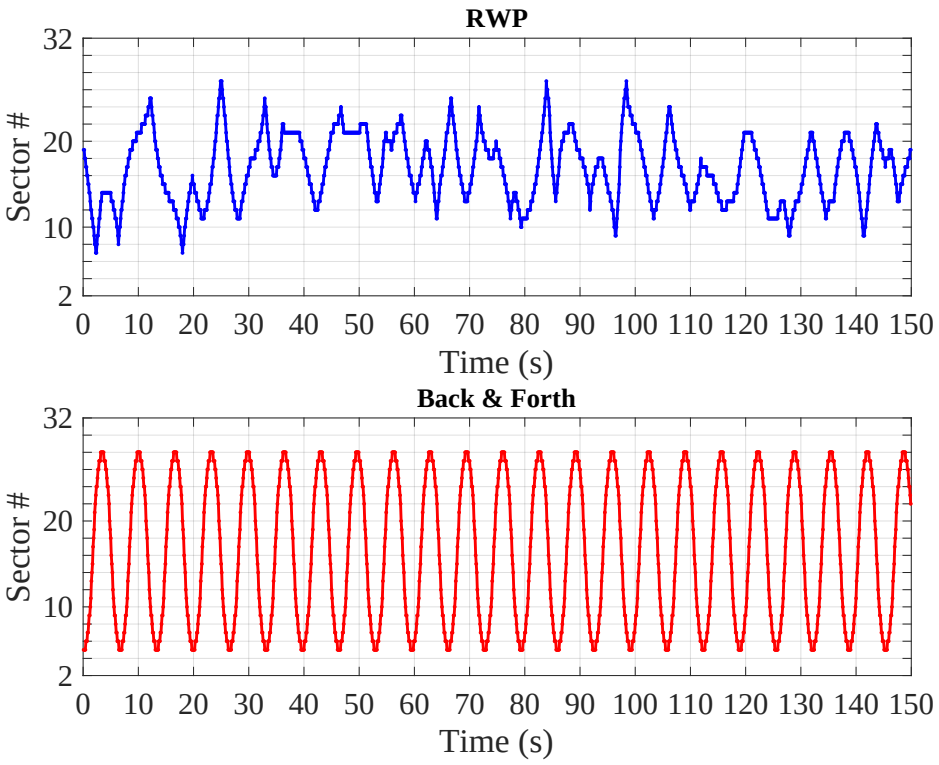

Fig. 6.5: Sector variation over time for RWP and B&F mobility

The goal of beamforming is to select the aligned sector between user and AP, continuously. Hence, in this section we insight into the variation of align sector at time t, $Sec_{\theta}(t)$, corresponding to the ground truth, θ. To see how the align sector varies by users mobility over the time, we plot sector variation of RWP (upper) and B&F (lower) mobility per ms in Figure 6.5. It can be concluded from the figure that mobility of the user causes that the align sector direction is frequently switched into a different sector. Recall that the sector antenna coverage and its geometry has discussed in section 6.2.3. Note that the same repetitive trend related with B&F is obtained for the sector tracking, as well.

6.5.2.2 Distance & Time

To have a better understanding, we have plotted the distance variation of the user corresponding to the AP, every ms by Figure 6.6 for both considered mobility models.

Two-dimensional distance between user and AP is simply obtained by:

$$d_{u,AP}(t) = \sqrt{(X_{AP} - X(t))^2 + (Y_{AP} - Y(t))^2} \tag{6.11}$$

where $[X_{AP}, Y_{AP}]$ is the coordination of AP and placed at $(0, 0)$. Note that user's coordination at time t can be obtained by Equation (6.9). Moreover, we highlighted user's distance at point A, the farthest point shown in figure 6.4. While RWP obtains various distance to AP within RoI, the distance traveled in B&F mobility model has kept constant and periodic between a distance interval, e.g., 1 m to 2.5 m.

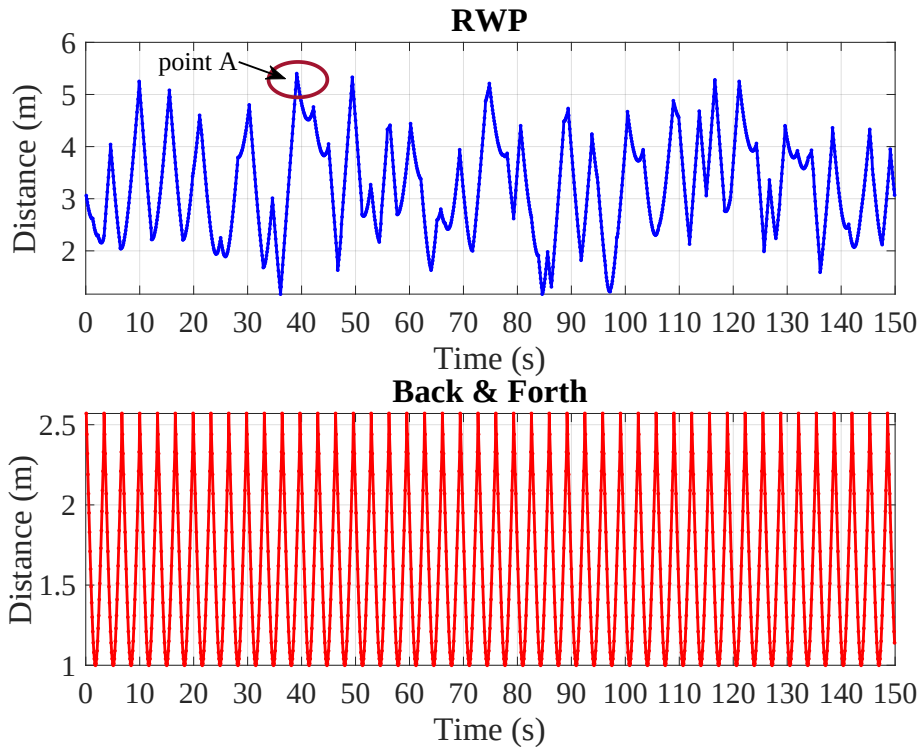

Fig. 6.6: Distance Variation over time for RWP and B&F mobility model

6.5.2.3 Sound Signal to Noise Ratio

To study the performance of the proposed sound-assisted beam alignment method, we analyse the signal-to-noise ratio, SNR, corresponding to inaudible signal of mobile user every ms. As investigated in section 5.2.2, path loss model for sound pressure level (dB) is distance-related variable. Intuitively, the further the distance from the sound source, the higher the loss in received sound pressure level. Assuming that $x(t)$ denotes time-domain chirp signal of received sound at distance 1 m, as explained by Equation(5.5). To measure SNR at time t, we take the following steps:

1. Distance $d(t)$ is calculated in specific time using Equation (6.11).

2. Distance-related loss value, $Loss_d(dB)$, is measured by Equation (5.6).

3. Received signal plus noise at distance $d(t)$ is measured by:

$Rec_{sig}(t) = x(t) - Loss_d.$

4. Received signal plus Noise power, $P_{signal+Noise}$ is calculated using:

   $(FFT(Rec_{sig}(t))).$

5. SNR is measured by:

   $SNR = P_{signal+Noise}(dB) - P_{Noise}(dB) - 1.$

Note that we measured the background noise value $P_{Noise}(dB) = -56.47\ dB$. Recall that noise measurement methodology has explained by Section 5.3.1. Figure 6.7 plots SNR value over time for particular RWP trace (illustrated in figure 6.4).

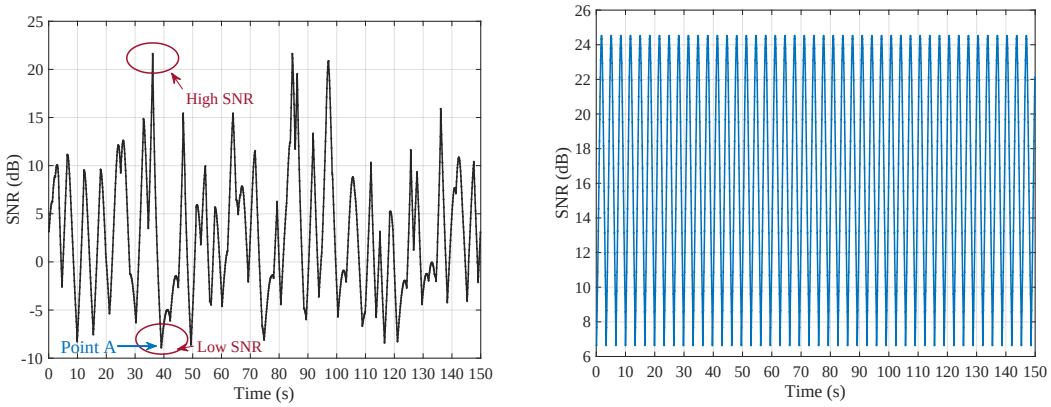

Fig. 6.7: SNR Variation, for RWP and B&F mobility

The corresponding SNR value for point A is also indicated. As expected, point A obtains the lowest SNR value due to the farthest distance. Further, we plot SNR variation for mobile user traveling along B&F mobility model in Figure 6.7. As obvious from the figure, SNR variation has a repetitive behaviour over the time for B&F mobility model, as well the distance and sector variation (plotted by the previous figures). SNR varies over time between a specific range ($[6.64\ dB, 24.51\ dB]$). Note that the particular user' distance has changed between 1 to 2.5, as shown by figure 6.6.

6.5.2.4 RMSE Variation

In this section, we report RMSE variation according to the received signal and corresponding estimated angle. Note that we defined RMSE measurement in section 6.3.1. Figures 6.8 show measured RMSE variation by Sound-Align over the time for RWP and B&F mobility.

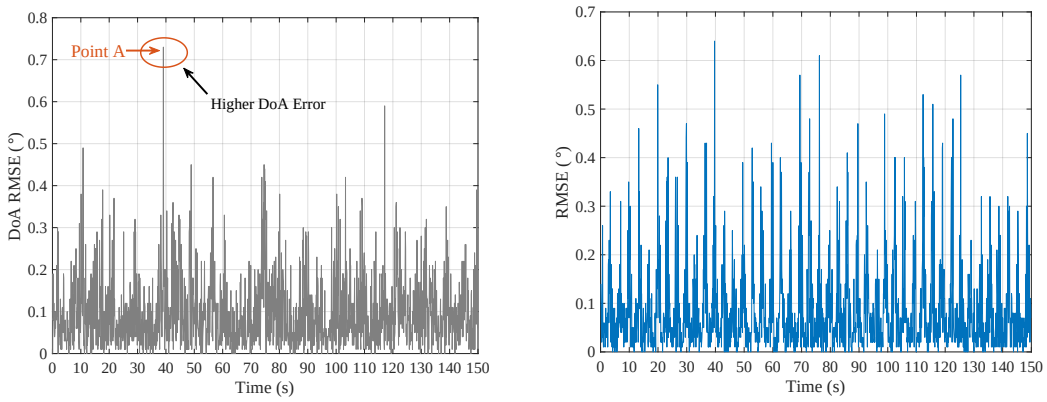

Fig. 6.8: RMSE variation for RWP and B&F mobility

As can be seen from Figure 6.8, highest value of DoA error is relevant to point A, the farthest point with lower SNR value. In addition, B&F mobility obtained less variation compared with RWP. The obtained mean RMSE within the observation time is 0.09° for B&F while the corresponding value for RWP is 0.10°. However, in both cases, Sound-Align provides a high accuracy for direction estimation.

6.5.2.5 Instantaneous Gain

Now, we study the gain achieved by a single mobile user in two different antenna configuration. Figures 6.9 and 6.10 compare Instantaneous gain per degree movement in 802.11 ad and Sound-Align for $N_{Sec} = 16$ and 64, respectively.

As observed from the figure, for single user scenario, there is no difference

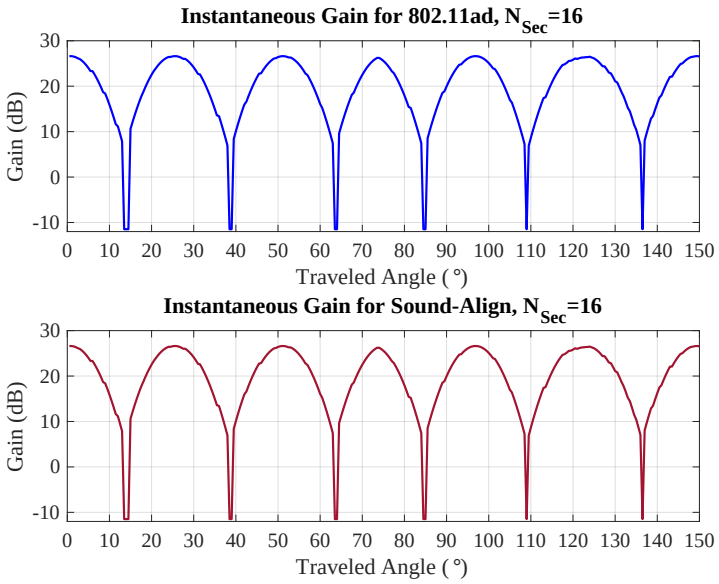

Fig. 6.9: Instantaneous gain for single user, $N_{Sec} = 16$

between the achieved gain by 11.*ad* and Sound-Align for this antenna setting. In the case of single user scenario, 802.11 ad enables to access slot per beacon interval. Thus, there is no competition for antenna training. Moreover, a single slot is sufficient for antenna training up to $N_{Sec} = 16$ (explained by Section 4.2.3). Thus, every 100 ms, both methods can successfully align their beam with AP and achieve the potential gain of antenna.

However, there is a significant difference between instantaneous gain achieved by Sound-Align and 802.11 ad for $N_{Sec} = 64$, as observed from Figure 6.10. we draw the following observations from the figure:

- In $N_{Sec} = 64$, IEEE 802.11 ad obtains more side lobe gain than Sound-Align, even for single-user scenario (no competition for antenna training). This achievement is supported by required number of slots for antenna training explained in Section 4.2.3.

- The aligned beam is frequently misaligned compared with $N_{Sec} = 16$. This is because of the narrower beamwidth in higher directional antenna.

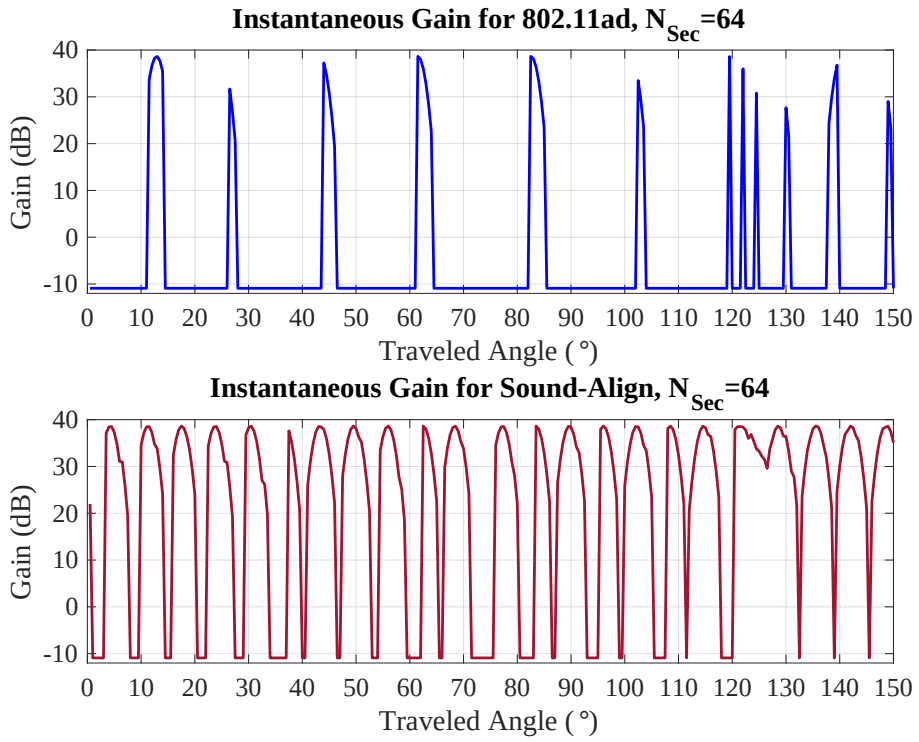

Fig. 6.10: Instantaneous gain for single user, $N_{Sec} = 64$

In the following section, we insight into the performance evaluation of the proposed beam alignment in multi-users scenario.

6.5.3 Performance Impact of Multi Users

The objective of this study is to address multi-users beamforming issue in IEEE 802.11ad. Thus, in this section, we present an extensive evaluation of the system performance for multi-users scenario.

6.5.3.1 Slot Access Success Rate Validation with different number of users

As discussed and extensively analysed by section 4.2.3, slot access probability reduces significantly at the presence of higher number of users attempting to perform beamforming. From the probabilistic point of view, the probability

that a user can successfully occupy a slot in a beamforming cycle can be obtained as:

$$P_{(Slot\ \ Access)} = \left(\frac{N_s - 1}{N_s}\right)^{N_{Users}-1} \tag{6.12}$$

where $N_s = 8$ and N_{Users} show the number of available slots in IEEE 802.11ad standard and the number of users, respectively. Consequently, the first result is to compare the analytical slot access success rate and and simulation values in multi-users scenario. Figure 6.11 reports the values for both analytical and simulation.

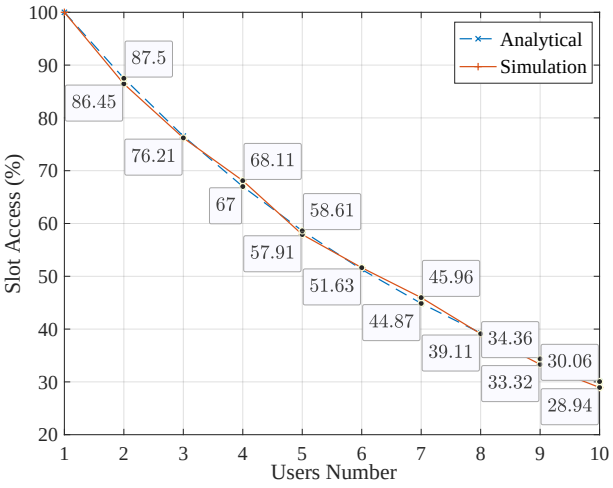

Fig. 6.11: Slot Access Success Rate Validation

As obvious from the figure, the simulation test bed is perfectly validated by the proposed analytical expression for slot access success rate. Moreover, access rate is exponentially dropped from 100% to about 29% by increasing the number of users from 1 to 10. Note that slot access success rate has no dependency to the number of antenna sector.

6.5.3.2 Validation of the Number of Required Slots for Antenna Training

We compare the required beacon intervals, BIs, (or beamforming cycles) for both simulation and analytical formulation. Recall that, in section 4.2.3, we have analytically formulated the required number of beacon intervals to successfully complete antenna training. As obvious from the analytical formulation, the numbers of antenna sector, N_{Sec} incurred more required beacon intervals for antenna training. Accordingly, Figure 6.12 illustrates the required BIs for $N_{Sec} = 32, 64$ in the case of different number of users.

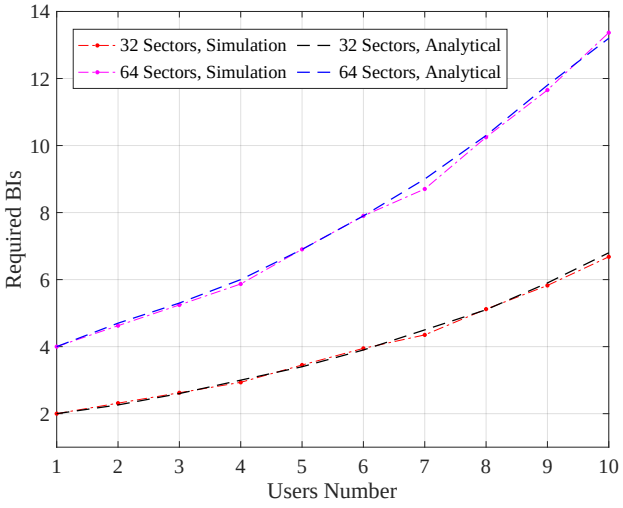

Fig. 6.12: Required number of BIs for $N_{Sec} = 32, 64$

The plot compares both analytical and simulation results. As can be seen, the validity of the simulation test bed is strongly confirmed by the analytical model.

6.5.3.3 DoA RMSE and Number of Users

We previously examined the achieved DoA accuracy of sound-align for single user in section 6.5.2.4. Here, we insight into DoA RMSE when multi-users are

moving within the RoI. Figure 6.13 depicts box plot for 10 various RWP users.

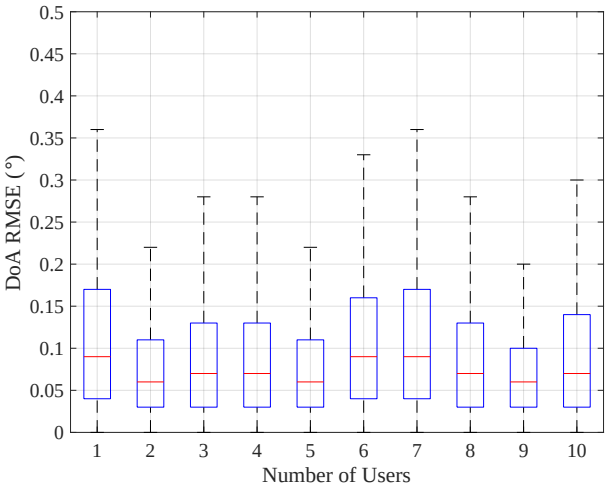

Fig. 6.13: DoA RMSE for Sound-Align in RWP mobility

Given that each user is individually travels within the RoI for $T_{Obs} = 150 \times 10^3\ ms$. DoA RMSE is measured by Equation 6.1 every ms. As obvious from the figure, all users obtain RMSE between 0.05° and 0.1° which is a significant precision achieved by Sound-Align. Moreover, the number of users incurs no negative effect on DoA RMSE because of FDM filtering approach (explained in Section 5.4). Note that we assume IEEE 802.11*ad* is perfectly aligned upon successfully accessing the slot and training antenna sectors.

6.5.3.4 Alignment Percentage

In this section, we present the results related to the average percentage of time that user spent within main lobe antenna for both Sound-Align and IEEE 802.11ad. Recall that we defined the metric in section 6.5.3.4.

Figure 6.14 represents the average alignment percentage versus different number of users. The results were collected for 5 different antenna configurations, $N_{Sec} = 4, 8, 16$ and $N_{Sec} = 32, 64$ (figure (6.15)). From Figure 6.14 the following observations can be drawn:

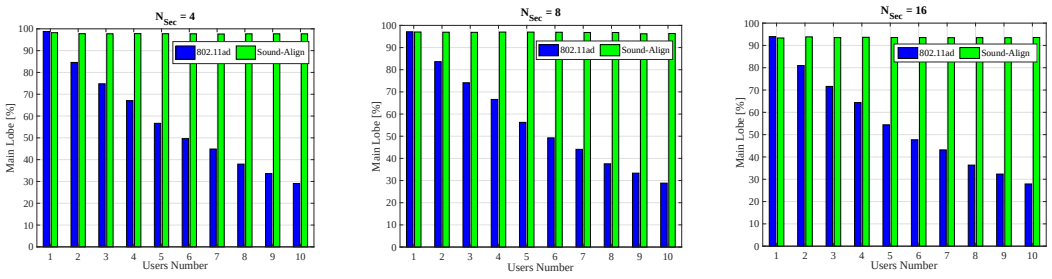

Fig. 6.14: Main lobe percentage for $N_{Sec} = 4, 8, 16$ in RWP mobility

- Given a fixed number of antenna sector, i.e., $N_{Sec} = 4$, increasing the number of users in the RoI decreases the obtained average alignment percentage in IEEE 802.11ad while has no significant impact on Sound-Align. The possible explanation is that a large number of users have less slot access rate, confirmed by Figure 6.11. Upon accessing a slot, user enables to train its antenna sectors to align with AP. Consequently, the average time that users spent in main lobe antenna decreases noticeably in 802.11ad. For example, the average alignment time in $N_{Sec} = 4$ decreases from 85% to about 30% by increasing the number of users from 2 to 10.

- In the considered antenna configurations, the effect of number of antenna sector is negligible for 802.11ad beamforming. This is because of the assumption that 802.11ad successfully selects the correct sector upon accessing the slot for antenna training (no DoA error).

- Compared with the baseline beamforming method, our proposed beam alignment enables to successfully maintain the alignment percentage significantly high, regardless of the number of users. This stable and significantly high alignment percentage has led by FDM and frequency filtering approach (discussed in section 5.4). However, increasing the antenna sector from 4 to 8 and 16 decreases main lobe percentage from 97% to 93%.

This behaviour can be explained by lower sector selection success rate for higher number of sectors.

Next, we examine the alignment percentage for higher number of sectors, $N_{Sec} = 32$ and 64. Figure 6.15 depicts the results.

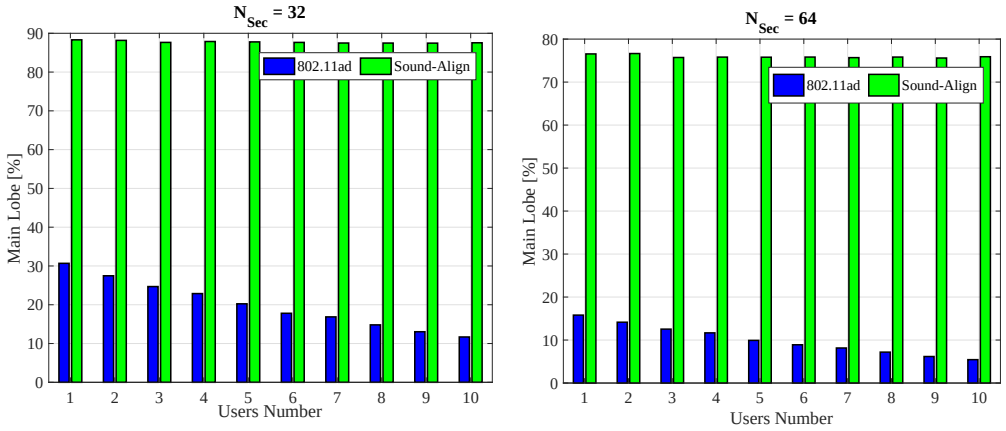

Fig. 6.15: Main lobe percentage for $N_{Sec} = 32, 64$ in RWP mobility

From the figure, following observations can be drawn:

- There has been a dramatic decline in 802.11ad alignment percentage for $N_{Sec} = 32$ and 64. For example, having 2 users in RoI, the achieved alignment percentage suffers a sharp decline from 80% to 28% and 15%, with increasing antenna sector from 16 to 32 and 64, respectively. This is caused by the more required slots for antenna training in configuration of $N_{Sec} > 16$. The obtained results can be confirmed by Figure 6.12.

- Regardless the number of users, there is a large improvement achieved by Sound-Align for more number of antenna sectors. Compared with the benchmark beamforming, Sound-Align obtained a significant improvement, reaching up to around 87% and 77% alignment with 10 users for $N_{Sec} = 32$ and 64, respectively. The achievement is because of the out-of-band and filtering approach of the proposed method.

6.5.3.5 Gain Comparison

Ultimately, in this section, we represent the average gain of directional antenna for both baseline and proposed beamforming methods, $\overline{Gain}_{11ad}$ and $\overline{Gain}_{SA}$.

Table 6.2: $\overline{Gain}$ comparison of 802.11ad and Sound-Align beam alignment, RWP mobility model and $v = 1.4m/s$

N_{User}	$N_{Sec} = 4$		$N_{Sec} = 8$		$N_{Sec} = 16$	
	$\overline{G_{11ad}}$	$\overline{G_{SA}}$	$\overline{G_{11ad}}$	$\overline{G_{SA}}$	$\overline{G_{11ad}}$	$\overline{G_{SA}}$
1	9.63	9.63	17.02	17.02	22.55	22.55
2	8.46	9.09	16.70	16.93	21.89	22.57
3	7.91	9.11	15.80	16.97	21.46	22.57
4	7.45	9.09	15.38	17	20.95	22.59
5	6.66	9.07	14.71	17.02	20.25	22.60
6	6.06	9.00	13.99	16.95	19.71	22.63
7	5.57	8.95	13.54	16.92	19.30	22.62
8	4.99	9.02	12.80	16.90	18.54	22.63
9	4.37	9.03	12.24	16.89	18.05	22.62
10	3.67	8.91	11.64	16.88	17.39	22.63

We have split the gain results into two separate tables, Table 6.2 and 6.3 for $N_{Sec} = 4, 8, 16$ and $N_{Sec} = 32, 64$, respectively.

From the tables, we can draw the following observations:

- intuitively, the higher directional antenna, the greater average gain for both beam alignment methods, regardless the number of users.

- Regardless the numbers of antenna sectors, N_{Sec}, the benchmark method provides significantly lower gain with more number of users. This finding is explained by contention-based antenna training feature of 802.11 ad. It is entirely confirmed by the alignment percentage results represented in section 6.5.3.4.

Table 6.3: $\overline{Gain}$ comparison of 802.11ad and Sound-Align beam alignment, $v = 1.4m/s$

N_{User}	$N_{Sec} = 32$		$N_{Sec} = 64$	
	$\overline{G_{11ad}}$	G_{SA}	$\overline{G_{11ad}}$	G_{SA}
1	24.07	28.59	27.11	34.01
2	23.35	28.59	26.57	34.04
3	23.03	28.48	26.25	33.97
4	22.78	28.57	25.81	33.98
5	22.13	28.51	25.13	33.98
6	21.62	28.48	24.63	33.98
7	21.34	28.49	24.42	33.98
8	20.91	28.53	23.72	33.98
9	19.79	28.51	23.08	33.97
10	19.72	28.5	22.59	33.98

- Our proposed method has successfully outperforms the benchmark beam alignment method in all multi-users scenarios. For example, in the case of $N_{User} = 10$, $\overline{G_{SA}}$ provides significantly higher gain from 5 dB to 11 dB for $N_{Sec} = 4, 8, 16$ and $N_{Sec} = 32, 64$, respectively. Note that the proposed method obtains a slight decline in $\overline{G}$ in different antenna settings. Moreover, device population has no incur on the offered $\overline{G}$ by Sound-Align.

6.5.3.6 Performance Impact of Mobility Model on Average Gain

In the previous section, we demonstrated the significant improvement of Sound-align compared with the baseline beamforming. The reported results collected for users moving according to RWP mobility model. In this section we investigate the performance impact of mobility model on the proposed system in terms of average gain of directional antenna. Accordingly, we evaluate Sound-Align beamforming when all users on the RoI are moving along B& F mobility

model (discussed in section 6.2.2). Tables 6.4 and 6.5 report the average gain results for $N_{Sec} = 4, 8, 16$ and $N_{Sec} = 32, 64$, respectively. Note that the blue columns represent average gain for Sound-Align and gray columns for IEEE802.11 ad.

Table 6.4: $\overline{Gain}$ comparison of 802.11ad and Sound-Align beam alignment, Back & Forth mobility model and $v = 1.4m/s$

N_{User}	$N_{Sec} = 4$		$N_{Sec} = 8$		$N_{Sec} = 16$	
	$\overline{G_{11ad}}$	$\overline{G_{SA}}$	$\overline{G_{11ad}}$	$\overline{G_{SA}}$	$\overline{G_{11ad}}$	$\overline{G_{SA}}$
1	11.81	11.82	16.74	16.29	22.75	22.97
2	11.21	11.81	15.77	16.15	22.20	22.70
3	10.55	11.77	15.21	16.25	21.54	22.62
4	9.93	11.57	14.68	16.44	20.97	22.69
5	8.92	11.32	14.28	16.65	20.44	22.79
6	8.07	11.04	13.86	16.83	19.91	22.81
7	7.34	10.73	13.55	16.97	19.41	22.75
8	6.45	10.44	12.93	16.98	18.67	22.67
9	5.57	10.15	12.44	17.01	18.03	22.60
10	4.60	10.02	11.92	17.02	17.32	22.54

From the tables, we can draw the following observations:

- Similar to RWP mobility, B&F also obtains a significant improvement in multi-users scenario compared with 802.11 ad. For example, there is about 5 dB improvement on average gain of antenna for $N_{Sec} = 4, 8, 16$ in the case of 10 users. Moreover, Sound-Align achieves more than 9 dB improvement for $N_{Sec} = 32, 64$.

- Average gain obtained by B&F for all antenna configurations and various number of users are almost similar with the values obtained by RWP. This result can confirm the performance of the proposed beam alignment, regardless the mobility model.

Table 6.5: $\overline{Gain}$ comparison of 802.11ad and Sound-Align beam alignment, B&F mobility model and $v = 1.4m/s$

N_{User}	$N_{Sec} = 32$		$N_{Sec} = 64$	
	$\overline{G_{11ad}}$	$\overline{G_{SA}}$	$\overline{G_{11ad}}$	$\overline{G_{SA}}$
1	24.85	28.57	27.11	34.60
2	23.35	28.55	26.57	33.99
3	22.84	28.53	26.25	33.96
4	22.69	28.52	25.81	33.91
5	22.17	28.46	25.13	33.86
6	21.60	28.46	24.63	33.75
7	21.37	28.46	24.42	33.67
8	20.94	28.36	23.72	33.52
9	20.15	28.36	23.08	33.35
10	19.74	28.30	22.59	33.18

6.6 Conclusion

In this chapter, we proposed sound-assisted beam alignment scheme for multi users, which are constantly walking within a RoI and desire to align their beam with mmWave AP. We have examined different antenna configurations and two different mobility pattern to evaluate the system performance. We compared our proposed beam alignment algorithm with baseline beamforming method in IEEE 802.11ad. The results proved that our proposed method improve antenna gain, significantly for multi-users scenario. Moreover, it was shown that our algorithm obtained a highly significant improvement for more directional antenna, e.g., $N_{Sec} = 32, 64$. These advancements can be brought by low complexity (2 microphones) and extremely fast (50 ms chirp signal) features.

Chapter 7

Conclusion and Future Work

This chapter concludes the thesis by highlighting the key outcomes of the research undertaken followed, and discussing possible future researches.

7.1 Key Outcomes and Concluding Remarks

This thesis surveyed the emerging research area of Millimeter Wave (MmWave) wireless communication to assess the state-of-the-art, its potential, and its challenges. We showed that MmWave wireless communication is an enabling technology to provide multi-Gbps data rates using 60GHz unlicensed band. We discussed that despite the immense potential of MmWave, its realization is challenging due to severe path loss, atmospheric absorption, and blockage. IEEE 802.11 ad mitigates these issues employing antenna arrays with beamfoming (BF) to establish a narrow directional communication link between the transmitter and the receiver. However, beamforming performance in a mobile MmWave network is still unexplored by the researchers, specially for multi-users scenario.

In this thesis, we went beyond the basic advantage of MmWave communica-

tion and sought further benefits that these emerging communication interface could bring to mobile wireless networks. We have proposed out-of-band beam alignment scheme for consumer electronic devices to improve MmWave beamforming performance while serving multiple mobile users.

The key outcomes and conclusions of this thesis are presented below:

- Our study revealed that despite the plethora of work in MmWave beamforming, its real constraints and limitations have not been well studied in the literature. MmWave beamforming which is performed in MAC layer through beacon interval channel access, is a contention-based method. Thus, device population on the network causing significant performance degradation for the gain of antenna. As a result, it is crucial to understand the constraints of beamforming in MmWave networks.

- We analytically studied the beam alignment performance of 802.11ad in the presence of multiple devices. We came up with a probabilistic model for required number of beacon intervals to complete antenna training in multi-users scenario for 802.11 ad. We further considered a practical rotation movement for clients to investigate the deficiency of beamforming procedure proposed in the standard in a mobile applicable environment.

- Utilizing the developed probabilistic model, we conducted a numerical performance comparison between the Oracle-based, IEEE 802.11 ad, and sensor-based beamforming for rotating devices to investigate the limitations of the standard. Our evaluation showed the limitations of the standard for highly directional antenna training in multi-users mobile devices.

- We explored the feasibility of exploiting inaudible acoustic channels on

the COTS devices to improve MmWave beamforming in multi-users network. By performing a combination of experimental-simulation evaluation, we sought the available inaudible bandwidth on the consumer electronic devices to accommodate concurrent multiple users for acoustic direction finding and beamforming. Our comprehensive experiments revealed that up to 20 channles with the frequency band of 50 Hz and signal length of 50 ms could be addressed within $18-19.2$ KHz inaudible acoustic bandwidth.

- Exploiting the developed inaudible acoustic channel, we investigated the performance of well-designed MUSIC algorithm for direction finding of multiple sound sources. Despite the wide popularity of MUSIC as a sub-space DoA method, MUSIC has not yet been leveraged for DoA in inaudible sound frequencies. We also designed a filtering approach to access the channel using FDM method for MUSIC direction estimation. Our results showed the performance of the designed sound-assisted direction finding as a low complexity (just 2 microphones), reliable (highly precise), and fast (just 50 ms chirp duration) DoA method for smart devices, such as smart phones.

- We conducted a large number of simulations to evaluate the performance of proposed inaudible sound-assisted direction estimation, called Sound-Align, for MmWave beamforming. Considering the directional communication in MmWave, we measured the antenna gain in various configuration of antenna sector numbers. Moreover, we examine the impact of device population on the efficiency of the proposed beamforming scheme. The results confirmed that Sound-Align has significantly outperformed IEEE 802.11 ad beamforming.

- We further validated the developed probabilistic model presented for required number of beacon intervals in a multi-users scenario using simulation. The findings confirmed the validity of the proposed analytical model, perfectly.

- Additionally, we evaluated our proposed beamforming algorithm for two different mobility models, RWP and Back&Forth. The findings demonstrated that in both mobility patterns Sound-Align obtained significantly higher performance than the standard by up to 11 dB avrage gain of antenna for 10 users and 64 antenna sectors.

7.2 Future Work

Our work opens up several directions of new research. This section summarize some of the ongoing and future research directions on this research.

- Our theoretical study was based on the well-studied directional antenna model provided on the implemented antenna in NS3 60 GHz module [75]. In this antenna model which is inherited from the base model in [76], the attributes of radiation pattern are defined mathematically. As a first step in future work, we will reconsider alternative antenna pattern to study more realistic radiation model. It is suggested to reconsider the achieved gain on side lobe antenna while the current model just assumed a constant value.

- The extensive inaudible sound DoA analysis obtained by conducting a set of controlled experiments provided in this thesis, was a big step towards understanding the feasibility of multiple devices direction finding. Although we conducted experiments at the reference points of 1 m with

the generally-used smart phone models and laptop embedded with 2 microphone array and then post-processing using simulation model, a thoroughly experimental evaluation with various hardware type is needed.

- In this research, we assumed LOS condition given the installment of AP in the height of users devices. Considering NLOS communication either by users' body organs or surrounding objects and evaluating the performance of Sound-Align beam alignment would be an interesting direction for future work.

- In our future work, we aim to experimentally validate the findings of this study by developing prototype Sound-Align system and MmWave hardwar (e.g., 60 GHz compatible AP) to measure the gain performance of the proposed system.

Bibliography

[1] CISCO. Cisco visual networking index: Global mobile data traffic forecast update, 2016–2021. February.

[2] CISCO. Cisco visual networking index: Global mobile data traffic forecast update, (2017–2022), February 18, 2019.

[3] T.S. Rappaport, R.W. Heath, R.C. Daniels, and J.N. Murdock. *Millimeter Wave Wireless Communications*. Pearson Education, 2014.

[4] K.C Huang and Z. Wang. *Millimeter Wave Communication Systems*. Wiley, Feb 2011.

[5] IEEE Standards Association Working Group. Amendment 3, enhancements for very high throughput in the 60 ghz band. Dec 2012.

[6] Ieee standard for information technology– local and metropolitan area networks– specific requirements– part 15.3: Amendment 2: Millimeter-wave-based alternative physical layer extension. *IEEE Std 802.15.3c-2009 (Amendment to IEEE Std 802.15.3-2003)*, pages 1–200, Oct 2009.

[7] Wonil Roh, Ji-Yun Seol, Jeongho Park, Byunghwan Lee, Jaekon Lee, Yungsoo Kim, Jaeweon Cho, Kyungwhoon Cheun, and Farshid Aryanfar. Millimeter-wave beamforming as an enabling technology for 5g cellular

communications: Theoretical feasibility and prototype results. *Communications Magazine, IEEE*, pages 106–113, 02 2014.

[8] Sanjib Sur, Xinyu Zhang, Parmesh Ramanathan, and Ranveer Chandra. Beamspy: Enabling robust 60 ghz links under blockage. In *Proceedings of the 13th Usenix Conference on Networked Systems Design and Implementation*, NSDI'16. USENIX Association, 2016.

[9] Y. M. Tsang and A. S. Y. Poon. Detecting human blockage and device movement in mmwave communication system. In *2011 IEEE Global Telecommunications Conference - GLOBECOM 2011*, pages 1–6, Dec 2011.

[10] S. Kutty and D. Sen. Beamforming for millimeter wave communications: An inclusive survey. *IEEE Communications Surveys Tutorials*, 18(2):949–973, Secondquarter 2016.

[11] Nitin Jonathan Myers, Jarkko Kaleva, Antti Tölli, and Robert W. Heath Jr. Message passing-based link configuration in short range millimeter wave systems. 2019.

[12] T. Nitsche, C. Cordeiro, A. B. Flores, E. W. Knightly, E. Perahia, and J. C. Widmer. Ieee 802.11ad: directional 60 ghz communication for multi-gigabit-per-second wi-fi [invited paper]. *IEEE Communications Magazine*, 52(12):132–141, December 2014.

[13] H. T. Friis. A note on a simple transmission formula. *Proceedings of the IRE*, May 1946.

[14] S. Jayaprakasam, S. K. A. Rahim, and C. Y. Leow. Distributed and collaborative beamforming in wireless sensor networks: Classifications,

trends, and research directions. *IEEE Communications Surveys Tutorials*, 19(4):2092–2116, 2017.

[15] T. Nitsche, A. B. Flores, E. W. Knightly, and J. Widmer. Steering with eyes closed: Mm-wave beam steering without in-band measurement. In *2015 IEEE Conference on Computer Communications (INFOCOM)*, pages 2416–2424, April 2015.

[16] www.qualcomm.com. Qualcomm atheros and wilocity announce triband wi-fi: Industry's first standards-compliant, multi-gigabit wireless chipset. https://www.qualcomm.com/news/releases/2011/05/31/qualcomm-atheros-and-wilocity-announce-tri-band-wi-fi-industrys-first, 2011.

[17] Sanjib Sur, Ioannis Pefkianakis, Xinyu Zhang, and Kyu-Han Kim. Wifi-assisted 60 ghz wireless networks. In *Proceedings of the 23rd Annual International Conference on Mobile Computing and Networking*, MobiCom '17. ACM, 2017.

[18] SAMSUNG. Feasibility of mobility for 28 ghz millimeter-wave systems. September 2018.

[19] M. Park, P. Gopalakrishnan, and R. Roberts. Interference mitigation techniques in 60 ghz wireless networks. *IEEE Communications Magazine*, 47(12):34–40, Dec 2009.

[20] Y. M. Tsang, A. S. Y. Poon, and S. Addepalli. Coding the beams: Improving beamforming training in mmwave communication system. In *2011 IEEE Global Telecommunications Conference - GLOBECOM 2011*, pages 1–6, Dec 2011.

[21] M. Fakharzadeh, M. Nezhad-Ahmadi, B. Biglarbegian, J. Ahmadi-Shokouh, and S. Safavi-Naeini. Cmos phased array transceiver technology for 60 ghz wireless applications. *IEEE Transactions on Antennas and Propagation*, 58(4):1093–1104, April 2010.

[22] Z. Li, N. Rupasinghe, O. Y. Bursalioglu, C. Wang, H. Papadopoulos, and G. Caire. Directional training and fast sector-based processing schemes for mmwave channels. In *2017 IEEE International Conference on Communications (ICC)*, May 2017.

[23] J. Palacios, D. De Donno, and J. Widmer. Tracking mm-wave channel dynamics: Fast beam training strategies under mobility. In *IEEE INFOCOM 2017 - IEEE Conference on Computer Communications*, pages 1–9, May 2017.

[24] N. Celik, M. F. Iskander, R. Emrick, S. J. Franson, and J. Holmes. Implementation and experimental verification of a smart antenna system operating at 60 ghz band. *IEEE Transactions on Antennas and Propagation*, 56(9), Sep. 2008.

[25] N. Celik, M. F. Iskander, and Z. Zhang. Experimental verification of the hybrid smart antenna algorithm with modulated waveforms. *IEEE Antennas and Wireless Propagation Letters*, 2009.

[26] Taeyoung Kim, Jeongho Park, Ji-Yun Seol, Suryong Jeong, Jaeweon Cho, and Wonil Roh. Tens of gbps support with mmwave beamforming systems for next generation communications. In *2013 IEEE Global Communications Conference (GLOBECOM)*, pages 3685–3690, Dec 2013.

[27] D. Zhu, J. Choi, and R. W. Heath. Auxiliary beam pair enabled aod and aoa estimation in closed-loop large-scale millimeter-wave mimo systems.

IEEE Transactions on Wireless Communications, 16(7):4770–4785, July 2017.

[28] Masazumi Ueba, Amane Miura, Shoichi Kitazawa, Shigeru Saito, and Takashi Ohira. Feasibility study on millimetre wave multi-gigabit wireless lan system. In *2007 European Microwave Conference*, pages 688–691, Oct 2007.

[29] K. Hosoya, N. Prasad, K. Ramachandran, N. Orihashi, S. Kishimoto, S. Rangarajan, and K. Maruhashi. Multiple sector id capture (midc): A novel beamforming technique for 60-ghz band multi-gbps wlan/pan systems. *IEEE Transactions on Antennas and Propagation*, 63(1):81–96, Jan 2015.

[30] B. Yin, S. Abu-Surra, Gary Xu, T. Henige, E. Pisek, Z. Pi, and J. R. Cavallaro. High-throughput beamforming receiver for millimeter wave mobile communication. In *2013 IEEE Global Communications Conference (GLOBECOM)*, pages 3697–3702, Dec 2013.

[31] Joan Palacios Beltran, Danilo De Donno, and Jörg Widmer. Tracking mm-wave channel dynamics: Fast beam training strategies under mobility. *CoRR*, abs/1612.07957, 2016.

[32] Jiahui Li, Yin Sun, Limin Xiao, Shidong Zhou, and C. Emre Koksal. Fast analog beam tracking in phased antenna arrays: Theory and performance, 2017.

[33] C. Qin, J. A. Zhang, X. Huang, and Y. J. Guo. Virtual-subarray-based angle-of-arrival estimation in analog antenna arrays. *IEEE Wireless Communications Letters*, 9(2):194–197, 2020.

[34] H. Shokri-Ghadikolaei, L. Gkatzikis, and C. Fischione. Beam-searching and transmission scheduling in millimeter wave communications. In *2015 IEEE International Conference on Communications (ICC)*, pages 1292–1297, June 2015.

[35] B. Li, Z. Zhou, W. Zou, X. Sun, and G. Du. On the efficient beam-forming training for 60ghz wireless personal area networks. *IEEE Transactions on Wireless Communications*, 12(2):504–515, February 2013.

[36] O.Abari, Haitham H, Michael Rodriguez, and Dina Katabi. Millimeter wave communications: From point-to-point links to agile network connections. In *Proceedings of the 15th ACM Workshop on Hot Topics in Networks*, HotNets '16, pages 169–175, New York, NY, USA, 2016. ACM.

[37] T. Bai, R. Vaze, and R. W. Heath. Analysis of blockage effects on urban cellular networks. *IEEE Transactions on Wireless Communications*, 13, September 2014.

[38] O. Abari, B. Dinesh, Austin Duffield, and Dina Katabi. Cutting the cord in virtual reality. In *Proceedings of the 15th ACM Workshop on Hot Topics in Networks*, HotNets '16, pages 162–168, New York, NY, USA, 2016. ACM.

[39] A. Maltsev, R. Maslennikov, A. Sevastyanov, A. Khoryaev, and A. Lomayev. Experimental investigations of 60 ghz wlan systems in office environment. *IEEE Journal on Selected Areas in Communications*, 27, October 2009.

[40] K. Venugopal and R. W. Heath. Millimeter wave networked wearables in dense indoor environments. *IEEE Access*, 4, 2016.

[41] K. Venugopal, M. C. Valenti, and R. W. Heath. Device-to-device millimeter wave communications: Interference, coverage, rate, and finite topologies. *IEEE Transactions on Wireless Communications*, 15, Sep. 2016.

[42] Q. Zhang, W. Saad, M. Bennis, and M. Debbah. Quantum game theory for beam alignment in millimeter wave device-to-device communications. pages 1–6, Dec 2016.

[43] Ieee draft amendment to ieee standard for information technology–telecommunications and information exchange between systems–local and metropolitan area networks specific requirements part 15.3c: Wireless medium access control (mac) and physical layer (phy) specifications for high rate wireless personal area networks (wpans): Amendment 2: Millimeter-wave based alternative physical layer extension. *IEEE Unapproved Draft Std P802.15.3c/D13, Jul, 2009*, 2009.

[44] Y. Niu, C. Gao, Y. Li, D. Jin, L. Su, and D. Wu. Boosting spatial reuse via multiple-path multihop scheduling for directional mmwave wpans. *IEEE Transactions on Vehicular Technology*, 65(8):6614–6627, Aug 2016.

[45] P. Zhou, X. Fang, Y. Fang, Y. Long, R. He, and X. Han. Enhanced random access and beam training for millimeter wave wireless local networks with high user density. *IEEE Transactions on Wireless Communications*, 16(12):7760–7773, Dec 2017.

[46] N. Gonzalez-Prelcic, A. Ali, V. Va, and R. W. Heath. Millimeter-wave communication with out-of-band information. *IEEE Communications Magazine*, 55(12):140–146, Dec 2017.

[47] Rajesh Mahindra, Hari Viswanathan, Karthik Sundaresan, Mustafa Y. Arslan, and Sampath Rangarajan. A practical traffic management sys-

tem for integrated lte-wifi networks. In *Proceedings of the 20th Annual International Conference on Mobile Computing and Networking*, MobiCom '14. ACM, 2014.

[48] WiFi Routers, AD7200. Talon ad7200 multi-band wi-fi router. https://www.tp-link.com/uk/home-networking/wifi-router/ad7200/, 2016.

[49] Multiple emitter location and signal parameter estimation. *Antennas and Propagation, IEEE Transactions on*, 34, mar 1986.

[50] J. Bao, D. Sun, and H. Li. Motion sensor aided beam tracking in mobile devices of millimeter-wave communications. In *2018 IEEE International Conference on Communications (ICC)*, pages 1–7, May 2018.

[51] H. Haitham, O. Abari, Michael Rodriguez, Mohammed Abdelghany, Dina Katabi, and Piotr Indyk. Fast millimeter wave beam alignment. In *Proceedings of the 2018 Conference of the ACM Special Interest Group on Data Communication*, SIGCOMM '18, pages 432–445. ACM, 2018.

[52] D. Shim, Cheol-Kwan Yang, Jae Kim, Joo Han, and Yong Cho. Application of motion sensors for beam-tracking of mobile stations in mmwave communication systems. *Sensors*, 14:19622?19638, Oct 2014.

[53] Z. Qi and W. Liu. Three-dimensional millimetre wave beam tracking based on handset mems sensors with extended kalman filtering. In *Radio Propagation and Technologies for 5G (2016)*, pages 1–6, Oct 2016.

[54] A. W. Doff, K. Chandra, and R. V. Prasad. Sensor assisted movement identification and prediction for beamformed 60 ghz links. In *2015 12th*

Annual IEEE Consumer Communications and Networking Conference (CCNC), pages 648–653, Jan 2015.

[55] Z. Yang, P. H. Pathak, Y. Zeng, and P. Mohapatra. Sensor-assisted codebook-based beamforming for mobility management in 60 ghz wlans. In *2015 IEEE 12th International Conference on Mobile Ad Hoc and Sensor Systems*, pages 333–341, Oct 2015.

[56] M.K. Haider and E.W. Knightly. itrack: Tracking indicator leds on aps to bootstrap mmwave beam acquisition and steering. In *Proceedings of the 19th International Workshop on Mobile Computing Systems and Applications*, HotMobile '18, pages 107–112, 2018.

[57] V. Va, T. Shimizu, G. Bansal, and R. W. Heath. Beam design for beam switching based millimeter wave vehicle-to-infrastructure communications. In *2016 IEEE International Conference on Communications (ICC)*, May 2016.

[58] I. Mavromatis, A. Tassi, R. J. Piechocki, and A. Nix. mmwave system for future its: A mac-layer approach for v2x beam steering. In *2017 IEEE 86th Vehicular Technology Conference (VTC-Fall)*, Sep 2017.

[59] M. Brambilla, M. Nicoli, S. Savaresi, and U. Spagnolini. Inertial sensor aided mmwave beam tracking to support cooperative autonomous driving. In *2019 IEEE International Conference on Communications Workshops (ICC Workshops)*, pages 1–6, May 2019.

[60] M. Park and H.K. Pan. Effect of device mobility and phased array antennas on 60 ghz wireless networks. In *Proceedings of the 2010 ACM International Workshop on mmWave Communications: From Circuits to Networks*, mmCom '10. ACM, 2010.

[61] M. E. Allam and J. F. Greenleaf. Isomorphism between pulsed-wave doppler ultrasound and direction-of-arrival estimation. i. basic principles. *IEEE Transactions on Ultrasonics, Ferroelectrics, and Frequency Control*, Sep. 1996.

[62] S. P. M., T. Panigrahi, M. Hassan, and M. Ding. Sampling free tdoa localization in millimeter wave networks. In *2019 IEEE Wireless Communications and Networking Conference (WCNC)*, April 2019.

[63] V. Krishnaveni, T. Kesavamurthy, and Aparna B. Beamforming for direction-of-arrival (doa) estimation-a survey. *International Journal of Computer Applications*, 61, 01 2013.

[64] J. Capon. High-resolution frequency-wavenumber spectrum analysis. *Proceedings of the IEEE*, 57, Aug 1969.

[65] R. Roy, A. Paulraj, and T. Kailath. Esprit–a subspace rotation approach to estimation of parameters of cisoids in noise. *IEEE Transactions on Acoustics, Speech, and Signal Processing*, 34(5), October 1986.

[66] K. Chintalapudi, V. Padmanabhan, and R.Venkatesan. Dhwani: Secure peer-to-peer acoustic nfc. In *SIGCOMM*. ACM, August 2013.

[67] Hyewon Lee, Tae Hyun Kim, Jun Won Choi, and Sunghyun Choi. Chirp signal-based aerial acoustic communication for smart devices. In *INFOCOM*, pages 2407–2415. IEEE, 2015.

[68] Q. Wang, K. Ren, M. Zhou, T. Lei, D. Koutsonikolas, and Lu Su. Messages behind the sound: real-time hidden acoustic signal capture with smartphones. In *Proceedings of the 22nd Annual International Confer-*

ence on Mobile Computing and Networking, MobiCom 2016, New York City, NY, USA, 2016, 2016.

[69] M. Uddin and T. Nadeem. Harmony: Content resolution for smart devices using acoustic channel. In *2015 IEEE Conference on Computer Communications, INFOCOM 2015,Kowloon, Hong Kong, April 26 - May 1, 2015*, pages 2182–2190, 2015.

[70] W. Wang, A.X. Liu, and S. Ke. Device-free gesture tracking using acoustic signals. In *Proceedings of the 22Nd Annual International Conference on Mobile Computing and Networking*, MobiCom '16, pages 82–94. ACM, 2016.

[71] H. Chen, F. Li, and Y. Wang. Echotrack: Acoustic device-free hand tracking on smart phones. In *IEEE INFOCOM 2017 - IEEE Conference on Computer Communications*, pages 1–9, May 2017.

[72] S. Adavanne, A. Politis, and T. Virtanen. Direction of arrival estimation for multiple sound sources using convolutional recurrent neural network. In *2018 26th European Signal Processing Conference (EUSIPCO)*, pages 1462–1466, Sep. 2018.

[73] W. Huang, Y. Xiong, X. Li, H. Lin, X. Mao, P. Yang, and Y. Liu. Shake and walk: Acoustic direction finding and fine-grained indoor localization using smartphones. In *IEEE INFOCOM 2014 - IEEE Conference on Computer Communications*, pages 370–378, April 2014.

[74] I. Constandache, S. Agarwal, I. Tashev, and Choudhury. R.R. Daredevil: Indoor location using sound. *SIGMOBILE Mob. Comput. Commun. Rev.*, 18(2), June 2014.

[75] H. Assasa and J. Widmer. Implementation and evaluation of a wlan ieee 802.11ad model in ns-3. In *Proceedings of the Workshop on Ns-3*, WNS3 '16, pages 57–64. ACM, 2016.

[76] R. Maslennikov, , and A. Lomayev. Implementation of 60 ghz wlan channel model. *Technical report, IEEE*, 2010.

[77] Damping of air at high frequencies. http://www.sengpielaudio.com/calculator-air.htm.

[78] D. Plamen. Crank it up! here are the 10 phones with the loudest speakers from 2017. https://www.phonearena.com/news/10-phones-smartphones-with-loudest-speakers-from-2017_id101333.

[79] S. Yun, Y.C. Chen, H. Zheng, L. Qiu, and W. Mao. Strata: Fine-grained acoustic-based device-free tracking. In *Proceedings of the 15th Annual International Conference on Mobile Systems, Applications, and Services*, MobiSys 17, pages 15–28. ACM, 2017.

[80] Preferred walking speed. https://en.wikipedia.org/wiki/Preferred_walking_speed.